UCLA
UCLA Electronic Theses and Dissertations

Title

Development of behavioral analysis tools for the assessment of threat avoidance learning in mPFC

Permalink

https://escholarship.org/uc/item/7v58t2ch

Author

Gabriel, Chris

Publication Date

2024

Peer reviewed|Thesis/dissertation

eScholarship.org Powered by the California Digital Library
University of California

UNIVERSITY OF CALIFORNIA

Los Angeles

Development of behavioral analysis tools for the assessment of threat avoidance learning in mPFC

A dissertation submitted in partial satisfaction of the requirements for the degree Doctor of Philosophy in Neuroscience

by

Christopher John Gabriel

2024

© Copyright by

Christopher John Gabriel

2024

ABSTRACT OF THE DISSERTATION

Development of behavioral analysis tools

for the assessment of threat avoidance learning in mPFC

by

Christopher John Gabriel

Doctor of Philosophy in Neuroscience

University of California, Los Angeles, 2024

Professor Laura A. DeNardo, Co-Chair

Professor Scott A. Wilke, Co-chair

The medial prefrontal cortex is involved in many functions, including memory, decision making, and emotional regulation. This region is strongly tied to a variety of psychiatric diseases, especially those involved in balancing approach-avoidance conflicts, such as anxiety disorders and depression. Understanding the cellular mechanisms that regulate mPFC functions is critical for learning how they become maladaptive and contribute to disease.

Threat avoidance is a critical behavior for surviving in a dynamic environment. However, one must balance threat avoidance with other behaviors, such as foraging and nesting. Many psychiatric disorders including anxiety disorders, depression, and phobias feature excessive, maladaptive avoidance as a central symptom. Understanding how regulation of avoidance behavior emerges under normal circumstances is critical for understanding how maladaptive regulation produces excessive avoidance in patients.

As new methods in neuroscience allow the examination of neural activity in ever greater resolution, there is a growing need for tools that can automate the processing and analysis of animal behavior and align it with respect to simultaneously recorded data streams.
This thesis presents a new software program, BehaviorDEPOT, that allows forecasting of animal behavior from keypoint tracking and generates detailed reports of kinematic and postural behavior statistics to facilitate downstream analyses. This pipeline provides a new tool aimed at non-computational users that bridges estimation of an animal's location with the extraction of detailed information about the animal's posture, movement, location, and behavior.

This thesis combines the capabilities of BehaviorDEPOT with miniscope imaging of mPFC to examine the emergence of activity patterns associated with avoidance learning. Examining mPFC dynamics throughout rapid learning, this thesis reveals how changes in neural representations of threatening cues and safe locations are some of the first to emerge during learning. This thesis characterized signatures of learning in mPFC and identified an emergent population activity pattern during the onset of conditioned tones that correlates with learning rate and emerges before changes in behavior. This body of work contributes a useful tool that has already been adopted by neuroscientists and reveals activity patterns in mPFC that will contribute to our knowledge of maladaptive aversive learning.

The dissertation of Christopher John Gabriel is approved.

Daniel Aharoni

Michael S. Fanselow

Kate M. Wassum

Scott A. Wilke, Committee Co-Chair

Laura A. DeNardo, Committee Co-Chair

University of California Los Angeles

2024

Dedicated to Katelyn, Ellie, and Juno

Table of Contents

List of Figures

List of Tables

Acknowledgements

I would like to first thank my advisors, Dr. Laura DeNardo & Dr. Scott Wilke, for their mentorship and the opportunity to join each lab at its start. I will always value having had the unique opportunity to help shape the direction of the lab and to receive training in an environment where I was able to develop new skills and perspective on how to build a thriving research lab. I would like to thank Laura for always being an encouraging and supportive mentor. I am constantly inspired by her creativity, passion, and kindness. Throughout graduate school, Laura has always made me feel valued for my ideas and gave me the freedom to develop newfound interests. I would like to thank Scott for his mentorship and support of my project. Scott is always a source of thoughtful feedback and provided hands-on training that was essential for mastering the difficult surgeries required for my project. Though the pandemic added many unforeseen challenges, Laura & Scott encouraged me to adapt to the circumstances, supporting my exploration into computational analysis and programming.

I would like to thank the members of my committee, Dr. Kate Wassum, Dr. Michael Fanselow, and Dr. Daniel Aharoni for their guidance and feedback that have helped shape my project and make me a better scientist. I'd like to thank Peter Schuette for providing early guidance and inspiration for the project that would later turn into BehaviorDEPOT. Thanks to Federico and Chang from the Aharoni lab for their support and guidance troubleshooting miniscope issues. I would also like to thank Isha, Austin, and Ayesha for contributing time and effort in support of my projects.

I would like to thank the members of the DeNardo & Wilke labs, for their insightful advice and friendship. Thank you to Cassie and Benita for your comradery and collaboration over the years as we rotated through and helped start the lab together. Thank you to Zach for your help growing as a scientist through your supportive advice and encouraging energy in lab. Thank you to Tanya, Asai, and Caitlin for helping me develop analysis critical for my project. I'd also like to thank Michael, Sara, and Marta for being wonderful lab mates that made graduate school less

of a challenge. I would like to thank the many friends and coworkers in the 7th floor CHS community that made day to day work a delight. Thank you to the DeBiase lab in particular for helping to create a vibrant and fun community of peers to work with and get advice from.

Lastly, I would like to thank my family for supporting and believing in me throughout the ups and downs of graduate school. Thank you to my mother for always encouraging me to pursue my passions and instilling a value for education in me. Thank you to my sister for always paving the road ahead of me and being someone to look up to and to come to for help. Most of all, thank you to my wife, Katelyn, who packed up her life and moved to Los Angeles to support my education and whose love, encouragement, and support was critical for overcoming the many challenges of graduate school.

Permissions

Chapter 2 is a version of Gabriel, C.J., Zeidler, Z., Jin, B., Guo, C., Goodpastor, C.M., Kashay, A.Q., Wu, A., Delaney, M., Cheung, J., DiFazio, L.E., Sharpe, M.J., Aharoni, D., Wilke, S.A., & DeNardo, L.A. (2022). BehaviorDEPOT is a simple, flexible tool for automated behavioral detection based on markerless pose tracking. eLife, 10, e74314. https://doi.org/10.7554/eLife.74314

Author Contributions: C.J.G. Z.Z., D.A., S.A.W. and L.A.D. designed the research; C.J.G., Z.Z., B.J., C.G., and C.M.G contributed to software development; C.J.G., Z.Z., B.J., C.M.G., A.Q.K., A.W., S.A.W. and L.A.D. performed data curation and analysis; C.J.G., Z.Z., B.J., C.G., C.M.G., M.J.S., D.A., S.A.W. and L.A.D. wrote and edited the manuscript; M.D., J.C., and L.E.D. performed investigation.

Chapter 3 is in preparation for publication.

Author Contributions: C.J.G. and L.A.D designed the research; C.J.G. performed experiments. C.J.G., T.A.G., and A.S.F. performed data analysis. C.J.G. and L.A.D. wrote the manuscript. C.J.G., T.A.G., A.S.F, S.A.W., and L.A.D. edited the manuscript.

Funding

This work was funded by NIH K01MH116264 (L.A.D.), Whitehall Foundation Research Grant (L.A.D), Klingenstein-Simons Foundation Grant (L.A.D.), NARSAD Young Investigator Award (L.A.D.), NIH T32MH073526 (B.J.), ARCS Pre-doctoral Fellowship (C.J.G.).

Vita

Education

University of California Los Angeles
PhD Candidate, Neuroscience Interdepartmental Ph.D. Program 2018 - Present

North Carolina State University
Bachelor of Science in Biology 2011 - 2015
Bachelor of Arts in Psychology 2011 - 2015
Honors: Summa Cum Laude, Valedictorian

Awards and Honors

ARCS Predoctoral Fellowship 2019 - 2023
Thomas Jefferson Scholar 2011 - 2015

Selected Publications

Gabriel C.J., Gupta T.A., Sanchez-Fuentes A., Wilke S.A., & DeNardo L.A. *Transformations in prefrontal ensembles activity underlying rapid threat avoidance learning*. [In Preparation].

Klune C.B., Goodpaster C.M., Gongwer M.W., **Gabriel C.J.**, Chen R., Jones N.S., Schwarz L.A. & DeNardo L.A. *Developmentally distinct architectures in top-down circuits*. Nature Neuroscience [In Revision], Submitted Sept 14th, 2023.

Thorson M.T., Wei S.E., Johnson C., **Gabriel C.J.**, Arshavsky V.A., & Pearring J.A. (2023). *Nrl:CreERT2 mouse model to induce mosaic gene expression in rod photoreceptors.* Frontiers Mol Neurosci, Apr 25th, 2023. DOI: 10.3389/fnmol.2023.1161127

Kashay A.Q., Cheung J.Y., Vaknalli R.N., Delaney M.J., Navarro, M.B., Jr., Junaidi C., Veenker F., Neuwirth M.E., **Gabriel C.J.**, DeNardo L.A., & Wilke S.A. (2022). *Neural activity in the anterior cingulate cortex in required for effort-based decision making*. Pre-print on bioRxiv. DOI: 10.1101/2022.03.22.485350

Gabriel, C.J., Zeidler, Z., Jin, B., Guo, C., Goodpastor, C.M., Kashay, A.Q., Wu, A., Delaney, M., Cheung, J., DiFazio, L.E., Sharpe, M.J., Aharoni, D., Wilke, S.A., & DeNardo, L.A. (2022). *BehaviorDEPOT is a simple, flexible tool for automated behavioral detection based on markerless pose tracking*. eLife, 10, e74314. DOI: 10.7554/eLife.74314

Selected Presentations

Gabriel C.J., Wilke S.A., & DeNardo L.A. *Mechanisms of mPFC Control of Threat-induced Behaviors: Role of Prelimbic Cortex in Platform-mediated Avoidance.* Gordon Research Conference, Neurobiology of Cognition. July 26th, 2022.

Gabriel C.J., DeNardo L.A., & Wilke S.A. *BehaviorDEPOT: a simple, flexible tool for automated behavior classification based on markerless pose tracking.* Integrative Center for Learning & Memory Journal Club. Apr 22nd, 2022.

Gabriel C.J., Zeidler Z., Wilke S.A., & DeNardo L.A. *BehaviorDEPOT: a novel tool for automated behavior classification based on markerless pose tracking.* Society for Neuroscience Conference, Nov 8th, 2021.

Gabriel C.J., Jin B., Zeidler Z., Wu A., & DeNardo L.A. *BehaviorDEPOT: a novel tool for automated behavior classification and analysis in rodents.* Society for Neuroscience, Global Connectome Meeting. Jan 11-13th, 2021.

Gabriel C.J.*, Jin B.*, Klune C.*, & DeNardo L.A. *Mapping the assembly and function of prefrontal circuits.* Brain Research Institute, 31st Annual Neuroscience Poster Session, UCLA. Nov 12th, 2019. (*equal contribution)

Extracurricular/Leadership/Teaching

Biological Sciences Council, NSIDP Representative	2020 - 2023
NSIDP Social Committee Member	2019 - 2023
Knowing Neurons, Contributing Writer & Editor	2022 - Present
Teaching Assistant, Cellular Neurophysiology Graduate Course	Fall Quarter 2023

Chapter 1: Introduction

Functions of mPFC

The medial prefrontal cortex (mPFC) is a key brain region with demonstrated roles in a variety of functions, including decision-making, emotional regulation, motivation, and social behavior (Euston et al., 2012; Giustino & Maren, 2015; Mack et al., 2024). Altered mPFC activity is associated with numerous neuropsychiatric disorders, including schizophrenia, autism spectrum disorders, anxiety disorders, depression, specific phobias, and Alzheimer's disease (Buxhoeveden et al., 2006; Maner & Schmidt, 2006; Papaleo et al., 2012; Xu et al., 2019; Ironside et al., 2020). Understanding how mPFC contributes to the emergence of adaptive behavior – at the level of cells and circuits – will elucidate the nature of its specific and general functions as well as its contribution to disease states.

The mPFC plays a role in both appetitive and aversive learning processes and controls decision making after learning has occurred. In each case, mPFC promotes the behavioral flexibility required to learn associations and strategies that lead to ideal outcomes (Ragozzino, 2007; Laskowski et al., 2016). This positions mPFC to have an important role in learning the value of cues and adaptive strategies in both appetitive and aversive scenarios.

Role of mPFC in Fear Learning and Memory and Threat Avoidance

mPFC is important for learning about and responding to threatening stimuli (Shin & Liberzon, 2010; McKlveen et al., 2015). One subregion of the mPFC, the prelimbic cortex (PL), plays a key role in expression and regulation of conditioned fear and threat avoidance (Corcoran & Quirk, 2007; Courtin et al., 2013). This region is implicated in control of emotional responses as well as selection of appropriate adaptive actions (Euston et al., 2012).

Though PL projects to and receives inputs from a variety of brain regions, fear expression is especially tied to input from the hippocampus and the amygdala. PL integrates

inputs from these regions to regulate expression of fear memory (Burgos-Robles et al., 2009; Sharpe & Killcross, 2014). PL signaling appears to enhance the expression of learned fears, including interfering with fear extinction, though its role may vary based on task parameters (Guistino & Maren, 2015). During expression of fear, PL activity correlates with freezing, both during memory retrieval and after failing to extinguish previously learned fear (Burgos-Robles et al., 2009).

The neural mechanisms by which PL controls expression of learned fear have been the subject of increased study but remain poorly understood. At the level of single cells, PL encodes threat-predictive cues; however, these cells acquire highly heterogeneous responses to these cues and frequently encode variable mixtures of them (Herry & Jercog, 2022). Prefrontal regulation of behavior appears to depend on a variety of complementary mechanisms. Information can be encoded in both the frequency and temporal patterns of PL neural activity (Rozeske & Herry, 2018) and in interneuron-mediated disinhibition of neural circuits during fear learning (Tovote et al., 2015). There is also growing evidence that neural oscillations in mPFC regulate fear expression (Herry & Johansen, 2014).

Compared to conditioned fear, less is known about the prefrontal mechanisms underlying threat avoidance. Recent studies showed that PL plays a critical role in learning and expression of threat avoidance, in which animals learn to exhibit a response to avoid a predicted threat (Moscarello & LeDoux, 2013; Jiao et al., 2015; Diehl et al., 2018). Projections from PL bidirectionally modulate expression of avoidance in well-trained animals (Diehl et al., 2020). However, it remains poorly understood how PL rapidly encodes the predictive relationships between conditioned cues and adaptive actions required for threat avoidance.

Threat Avoidance is Necessary for Survival but Comes with Costs

The ability to predict and preemptively avoid encounters with threatening stimuli is essential for survival. Avoidance can be innate, such as rodent's natural avoidance of bright

locations or urine from a predator (Staples, 2010). But to survive in a dynamic environment, animals also require learned avoidance capabilities. Associative learning can motivate avoidance of novel stimuli, and stimuli previously paired with threat are sufficient to drive avoidance behavior (Bechterev, 1913).

Though avoidance is an effective strategy for mitigating threats, it also comes with costs. To avoid a threat also means missing opportunities for other behaviors essential to survival and procreation, such as foraging, mating, and nest building. When avoidance becomes excessive relative to the level of threat, this behavior becomes maladaptive. Excessive avoidance at the cost of more productive activities is commonly seen in human psychiatric disorders, including depression and obsessive-compulsive disorder (OCD) (Dickson & MacLeod, 2006; Gillan et al., 2014). Avoidance is also a central symptom of anxiety disorders and can be highly generalized or domain-specific (Stein & Stein, 2008; DiMartini et al., 2019). In each of these disorders, excessive avoidance responses negatively impact the well-being of the patient. Anxiety disorders are among the most prevalent human psychiatric diagnoses, are frequently co-morbid with other disorders, and can be significantly exacerbated by environmental stressors (Wittchen et al., 2002; Lester & Michelson, 2024).

The Problem of Avoidance Learning

The topic of avoidance learning has been extensively studied over the last century with studies and reviews dissecting the complexities inherent to avoidance learning (Bolles, 1972). Threat avoidance was first studied in the context of classical conditioning, with the earliest studies examining conditioned finger withdrawal to shock in humans (Bechterev, 1913; Watson, 1916). By the 1930s, the focus had shifted to instrumental learning and researchers adopted new procedures for behavioral testing, including the shuttle box assay (Warner, 1932; Hunter, 1935; Brogden, Lipman, & Culler, 1938). In the shuttle box assay, the animal is placed in a two-chamber arena and must respond to the presentation of a tone with movement to the opposite

chamber. Failure to shuttle by the end of the presented tone results in the animal receiving a mild shock. Tones are presented at random intervals to prevent the animal from predicting upcoming trials. This task was used to study avoidance across different species (Solomon & Wynne, 1953) and was combined with other paradigms to study the impacts of learning outside of the avoidance context (Kamin et al., 1963; Morris, 1974). Yet, the insights gleaned from studying threat avoidance created more questions than they answered.

One proposed mechanism was reinforcement of avoidance actions by reduction of fear elicited by the conditioned stimulus (Mowrer & Lamoreaux, 1942). This theory brought the escape response into the mechanism of learning–while experiencing shock, the animal makes a variety of responses and whatever stops the effect of the shock (i.e. escape) ends up strongly reinforced. This also proposed a role for fear in acquisition of avoidance; fear would motivate avoidance and reduction of that fear would reinforce it. This led to experiments that would establish the two-factor theory of threat responses as the leading theory. In this framework, threat responses are established through classical conditioning, then avoidance responses are reinforced by the reduction of previously established fear (Mowrer, 1947 and 1950).

However, there are significant shortcomings with two-factor theory. In one experiment involving dogs learning a shuttle box avoidance response, the animals reached peak performance and remained at this high level of performance for long blocks of many trials (Solomon & Wynne, 1953). If fear reduction is motivating avoidance behavior, then why doesn't the avoidance response extinguish when animals avoid hundreds of shocks in a row? The observation that well-trained animals tend to only express fear when delaying the avoidance response clarified that fear was not present on most successful trials.

Attention soon turned away from the explicit mechanisms that guide fear learning to the experimental contingencies that could manipulate learning. Examining the impact of conditioned stimulus (CS) termination and ability to avoid revealed that each factor was approximately equal in importance. Only rats with both contingencies available learned robustly (Kamin, 1956).

However, this was further complicated by the interaction between the demands of each task and the response required to avoid. Ultimately, the contingencies that permitted strong learning in some tasks were ineffective in others (Mogenson, Mullin, & Clark, 1965). For instance, in the shuttle box assay, the avoidance, escape, and CS termination contingencies make equal contributions to performance; in a running wheel avoidance task, only the avoidance contingency has a large effect (Bolles, Stokes, & Younger, 1966).

In several experiments, there were no behavior differences observed between rodents conditioned with avoidable versus unavoidable shock (Schlosberg, 1936; Munn, 1939). Conversely, in other experiments, the avoidance contingency produced markedly better performance over the unavoidable condition (Brogden, Lipman, & Culler, 1938). These contradictions reveal that the nature of the avoidance response matters: if the requirements to avoid do not match with the animal's innate repertoire of threat responses, then avoidance learning does not occur. As an example, rodents and opossums will fail to acquire an avoidance response that requires foot withdrawal (Schlosberg, 1936; Kappauf & Scholsberg, 1937; James, 1937) while similar leg withdrawal procedures have been successful in dogs, pigs, and other animals (Liddell, 1934; Whatmore, Morgan, & Kleitman, 1946). Similarly, rodents will readily learn an avoidance response that requires running, a natural response to threat for those species, but will fail to learn responses like foot flexion, which do not align with their natural response to threat. These data indicate that avoidance responses and the principles that guide their learning cannot be generalized across different assays or species. Instead, the single biggest consideration for successful learning may be how well the specific avoidance response aligns with an animal's species-specific avoidance repertoire.

Animals appear to express a fixed set of innate defensive responses that are specific to each species. One study observed the natural defensive behaviors of goats and observed that they also expressed a variety of those behaviors throughout the process of learning a foot flexion avoidance task (Gibson, 1952). Another study compared two similar avoidance tasks in

rodents, noting that an avoidance response that aligns with a rodent's natural defensive behavior will be learned more quickly and more thoroughly than one that does not (Grossen & Kelley, 1972). This led to the species-specific defense reaction (SSDR) hypothesis, which posits that rodents will readily perform an avoidance response if it requires the use of its innate SSDRs and will not readily perform responses that do not invoke a SSDR (Bolles, 1970; Crawford & Masterson, 1982).

Studies of threat avoidance experienced a boom through the 1960's, but then fell out of fashion due to difficulty resolving contradictory results of various assays and animals with a universal framework that could explain them all (Bolles, 1972; LeDoux et al., 2017). Since the 2000s, studies of threat avoidance have been rising again, perhaps because of the relevance of threat avoidance to human mental health and because of the advent of new technology permitting neurobiological exploration and manipulation of neural circuitry with greater resolution and control.

Platform-mediated Avoidance

Another model of avoidance which has been increasingly utilized is the platform-mediated avoidance (PMA) assay (Grossen & Kelley, 1972; Bravo-Rivera et al., 2014, Diehl et al., 2019). In PMA, an opaque platform covers part of an electrified grid floor, and a series of presented tones all co-terminate with a foot shock. To avoid the foot shock, the animal must access the safety platform before the shock is delivered. Animals first learn the association between tone and shock. Then they learn that the tone-predicted shock can be avoided by accessing the platform before the end of the tone. In other words, animals must learn to preemptively avoid a foot shock by choosing to access the platform when the tone is presented.

In contrast to the shuttle box assay – in which every location can potentially result in a shock – PMA has a location (the platform) for animals to associate with safety. Additionally, in many implementations of the shuttle box, the avoidance response results in early termination of

the conditioned tone. In PMA, animals do not have this level of unrealistic control over predictive cues. These aspects of PMA better model real-world scenarios involving threat avoidance. The PMA assay also offers opportunities to discover a unique set of neurobiological mechanisms, such as the encoding of safe vs. threatening locations, and how entries and exits out of safe locations are modulated by the presence of threat-conditioned stimuli. Using this task, I will examine how the presence of the safety platform shapes the neural responses to avoidance and how the significance of the conditioned tone is modulated by learning.

Neural Circuitry Underlying PMA

Activity within PL circuits is associated with acquisition of PMA. Encoding in PL reflects both fear and context after a single aversive event, regardless of behavioral outcome (Zelikowsky et al., 2014). Inactivation of PL impairs avoidance expression without effects on conditioned freezing behavior (Bravo-Rivera et al., 2014). Expression of the immediate early gene c-Fos – a marker of neuronal activity – in PL positively correlates with avoidance levels, including in cases of excessive avoidance (Bravo-Rivera et al., 2014 and 2015). Similarly, optogenetic and pharmacologic manipulations of PL activity revealed that PL manipulations can bidirectionally influence avoidance expression (Diehl et al., 2018 and 2020). Thus, PL function may be integral to the adaptive performance of threat avoidance.

PL bidirectionally controls threat avoidance behavior through divergent outputs to the basolateral amygdala (BLA) and the ventral striatum (VS), both of which are necessary for avoidance expression (Darvas et al., 2011; Ramirez et al., 2015; Hormigo et al., 2016). Activating PL-BLA projections enhances threat avoidance while activating PL-VS projections reduces avoidance levels (Diehl et al., 2020). Given that there are PL neurons that uniquely project to each region (Gao et al., 2022), these findings suggest that distinct ensembles of neurons enable PL to bidirectionally influence avoidance behavior depending on the situation.

While PL plays a key role in threat avoidance, the emergent PL activity patterns that allow animals to rapidly associate predictive cues with adaptive actions remain poorly understood. Sustained excitatory responses in this region are correlated with fear behavior and likely arise from an integration of synaptic input from relevant brain regions (Burgos-Robles et al., 2009). Local PL interneurons are also important for coordinating fear expression and are responsible for controlling disinhibition and synchrony of PL circuits (Courtin et al., 2014). It has become increasingly apparent that PL uses multiple overlapping encoding mechanisms, with information encoded in both the spike frequency of cells as well as the alignment to local neural oscillations (Dejean et al., 2016).

In line with its complex encoding mechanisms, this region also encodes more abstract representations of threat and safety. Recently, activity in this region has been shown to encode both the overall level of danger and specific representations of potential threats (Martin-Fernandez et al., 2023). In avoidance paradigms, PL activity is important for the expression of avoidance behavior, which may be primarily mediated through inhibitory signaling (Diehl et al., 2018). Though PL populations encode representations of threat, we are only beginning to understand how PL activity links representations of threat-predicting cues with motor programs associated with avoidance (Jercog et al., 2021).

Most studies have focused on the mechanisms that encode freezing behavior during conditioned fear, or on the mechanisms of threat avoidance behavior after learning has occurred, usually following many days of training. But to survive in the wild, animals must rapidly and reliably learn to avoid threats. To understand the mechanisms underlying more naturalistic forms of behavior, we need new studies that examine the evolution of PL activity patterns during rapid acquisition of learned threat avoidance.

High-throughput Analysis of Freely Moving Behaviors

Advances in neural recording technology have made it easier than ever to collect large, detailed datasets of neural activity and simultaneously record freely moving behavior in rodents (Aharoni & Hoogland, 2019; Guo et al., 2023). However, these powerful tools come with new logistical challenges associated with their use. Aligning neural data to behavior is difficult and becomes more complicated when considering freely moving behaviors that are spatially and temporally defined but do not always strictly adhere to a trial structure.

Many software solutions exist to track and analyze rodent behavior; however, each tool is typically designed to fit a particular need (e.g. to mark instances of freezing behavior) and usually reports when the animal behaved, but not where it was located when the behavior occurred. The performance of these tools is also limited by the experimental setup. Visually complex areas (e.g. high contrast bars versus solid flooring) as well as the appearance of the animal (e.g. inclusion of implants and associated wires) can impede accurate scoring of behavior. Lastly, many of these software programs are prohibitively expensive, limiting their access to groups that cannot afford a costly fee or subscription.

Determining the neural correlates of PMA necessitates an integrative analysis of different behaviors at the intersection of spatial (platform) and temporal (tone) features. Free, open-source software for animal pose estimation, such as DeepLabCut, leverage deep learning to allow custom tracking of subjects in a variety of arenas and with invariance to head-mounted hardware and cabling (Mathis et al., 2018). However, these tools do not extend to the classification of behavior and fail to provide a means to account for spatiotemporal variables.

To fill this gap, I set out to develop a new behavioral analysis pipeline that could utilize pose estimation algorithms to integrate flexible behavior classification (of freezing and threat avoidance) with spatiotemporally defined environmental features. Though the early intentions of the software I developed, BehaviorDEPOT, were to create an automated pipeline for analyzing complex rodent behaviors during PMA, interest in additional capabilities led us to expand the

software. I added analysis packages for commonly used behavioral assays including novel object exploration, elevated plus maze, and open field test. To reach the greatest number of users, I built free and easy to use software that is accessible to researchers with little or no coding experience.

An additional benefit of having highly detailed readouts of behavior is the ability to then pair the behavior profiles of animals with simultaneous neural recordings. Analyzing neural data relies on obtaining an accurate account of each behavioral variable to be examined. With the ability to obtain accurate labels for multiple behaviors and intersect them with relevant spatiotemporal information, BehaviorDEPOT enables a deeper understanding of both neural activity and behavior.

I used BehaviorDEPOT's detailed descriptions of behavior to investigate the neural correlates of rapid threat avoidance learning. Detailed descriptions of movement and freezing combined with precisely aligned descriptions of the animal's location in threatening or safe zones allowed extensive investigation into the single cell responses during learning, including functional analyses across time. Because BehaviorDEPOT can easily and automatically identify the intersection between different behaviors and salient task features, it greatly facilitated my investigation of the neural changes that occur as animals learn to avoid signaled threats.

REFERENCES

Aharoni, D., & Hoogland, T. M. (2019). Circuit Investigations With Open-Source Miniaturized Microscopes: Past, Present and Future. Frontiers in Cellular Neuroscience, 13, 141. https://doi.org/10.3389/fncel.2019.00141

Bekhterev, V. M. (1913). La psychologie objective. Librairie F. Alcan.

Bolles, R. C. (1970). Species-specific defense reactions and avoidance learning. Psychological Review, 77(1), 32–48. https://doi.org/10.1037/h0028589

Bolles, R. C. (1972). The Avoidance Learning Problem. In G. H. Bower (Ed.), Psychology of Learning and Motivation (Vol. 6, pp. 97–145). Academic Press. https://doi.org/10.1016/S0079-7421(08)60385-0

Bolles, R. C., & Seelbach, S. E. (1964). Punishing and reinforcing effects of noise onset and termination for different responses. Journal of Comparative and Physiological Psychology, 58(1), 127–131. https://doi.org/10.1037/h0040356

Bolles, R. C., Stokes, L. W., & Younger, M. S. (1966). Does CS termination reinforce avoidance behavior? Journal of Comparative and Physiological Psychology, 62(2), 201–207. https://doi.org/10.1037/h0023678

Bravo-Rivera, C., Roman-Ortiz, C., Brignoni-Perez, E., Sotres-Bayon, F., & Quirk, G. J. (2014). Neural structures mediating expression and extinction of platform-mediated avoidance. The Journal of Neuroscience: The Official Journal of the Society for Neuroscience, 34(29), 9736–9742. https://doi.org/10.1523/JNEUROSCI.0191-14.2014

Bravo-Rivera, C., Roman-Ortiz, C., Montesinos-Cartagena, M., & Quirk, G. J. (2015). Persistent active avoidance correlates with activity in prelimbic cortex and ventral striatum. Frontiers in Behavioral Neuroscience, 9, 184. https://doi.org/10.3389/fnbeh.2015.00184

Brogden, W. J., Lipman, E. A., & Culler, E. (1938). The role of incentive in conditioning and extinction. The American Journal of Psychology, 51, 109–117. https://doi.org/10.2307/1416419

Burgos-Robles, A., Vidal-Gonzalez, I., & Quirk, G. J. (2009). Sustained conditioned responses in prelimbic prefrontal neurons are correlated with fear expression and extinction failure. The Journal of Neuroscience: The Official Journal of the Society for Neuroscience, 29(26), 8474–8482. https://doi.org/10.1523/JNEUROSCI.0378-09.2009

Buxhoeveden, D. P., Semendeferi, K., Buckwalter, J., Schenker, N., Switzer, R., & Courchesne, E. (2006). Reduced minicolumns in the frontal cortex of patients with autism. Neuropathology and Applied Neurobiology, 32(5), 483–491. https://doi.org/10.1111/j.1365-2990.2006.00745.x

Corcoran, K. A., & Quirk, G. J. (2007). Activity in prelimbic cortex is necessary for the expression of learned, but not innate, fears. The Journal of Neuroscience: The Official Journal of the Society for Neuroscience, 27(4), 840–844. https://doi.org/10.1523/JNEUROSCI.5327-06.2007

Courtin, J., Bienvenu, T. C. M., Einarsson, E. Ö., & Herry, C. (2013). Medial prefrontal cortex neuronal circuits in fear behavior. Neuroscience, 240, 219–242. https://doi.org/10.1016/j.neuroscience.2013.03.001

Courtin, J., Chaudun, F., Rozeske, R. R., Karalis, N., Gonzalez-Campo, C., Wurtz, H., Abdi, A., Baufreton, J., Bienvenu, T. C. M., & Herry, C. (2014). Prefrontal parvalbumin interneurons shape neuronal activity to drive fear expression. Nature, 505(7481), 92–96. https://doi.org/10.1038/nature12755

Crawford, M., & Masterson, F. A. (1982). Species-specific defense reactions and avoidance learning. The Pavlovian Journal of Biological Science : Official Journal of the Pavlovian, 17(4), 204–214. https://doi.org/10.1007/BF03001275

Darvas, M., Fadok, J. P., & Palmiter, R. D. (2011). Requirement of dopamine signaling in the amygdala and striatum for learning and maintenance of a conditioned avoidance response. Learning & Memory, 18(3), 136–143. https://doi.org/10.1101/lm.2041211

Dejean, C., Courtin, J., Karalis, N., Chaudun, F., Wurtz, H., Bienvenu, T. C. M., & Herry, C. (2016). Prefrontal neuronal assemblies temporally control fear behaviour. Nature, 535(7612), 420–424. https://doi.org/10.1038/nature18630

DeMartini, J., Patel, G., & Fancher, T. L. (2019). Generalized Anxiety Disorder. Annals of Internal Medicine, 170(7), ITC49–ITC64. https://doi.org/10.7326/AITC201904020

Dickson, J. M., & MacLeod, A. K. (2006). Dysphoric adolescents' causal explanations and expectancies for approach and avoidance goals. Journal of Adolescence, 29(2), 177–191. https://doi.org/10.1016/j.adolescence.2005.03.007

Diehl, M. M., Bravo-Rivera, C., & Quirk, G. J. (2019). The study of active avoidance: A platform for discussion. Neuroscience & Biobehavioral Reviews, 107, 229–237. https://doi.org/10.1016/j.neubiorev.2019.09.010

Diehl, M. M., Bravo-Rivera, C., Rodriguez-Romaguera, J., Pagan-Rivera, P. A., Burgos-Robles, A., Roman-Ortiz, C., & Quirk, G. J. (2018). Active avoidance requires inhibitory signaling in the rodent prelimbic prefrontal cortex. eLife, 7, e34657. https://doi.org/10.7554/eLife.34657

Diehl, M. M., Iravedra-Garcia, J. M., Morán-Sierra, J., Rojas-Bowe, G., Gonzalez-Diaz, F. N., Valentín-Valentín, V. P., & Quirk, G. J. (2020). Divergent projections of the prelimbic cortex bidirectionally regulate active avoidance. eLife, 9, e59281. https://doi.org/10.7554/eLife.59281

Euston, D. R., Gruber, A. J., & McNaughton, B. L. (2012). The role of medial prefrontal cortex in memory and decision making. Neuron, 76(6), 1057–1070. https://doi.org/10.1016/j.neuron.2012.12.002

Gao, L., Liu, S., Gou, L., Hu, Y., Liu, Y., Deng, L., Ma, D., Wang, H., Yang, Q., Chen, Z., Liu, D., Qiu, S., Wang, X., Wang, D., Wang, X., Ren, B., Liu, Q., Chen, T., Shi, X., … Yan, J. (2022). Single-neuron projectome of mouse prefrontal cortex. Nature Neuroscience, 25(4), 515–529. https://doi.org/10.1038/s41593-022-01041-5

Gibson, E. J. (1952). The role of shock in reinforcement. Journal of Comparative and Physiological Psychology, 45(1), 18–30. https://doi.org/10.1037/h0057667

Gillan, C. M., Morein-Zamir, S., Urcelay, G. P., Sule, A., Voon, V., Apergis-Schoute, A. M., Fineberg, N. A., Sahakian, B. J., & Robbins, T. W. (2014). Enhanced avoidance habits in obsessive-compulsive disorder. Biological Psychiatry, 75(8), 631–638. https://doi.org/10.1016/j.biopsych.2013.02.002

Giustino, T. F., & Maren, S. (2015). The Role of the Medial Prefrontal Cortex in the Conditioning and Extinction of Fear. Frontiers in Behavioral Neuroscience, 9, 298. https://doi.org/10.3389/fnbeh.2015.00298

Grossen, N. E., & Kelley, M. J. (1972). Species-specific behavior and acquisition of avoidance behavior in rats. Journal of Comparative and Physiological Psychology, 81(2), 307–310. https://doi.org/10.1037/h0033536

Guo, C., Blair, G. J., Sehgal, M., Sangiuliano Jimka, F. N., Bellafard, A., Silva, A. J., Golshani, P., Basso, M. A., Blair, H. T., & Aharoni, D. (2023). Miniscope-LFOV: A large-field-of-view, single-cell-resolution, miniature microscope for wired and wire-free imaging of neural dynamics in freely behaving animals. Science Advances, 9(16). https://doi.org/10.1126/sciadv.adg3918

Herry, C., & Jercog, D. (2022). Decoding defensive systems. Current Opinion in Neurobiology, 76, 102600. https://doi.org/10.1016/j.conb.2022.102600

Herry, C., & Johansen, J. P. (2014). Encoding of fear learning and memory in distributed neuronal circuits. Nature Neuroscience, 17(12), 1644–1654. https://doi.org/10.1038/nn.3869

Hormigo, S., Vega-Flores, G., & Castro-Alamancos, M. A. (2016). Basal Ganglia Output Controls Active Avoidance Behavior. The Journal of Neuroscience: The Official Journal of the Society for Neuroscience, 36(40), 10274–10284. https://doi.org/10.1523/JNEUROSCI.1842-16.2016

Hunter, W. S. (1935). Conditioning and extinction in the rat. British Journal of Psychology, 26, 135–148.

Ironside, M., Amemori, K.-I., McGrath, C. L., Pedersen, M. L., Kang, M. S., Amemori, S., Frank, M. J., Graybiel, A. M., & Pizzagalli, D. A. (2020). Approach-Avoidance Conflict in Major Depressive Disorder: Congruent Neural Findings in Humans and Nonhuman Primates. Biological Psychiatry, 87(5), 399–408. https://doi.org/10.1016/j.biopsych.2019.08.022

James, W. T. (1937). An experimental study of the defense mechanism in the opossum, with emphasis on natural behavior and its relation to mode of life. The Pedagogical Seminary and Journal of Genetic Psychology, 51, 95–100. https://doi.org/10.1080/08856559.1937.10534306

Jercog, D., Winke, N., Sung, K., Fernandez, M. M., Francioni, C., Rajot, D., Courtin, J., Chaudun, F., Jercog, P. E., Valerio, S., & Herry, C. (2021). Dynamical prefrontal population coding during defensive behaviours. Nature, 595(7869), 690–694. https://doi.org/10.1038/s41586-021-03726-6

Jiao, X., Beck, K. D., Myers, C. E., Servatius, R. J., & Pang, K. C. H. (2015). Altered activity of the medial prefrontal cortex and amygdala during acquisition and extinction of an active avoidance task. Frontiers in Behavioral Neuroscience, 9, 249. https://doi.org/10.3389/fnbeh.2015.00249

Kamin, L. J. (1956). The effects of termination of the CS and avoidance of the US on avoidance learning. Journal of Comparative and Physiological Psychology, 49(4), 420–424. https://doi.org/10.1037/h0088011

Kamin, L. J., Brimer, C. J., & Black, A. H. (1963). Conditioned suppression as a monitor of fear of the CS in the course of avoidance training. Journal of Comparative and Physiological Psychology, 56(3), 497–501. https://doi.org/10.1037/h0047966

Kappauf, W. E., & Schlosberg, H. (1937). Conditioned responses in the white rat. III. Conditioning as a function of the length of the period of delay. The Pedagogical

Seminary and Journal of Genetic Psychology, 50, 27–45. https://doi.org/10.1080/08856559.1937.10534267

Laskowski, C. S., Williams, R. J., Martens, K. M., Gruber, A. J., Fisher, K. G., & Euston, D. R. (2016). The role of the medial prefrontal cortex in updating reward value and avoiding perseveration. Behavioural Brain Research, 306, 52–63. https://doi.org/10.1016/j.bbr.2016.03.007

LeDoux, J. E., Moscarello, J., Sears, R., & Campese, V. (2017). The birth, death and resurrection of avoidance: A reconceptualization of a troubled paradigm. Molecular Psychiatry, 22(1), 24–36. https://doi.org/10.1038/mp.2016.166

Lester, K. J., & Michelson, D. (2024). Perfect storm: Emotionally based school avoidance in the post-COVID-19 pandemic context. BMJ Mental Health, 27(1), e300944. https://doi.org/10.1136/bmjment-2023-300944

Liddell, H. S. (1934). The conditioned reflex. In Comparative psychology (pp. 247–296). Prentice-Hall, Inc. https://doi.org/10.1037/11453-009

Mack, N. R., Bouras, N. N., & Gao, W.-J. (2024). Prefrontal regulation of social behavior and related deficits: Insights from rodent studies. Biological Psychiatry, S0006-3223(24)01146-6. https://doi.org/10.1016/j.biopsych.2024.03.008

Maner, J. K., & Schmidt, N. B. (2006). The role of risk avoidance in anxiety. Behavior Therapy, 37(2), 181–189. https://doi.org/10.1016/j.beth.2005.11.003

Martin-Fernandez, M., Menegolla, A. P., Lopez-Fernandez, G., Winke, N., Jercog, D., Kim, H.-R., Girard, D., Dejean, C., & Herry, C. (2023). Prefrontal circuits encode both general danger and specific threat representations. Nature Neuroscience, 26(12), 2147–2157. https://doi.org/10.1038/s41593-023-01472-8

Mathis, A., Mamidanna, P., Cury, K. M., Abe, T., Murthy, V. N., Mathis, M. W., & Bethge, M. (2018). DeepLabCut: Markerless pose estimation of user-defined body parts with deep

learning. Nature Neuroscience, 21(9), 1281–1289. https://doi.org/10.1038/s41593-018-0209-y

McKlveen, J. M., Myers, B., & Herman, J. P. (2015). The medial prefrontal cortex: Coordinator of autonomic, neuroendocrine and behavioural responses to stress. Journal of Neuroendocrinology, 27(6), 446–456. https://doi.org/10.1111/jne.12272

Mogenson, G. J., Mullin, A. D., & Clark, E. A. (1965). Effects of delayed secondary reinforcement and response requirements on avoidance learning. Canadian Journal of Psychology / Revue Canadienne de Psychologie, 19(1), 61–73. https://doi.org/10.1037/h0082893

Morris, R. G. M. (1974). Pavlovian conditioned inhibition of fear during shuttlebox avoidance behavior. Learning and Motivation, 5(4), 424–447. https://doi.org/10.1016/0023-9690(74)90002-2

Moscarello, J. M., & LeDoux, J. E. (2013). Active avoidance learning requires prefrontal suppression of amygdala-mediated defensive reactions. The Journal of Neuroscience: The Official Journal of the Society for Neuroscience, 33(9), 3815–3823. https://doi.org/10.1523/JNEUROSCI.2596-12.2013

Mowrer, O. H. (1947). On the dual nature of learning—A re-interpretation of “conditioning” and “problem-solving.” Harvard Educational Review, 17, 102–148.

Mowrer, O. H. (1950). Learning theory and personality dynamics: Selected papers (pp. xviii, 776). Ronald Press.

Mowrer, O. H., & Lamoreaux, R. R. (1942). Avoidance conditioning and signal duration—A study of secondary motivation and reward. Psychological Monographs, 54(5), i–34. https://doi.org/10.1037/h0093499

Munn, N. L. (1939). The Relative Effectiveness of Two Conditioning Procedures. The Journal of General Psychology. https://www.tandfonline.com/doi/abs/10.1080/00221309.1939.9710590

Papaleo, F., Yang, F., Garcia, S., Chen, J., Lu, B., Crawley, J., & Weinberger, D. (2012). Dysbindin-1 modulates prefrontal cortical activity and schizophrenia-like behaviors via dopamine/D2 pathways. Molecular Psychiatry, 17(1), 85–98. https://doi.org/10.1038/mp.2010.106

Ragozzino, M. E. (2007). The contribution of the medial prefrontal cortex, orbitofrontal cortex, and dorsomedial striatum to behavioral flexibility. Annals of the New York Academy of Sciences, 1121, 355–375. https://doi.org/10.1196/annals.1401.013

Ramirez, F., Moscarello, J. M., LeDoux, J. E., & Sears, R. M. (2015). Active Avoidance Requires a Serial Basal Amygdala to Nucleus Accumbens Shell Circuit. The Journal of Neuroscience, 35(8), 3470–3477. https://doi.org/10.1523/JNEUROSCI.1331-14.2015

Rozeske, R. R., & Herry, C. (2018). Neuronal coding mechanisms mediating fear behavior. Current Opinion in Neurobiology, 52, 60–64. https://doi.org/10.1016/j.conb.2018.04.017

Schlosberg, H. (1936). Conditioned responses in the white rat: II. Conditioned responses based upon shock to the foreleg. The Pedagogical Seminary and Journal of Genetic Psychology, 49, 107–138. https://doi.org/10.1080/08856559.1936.10533755

Sharpe, M., & Killcross, S. (2015). The prelimbic cortex uses contextual cues to modulate responding towards predictive stimuli during fear renewal. Neurobiology of Learning and Memory, 118, 20–29. https://doi.org/10.1016/j.nlm.2014.11.005

Shin, L. M., & Liberzon, I. (2010). The neurocircuitry of fear, stress, and anxiety disorders. Neuropsychopharmacology: Official Publication of the American College of Neuropsychopharmacology, 35(1), 169–191. https://doi.org/10.1038/npp.2009.83

Solomon, R. L., & Wynne, L. C. (1953). Traumatic avoidance learning: Acquisition in normal dogs. Psychological Monographs: General and Applied, 67(4), 1–19. https://doi.org/10.1037/h0093649

Staples, L. G. (2010). Predator odor avoidance as a rodent model of anxiety: Learning-mediated consequences beyond the initial exposure. Neurobiology of Learning and Memory, 94(4), 435–445. https://doi.org/10.1016/j.nlm.2010.09.009

Stein, M. B., & Stein, D. J. (2008). Social anxiety disorder. Lancet (London, England), 371(9618), 1115–1125. https://doi.org/10.1016/S0140-6736(08)60488-2

Tovote, P., Fadok, J. P., & Lüthi, A. (2015). Neuronal circuits for fear and anxiety. Nature Reviews. Neuroscience, 16(6), 317–331. https://doi.org/10.1038/nrn3945

Warner, L. H. (1932). The association span of the white rat. The Pedagogical Seminary and Journal of Genetic Psychology, 41, 57–90. https://doi.org/10.1080/08856559.1932.9944143

Watson, J. B. (1916). Behavior and the concept of mental disease. Journal of Philosophy, Psychology & Scientific Methods, 13, 589–596. https://doi.org/10.2307/2012555

Whatmore, G. B., Morgan, E. A., & Kleitman, N. (1946). The influence of avoidance conditioning on the course of non-avoidance conditioning in dogs. The American Journal of Physiology, 145, 432–435. https://doi.org/10.1152/ajplegacy.1946.145.3.432

Wittchen, H.-U., Kessler, R. C., Beesdo, K., Krause, P., Höfler, M., & Hoyer, J. (2002). Generalized anxiety and depression in primary care: Prevalence, recognition, and management. The Journal of Clinical Psychiatry, 63 Suppl 8, 24–34.

Xu, P., Chen, A., Li, Y., Xing, X., & Lu, H. (2019). Medial prefrontal cortex in neurological diseases. Physiological Genomics, 51(9), 432–442. https://doi.org/10.1152/physiolgenomics.00006.2019

Zelikowsky, M., Hersman, S., Chawla, M. K., Barnes, C. A., & Fanselow, M. S. (2014). Neuronal Ensembles in Amygdala, Hippocampus, and Prefrontal Cortex Track Differential Components of Contextual Fear. *The Journal of Neuroscience*, *34*(25), 8462–8466. https://doi.org/10.1523/JNEUROSCI.3624-13.2014

Chapter 2: BehaviorDEPOT is a simple, flexible tool for automated behavioral detection based on markerless pose tracking

ABSTRACT

Quantitative descriptions of animal behavior are essential to study the neural substrates of cognitive and emotional processes. Analyses of naturalistic behaviors are often performed by hand or with expensive, inflexible commercial software. Recently, machine learning methods for markerless pose estimation enabled automated tracking of freely moving animals, including in labs with limited coding expertise. However, classifying specific behaviors based on pose data requires additional computational analyses and remains a significant challenge for many groups. We developed BehaviorDEPOT (DEcoding behavior based on POsitional Tracking), a simple, flexible software program that can classify behavior from video timeseries and can analyze the results of experimental assays. BehaviorDEPOT calculates kinematic and postural statistics from keypoint tracking data and creates heuristics that reliably detect behaviors. It requires no programming experience and is applicable to a wide range of behaviors and experimental designs. We provide several hard-coded heuristics. Our freezing detection heuristic achieves above 90% accuracy in videos of mice and rats, including those wearing tethered head-mounts. BehaviorDEPOT also helps researchers develop their own heuristics and incorporate them into the software's graphical interface. Behavioral data is stored framewise for easy alignment with neural data. We demonstrate the immediate utility and flexibility of BehaviorDEPOT using popular assays including fear conditioning, decision making in a T-maze, open field, elevated plus maze, and novel object exploration.

INTRODUCTION

A central goal of neuroscience is to discover relationships between neural activity and behavior. Discrete behaviors represent outward manifestations of cognitive and emotional processes. Popular laboratory assays for memory, decision making, anxiety and novelty exploration typically require examination of behaviors occurring in particular locations in space or instances in time. However, it remains a major challenge to quantify naturalistic behaviors in the laboratory in a rapid, reliable, and spatiotemporally precise manner. In most labs, this work is done manually, a time-consuming process that is rife with inconsistency.

Automated detection of freely moving animal behaviors is faster, expands the parameter space that can be explored, and can eliminate errors associated with manual annotation such as inter-rater inconsistency due to insufficient rater training and rater fatigue. The standardization promised by such methods also enhances the rigor and reproducibility of results across research groups, which is a major concern in behavioral neuroscience. Commercially available software for automated behavior analysis is expensive and the underlying algorithms are hidden which prevents customization or interrogation to determine why a particular result is reported. Moreover, commercially available behavior detectors are prone to failure when animals are wearing head-mounted hardware for manipulating or recording brain activity. As open-source hardware for recording and manipulating neural activity become increasingly available (Luo et al., 2018), more labs are integrating optogenetics, miniscopes, fiber photometry and electrophysiological recordings into their behavioral experiments. This expansion of the research space includes labs without established computational expertise to quantify complex behaviors or align them with precisely timed manipulations or biological signals. Flexible, easy-to-use, open-source software is needed to automate analysis of freely-moving behaviors and facilitate subsequent analyses.

To label behaviors automatically, animals must first be segmented from their environment and tracked through space and time. Previously established methods use

techniques including background subtraction and pattern classifiers to estimate animal positions in video timeseries and then abstract animal movement to a center of mass or an ellipse for analysis (Ohayon et al., 2013; Branson et al., 2009; Noldus et al., 2001; Geuther et al., 2021). After segmentation and tracking, the challenge then is to use data about animal movements to classify discrete behaviors that represent useful information about the cognitive or emotional state of the animal. JAABA (Kabra et al., 2013) uses machine learning to classify behaviors based on the outputs of tracking systems such as MotionTracker (MoTr) (Ohayon et al., 2013) and Ctrax (Branson et al., 2009), which fit ellipses to track animal movements. JAABA requires no coding expertise and has been widely used in the fly community to report complex behaviors including social interactions and various kinds of locomotion. However, only a few rodent studies have employed JAABA (Sangiamo et al., 2020; Neunuebel et al., 2015; Phillips et al., 2019; Nomoto et al., 2015; van den Boom et al., 2017). One limitation is that ellipses cannot resolve the detailed spatiotemporal relationships between individual body parts that characterize many complex behaviors. Moreover, many methods that rely on background subtraction or similar approaches are not robust to environmental complexity and require behavioral assays that can be performed in an empty arena (Geuther et al., 2019).

Newer pose estimation algorithms that are based on machine learning can accurately track individual ‘keypoints’ on an animal’s body (e.g. nose, ears, joints) (Mathis et al., 2018; Pereira et al., 2019; Graving et al., 2019). Keypoint tracking is robust to environmental changes in behavioral arenas and the relationships between the locations of keypoints allow researchers to resolve temporal pose sequences with fine detail. Recently developed open-source software packages such as MARS (Segalin et al., 2021) and SimBA (Nilsson et al., 2020) use supervised machine learning to classify behaviors based on the positions of keypoints on an animals’ body. These methods are excellent solutions for classifying complex behaviors that are challenging for humans to label reliably, including multi-animal social behaviors or self-grooming. However, additional rounds of machine learning are computationally-intensive and require significant

amounts of human-labeled video data. This level of complexity is unnecessary to classify many widely studied behaviors and implementing these approaches may present an insurmountable challenge for labs with limited expertise in coding and machine learning.

Here we describe BehaviorDEPOT, which provides an easy way convert keypoint tracking into meaningful behavioral data in a wide variety of experimental configurations. BehaviorDEPOT not only detects behaviors in video timeseries but can analyze the results of widely used assays such as fear conditioning, open field test, elevated plus maze, novel object exploration, and T-mazes, and can accommodate varied designs including optogenetic manipulations. In these assays, behaviors of interest are typically defined based on criteria set by individual researchers. Definitions often include both the pose of the animal and a physical location in the behavioral arena. For example, in novel object exploration, bouts of exploration are typically defined as times when the animal's head is oriented towards the object and the animal is within 2 centimeters of the object. Keypoint tracking is ideally suited for these types of behaviors because it can track the spatial location of animals while also resolving fine-scale movements.

BehaviorDEPOT detects behaviors using heuristics – simple, efficient rules – that are based on human definitions. These heuristics operate by applying thresholds to metrics calculated from keypoint tracking data (e.g. velocity, angular velocity), and can also incorporate spatial and temporal cues of the experimenters choosing. BehaviorDEPOT heuristics have low error rates and, in contrast to classifiers built through additional rounds machine learning, can be developed based on small amounts of manually annotated video frames and can be easily tweaked to fit out-of-sample videos. Our freezing heuristic has excellent performance even in animals wearing tethered patch cords for optogenetics or Ca2+ imaging, thereby overcoming a major point of failure in commercially available freezing algorithms. BehaviorDEPOT organizes and saves behavioral data in structures that facilitate subsequent analyses, including alignment with neural recordings. It also helps users develop their own heuristics and incorporate them

into the graphical interface. The automated, intuitive, and flexible way in which BehaviorDEPOT quantifies behavior will propel new discoveries by allowing even inexperienced coders to capitalize on the richness of their data.

RESULTS

BehaviorDEPOT comprises six independent modules that form a flexible, multifunctional pipeline that can run experiments, detect behaviors in video timeseries, and analyze behavioral data (Fig. 1). Its graphical interface accommodates users with no prior coding experience. The Analysis Module imports keypoint tracking data, calculates postural and kinematic metrics (e.g. body length, head velocity) and uses these data as the basis of heuristic behavior detectors and analyzes the results of experiments (e.g. report the effects of an optogenetic manipulation during cued fear conditioning). We provide hard-coded heuristics for detecting freezing, jumping, rearing, escape, locomotion, and novel object exploration. We also provide analysis functions for the open field test, elevated plus maze, T-maze, and three chamber assays. The Analysis Module generates rich data structures containing spatial tracking data, postural and kinematic data, behavioral timeseries, and experimental parameters. All data is stored framewise for easy alignment with neural signals. We developed the Experiment Module as a companion to our heuristic for detecting freezing. The Experiment Module can run fear conditioning experiments by using Arduinos to control shockers, arenas, and lasers for optogenetics. Finally, to maximize the utility and flexibility of BehaviorDEPOT, we created the Inter-Rater, Data Exploration, Optimization and Validation Modules to guide users through developing their own heuristics and integrating them into the Analysis Module (Fig. 1). Here we describe how each module works and demonstrate BehaviorDEPOT's utility in fear conditioning, learned avoidance, open field, elevated plus maze, novel object exploration assays and in an effort-based decision task in a T-maze.

The Analysis Module

The main functions of the Analysis Module are to automatically detect behaviors and analyze the results of experiments. The Analysis Module imports videos and accompanying keypoint tracking data and smooths the tracking data. It can accommodate previously recorded videos since keypoint tracking models can be trained posthoc. Users can track any keypoints they choose. We used DeepLabCut (DLC) (Matthis et al., 2018) for keypoint tracking, which produces a list of comma-separated values that contains framewise estimates of the X-Y coordinates for designated body parts as well as a likelihood statistic for each estimated point. The Analysis Module applies a threshold based on DLC likelihood and performs a Hampel transformation (Hampel et al., 1974) to remove outliers. Then, a LOWESS, local regression smoothing method is applied to the data (Cleveland et al., 1981), and sub-threshold tracking values are estimated using surrounding data and spline interpolation (Fig. 2A). The module then performs a feature expansion step, calculating additional keypoint positions based on the originally tracked set (Supplementary File 1). We designed a set of postural and kinematic metrics that are calculated automatically for each keypoint (Supplementary File 2). These metrics serve as the inputs for BehaviorDEPOT's heuristics.

We created a set of heuristics to detect several human-defined behaviors including freezing, rearing, escape, locomotion, and novel object investigation. From the graphical interface of the Analysis Module, users can select a heuristic and indicate if they want to analyze behaviors during particular time windows or within regions of interest (ROI) and whether they plan to do batched analyses. The Analysis Module also includes spatial functions for analyzing the open field test, elevated plus maze, T-maze and three chamber assays. By allowing users to perform integrated spatial-temporal-behavioral analyses, BehaviorDEPOT's utility extends beyond existing open-source behavioral classification software, which typically just report which behaviors occur in each video frame. Later in the manuscript, we describe how users can create their own heuristics and incorporate them into the graphical interface.

The Analysis Module exports all relevant data in a set of MATLAB structures (Supplementary File 3) so that users can easily perform additional analyses if needs arise (Fig. 2A). For instance, users may want to align the data to neural signals, a process we discuss in upcoming sections. A structure called ‘Tracking’ stores raw and smoothed keypoint tracking data. ‘Params’ stores the parameters of video recordings, smoothing functions, heuristics used and arena metrics (e.g., ROI size and location). ‘Metrics’ stores kinematic and postural statistics calculated from keypoint positions (Supplementary File 2). ‘Behavior’ stores bout-wise and vectorized representations of identified behaviors across the entire video, or with respect to user-defined spatiotemporal filters.

The Analysis Module also generates a series of graphical data representations (Supplementary File 3). For instance, trajectory maps show when an animal was in a particular location and where behaviors occurred. Bout maps indicate when behaviors occurred and for how long. These visual representations help users understand behavioral phenotypes in great spatiotemporal detail and can inform further custom analyses using the data structures that the Analysis Module generates. In the following sections, we describe the development and validation of BehaviorDEPOT’s heuristics and demonstrate its utility in numerous behavioral assays.

Development and Validation of the BehaviorDEPOT Freezing Detection Heuristics

Freezing behavior, defined as the absence of movement except for respiration (Grossen et al., 1972; Fanselow et al., 1979; Fanselow et al., 1984), is widely studied as a proxy for both learned and innate fear (Anagnostaras et al., 1999; Anagnostaras et al., 2010; Perusini, J.N. & Fanselow, M.S., 2015). In many laboratory assays, rodents freeze in response to perceived environmental threats including conditioned cues, predator odor, or looming disks that mimic a predator approaching from above (Perusini, J.N. & Fanselow, M.S., 2015). Despite the heavy study of freezing behavior, most labs still score freezing manually or using expensive

commercially available software programs that often fail when animals have tethered headmounts. Here we describe the development and validation of the BehaviorDEPOT freezing detection heuristic and demonstrate its accurate performance across a range of experimental setups, including in mice wearing head-mounts for optogenetics and miniscopes.

The BehaviorDEPOT freezing detection heuristic combines a convolution-based smoothing operation with a low-pass velocity filter and then applies a minimum duration threshold to identify periods of freezing. To develop the freezing heuristic, we began by training a deep neural network in DLC on videos recorded with a high resolution and high frame-rate camera (Chameleon3 USB3, FLIR) at 50 frames per second (fps). The network tracks 8 points on the body and smooths the raw tracking data (Fig. 2B,C). An expert rater annotated freezing in 3 randomly selected videos (27,000 total frames). This served as a reference set for heuristic development. We reasoned that freezing could be reliably detected based on periods of low keypoint velocity. After exploring the predictive value of different keypoints using the Data Exploration Module (described below), we determined that thresholding the velocity of a midpoint on the back and the angular velocity of the head produced the most accurate freezing detection heuristic (Fig. 2D). We smoothed the heuristic output by applying a sliding window to produce a convolved freezing vector in which each value represented the number of freezing frames visible when the window is centered at a given frame. We then applied an adjustable count threshold to convert the convolved freezing vector into the final binary freezing vector (Fig. 2E).

To validate heuristic performance, we manually annotated a different, randomly selected set of videos that were never referenced while setting the parameters (Supplementary File 4). These videos were recorded in several different behavioral chambers under varied lighting conditions. BehaviorDEPOT freezing detection was highly consistent with human annotations (Fig. 2F). Accuracy of the freezing heuristic was estimated based on precision, recall, F1 and specificity. Precision and recall quantify the positive predictive value against the tendency to

produce false positive or false negative errors, respectively. The F1 score, the harmonic mean of the precision and recall, is useful as a summary statistic of overall performance. Specificity quantifies the ability to accurately label true negative values and helps ensure that the heuristic is capturing data from only a single annotated behavior. Our heuristic had very low error rates (Fig. 2F).

We also assessed how good the DLC tracking needed to be for the freezing heuristic to work well. We trained ten different DLC networks with mean tracking errors ranging from 1–8 pixels. We used each network to analyze a set of six videos and then used BehaviorDEPOT to automatically detect freezing in each video. A linear regression analysis revealed that tracking error had a significant effect on precision and on the F1 score without effecting recall or specificity (Fig. 2-figure supplement 1; Supplementary File 5), with tracking errors <4 pixels producing the highest F1 scores in our analysis.

To ensure that our heuristic would generalize to other camera types and DLC networks, we trained a second network based on videos recorded with a standard webcam at 30fps. On the webcam, lower sensor quality and lower frame rate produces more blur in the recorded images, so we tracked 4 body parts that are easy to see (nose, ears, tail base; Fig. 2G). When compared to human annotations (Supplementary File 4), the webcam videos also scored highly for precision, recall, F1 and specificity (Fig. 2G), indicating that our freezing heuristic can indeed generalize across camera types and DLC networks.

Since the same rules may not necessarily generalize to all settings, we developed a second freezing heuristic that uses a changepoint function to find frames at which the mean velocity changes most significantly and then separates frames into groups that minimize the sum of the residual error from the local mean. Binarized freezing vectors are then processed using a convolution algorithm and minimum duration threshold (Fig. 2E). This heuristic was also highly accurate, performing similarly to the velocity-based heuristic on videos recorded with a webcam (Fig. 2– figure supplement 2). Users can tune the heuristic by adjusting a minimum

residual threshold for the changepoint function. We termed this the ‘jitter’ heuristic since the minimum residual threshold will be determined by the pixel error in keypoint position estimates. In other words, the threshold will be determined by how much frame-to-frame ‘jitter’ there is in DLC’s estimate of the keypoint location. Keypoint tracking ‘jitter’ may arise as a function of video resolution, framerate, and number of frames used to train a keypoint tracking model. As such, the ‘jitter’ heuristic may accommodate a wider range of video qualities and keypoint tracking models. Also, in videos recorded from the side, the velocity-based freezing heuristic may be slightly affected by distortions in velocity calculations caused by the angle (e.g. when the mouse is moving towards/away from the camera).

The Experiment Module

As a companion to the heuristic for freezing, we also developed the ‘Experiment Module’, a MATLAB app that allows users to design and run fear conditioning experiments. This extends the utility of BehaviorDEPOT by providing a fully open-source software pipeline that takes users from data collection to data analysis. The Experiment Module controls commercially available shockers, lasers for optogenetics and sound generators via a set of Arduinos (Fig. 1–figure supplement 1). Users can download the ‘Fear Conditioning Experiment Designer’ app from our Github repository and install it with a single button click. From a graphical interface, users can design experimental protocols for contextual or cued fear conditioning, with or without optogenetics. All experimental parameters (e.g. timestamps for laser, tones, shocks) are saved in MATLAB structures that can be referenced by the BehaviorDEPOT analysis pipeline (Fig. 1).

Use Case 1: Optogenetics

In commercial freezing detection software, algorithms often fail when a rodent is wearing a patch cord for routine optogenetics experiments. To ensure that BehaviorDEPOT’s freezing heuristic maintains high levels of accuracy under these conditions, we tested its performance in

an optogenetics experiment. mPFC plays a well-established role in fear memory retrieval (Corcoran et al., 2007; Ledoux, J.E., 2000), extinction (Giustino, T.F. & Maren, S., 2015), and generalization (Giustino, T.F. & Maren, S., 2015; Xu et al., 2013; Pollack et al., 2018). While silencing mPFC subregions can promote fear memory generalization in remote memory (Xu et al., 2013; Frankland et al. 2004), less is known about its role in recent memory generalization. We used an adeno-associated virus (AAV) to express the soma-targeted neuronal silencer stGtACR2 (Mahn et al., 2018) bilaterally in the mPFC and implanted optogenetic cannula directly above the AAV injection sites (Fig. 3A, Fig. 3–figure supplement 1). We performed contextual fear conditioning (CFC) in context A. The next day, we measured freezing levels in the conditioned context (context A) as well as a novel context (context B) that was never paired with shocks. During these retrieval sessions, two-minute laser-on periods were separated by two minute laser-off intervals (Fig. 3B).

We first tested the accuracy of the freezing heuristic for animals wearing tethered head mounts. We trained an optogenetics-specific DLC network that tracks 9 points on the animal, including the fiber-optic cannula (Fig. 3C). Our rationale for creating a separate keypoint tracking network was two-fold. First, while you can train one ‘master’ DLC network that can track mice in many different arenas, we find that DLC tracking errors are lowest when you have dedicated networks for particular camera heights, arenas, and types of head-mounted hardware. DLC networks are easy to train and to make it even easier for new users, we provide links to download our DLC models in our GitHub repository (https://github.com/DeNardoLab/BehaviorDEPOT/wiki/Pretrained-DLC-Models). Second, this was another opportunity to test how well the BehaviorDEPOT freezing heuristic generalizes to a different DLC network with a different number of keypoints. For a randomly selected set of videos with different floors and lighting conditions, we compared heuristic performance to expert human raters (Supplementary File 4). Even with the patch cord attached, the freezing heuristic had excellent scores for precision, recall, F1 and specificity (Fig. 3D).

Having confirmed the accuracy of the freezing heuristic, we then used BehaviorDEPOT to quantify freezing behavior and compared the results to the annotations of an expert human rater. As expected, fear conditioned mice readily froze following shocks during CFC, while non-shocked controls did not (Fig. 3E). During retrieval sessions, silencing mPFC in previously shocked animals significantly enhanced freezing in the novel context but did not affect freezing in the fear conditioned context (Fig. 3F,G). mPFC silencing thereby produced a significant decrease in the discrimination index in fear conditioned mice (Fig. 3H), indicating that mPFC plays a key role in the specificity of recent fear memories. In all analyses, BehaviorDEPOT freezing estimates were comparable to a highly trained human rater (Fig. 3F–H). By maintaining performance levels even in videos with visual distractors like a patch cord, the BehaviorDEPOT freezing heuristic overcomes a major point of failure in commercially available freezing detection software.

Use Case 2: Ca2+ imaging with miniscopes during signaled avoidance

As new open-source tools for neurophysiology become available, more labs are performing simultaneous neurophysiological and behavioral recordings. Miniature head-mounted microscopes now allow us to image the activity of hundreds of neurons simultaneously in freely moving animals (Ghosh et al., 2011; Cai et al., 2016; Shuman et al. 2020). These miniscopes pair with genetically encoded Ca2+ indicators (Dana et al., 2019) that can be targeted to specific neuronal populations and GRIN lenses (Barretto et al., 2009) that can be targeted to many regions in the brain. With these tools in hand, we can discover how the encoding of complex cognitive and emotional behaviors maps onto specific cell types across the brain. By recording the activity of hundreds of neurons simultaneously, we can also study the population codes that produce complex behaviors (Jercog et al., 2021; Stout et al. 2020). To do so, however, we need improved open-source methods that allow us to quantify freely moving

behaviors with reference to salient environmental stimuli and to align these detailed behavioral measurements with neurophysiological recordings.

Here we demonstrate the utility of BehaviorDEPOT for aligning behavioral measurements with Ca2+ signals during a platform mediated avoidance (PMA) task that has temporally and spatially salient features. PMA (Grossen & Kelley, 1972; Bravo-Rivera et al., 2015) is an mPFC-dependent task in which a fear conditioned tone prompts mice to move to a safety platform that protects them from receiving a footshock (Diehl et al. 2020). We recorded the activity of hundreds of mPFC neurons in freely behaving animals using head-mounted microendoscopes (UCLA Miniscopes: Cai et al., 2016; Shuman et al., 2019) while simultaneously recording behavior using a new open-source USB camera, the UCLA MiniCAM.

Together with BehaviorDEPOT and the UCLA miniscopes, the MiniCAM provides a fully open-source data acquisition and analysis pipeline for in vivo Ca2+ imaging during freely moving behavior. The MiniCAM is an open-source behavioral imaging platform that natively integrates and synchronizes with open-source UCLA miniscope hardware and software (Fig. 4A). It is composed of an M12 optical lens mount, a custom printed circuit board housing a CMOS image senor and supporting electronics, an LED illumination ring, and a 3D printed case. The MiniCAM is powered and communicates over a single coaxial cable that can be up to 15 meters long. The coaxial cable connects to a miniscope data acquisition board (DAQ) which then connects over USB3 to a host computer. A range of commercial M12 lenses can be used to select the view angle of the camera system. The image sensor used is a 5MP CMOS image sensor (MT9P031I12STM-DP, ON Semiconductor) with 2592 x 1944 pixel resolution and a full resolution frame rate of approximately 14FPS. For this application, the MiniCAM's pixels were binned and cropped to achieve 1024x768 pixels at approximately 50FPS. The optional LED illumination ring uses 16 adjustable red LEDs (LTST-C190KRKT, Lite-On Inc., 639nm peak wavelength) for illumination in dark environments (Fig. 4A). We trained a separate DLC network for videos of animals wearing miniscopes recorded with MiniCAMs. Our network tracked 9

keypoints on the body (ears, nose, midback, hips, tailbase, and tail) and the miniscope itself (Fig. 4B). For these videos, BehaviorDEPOT freezing ratings were highly consistent with expert human annotations (Fig. 4C).

We used BehaviorDEPOT to analyze behavior during PMA so we could align it to the underlying neural activity. In this task, animals are placed in a fear conditioning chamber in which an acrylic safety platform occupies 25% of the electrified grid floor. Three baseline tones are followed by nine tones that co-terminate with a mild foot shock. The following day, we measure avoidance and freezing behaviors during six unreinforced tones (Fig. 4D). The Analysis Module automatically produces trajectory maps that make it quick and easy to assess the spatiotemporal characteristics of rodent behavior. In our representative example, the color-coded trajectory and freezing locations (denoted as black squares) converge on the platform at the end of the session, indicating the mouse indeed learned to avoid shocks by entering the platform (Fig. 4E). We used BehaviorDEPOT to produce summary data, showing that mice readily learned the cue-avoidance association during training (Fig. 4F) and remembered it the next day (Fig. 4G).

During a retrieval session, we recorded neural activity using a UCLA miniscope and behavior using a UCLA MiniCAM (Fig. 4H). Using MIN1PIPE43, we extracted and processed neural signals from 513 mPFC neurons across 3 mice. We then determined whether individual neurons encoded specific behaviors that we had quantified using BehaviorDEPOT (Fig. 4I). We computed a receiver operating characteristic (ROC) curve that measures a neuron's stimulus detection strength over a range of thresholds (Fig. 4J). We identified numerous neurons that were modulated by freezing and avoidance on the safety platform. These neurons were organized in a salt and pepper manner in mPFC (Fig. 4K). Nearly half of all neurons that exhibited task relevant behavior and were specific for either freezing or threat avoidance, or their combination (Fig. 4L). These experiments demonstrate that the BehaviorDEPOT heuristic for detecting freezing is robust across a wide variety of experimental setups with different

camera types, keypoint tracking networks, arenas and headmounts. Further, this suite of open-source hardware and software will enable a broader user base to combine Ca2+ imaging with high resolution behavioral analysis.

Use Cases 3–6: Open Field, Elevated Plus Maze, Novel Object Exploration, and Decision-Making

BehaviorDEPOT also supports behavioral analyses beyond the realm of conditioned fear. In a number of commonly used assays, behaviors are defined based on animal location or the intersection of location and specific movements (e.g. head turns in a choice zone, described below). Such assays, including elevated plus maze (EPM), open field test (OFT), novel object exploration (NOE), object location memory, social preference/memory, decision making assays (T-maze), and working memory assays (Y-mazes), examine a broad swath of cognitive and emotional processes including anxiety, memory and decision making and are published in tens of thousands of studies each year. To extend the utility of BehaviorDEPOT to this broad user base, the Analysis Module includes functions that quantify time spent in user defined ROIs. We demonstrate the utility of these functions in four representative assays, EPM, OFT, NOE and a T-maze. However, the same functions could be used to analyze numerous assays including Y-mazes, real-time or conditioned place preference, as well as social preference and social memory tests.

Elevated Plus Maze, Open Field Test, and Novel Objection Exploration

EPM and OFT are used to measure anxiety-related behaviors in the laboratory (La-Vu et al., 2020), but these assays are often scored manually or with expensive software such as Ethovision (Noldus et al., 2001). In the EPM, rodents navigate through an elevated (~1 foot off the ground) plus-shaped maze consisting of two open arms without walls and two enclosed arms with walls. Animals that spend more time in the closed arms are interpreted to have higher

anxiety (La-Vu et al., 2020). In the OFT, rodents are placed in an empty arena without a ceiling for 10–15 minutes. Experimenters measure the fraction of time spent in the perimeter of the box vs. the center. Increased time in the perimeter zone is interpreted as higher anxiety. OFT is also commonly used to measure locomotion in rodents. We trained a DLC network to track animals in an EPM or OFT. We used the BehaviorDEPOT functions to indicate the closed arms, open arms, and center zone for EPM (Fig. 5A) and the center zone for OFT (Fig. 5B). BehaviorDEPOT uses the midback keypoint to track the animal as it traverses the zones, reporting time spent in each zone. BehaviorDEPOT annotations were highly consistent with an expert human rater (Fig. 5D).

NOE assays can be used to assess exploration and novelty preference (Ennaceur et al., 1988; Leger et al., 2013; Vogel-Ciernia, A. & Wood. M.A., 2014; Zeidler et al., 2020). An object is placed in the center of an open field and investigation time is measured. NOE is typically defined as instances when the animal's head is within 2 centimeters (cm) of the object and oriented towards the object (Leger et al., 2013; Vogel-Ciernia, A. & Wood. M.A., 2014). After importing DLC tracking data, BehaviorDEPOT allows users to draw an ROI at a set radius around the object (Fig. 5C). The NOE heuristic uses a combination of head angle and distance with respect to the ROI to label 'investigation' frames. BehaviorDEPOT quantified NOE at levels that were highly consistent with expert human raters (Fig. 5F).

Automated Quantification of Decision-Making Behaviors

Decision making is a widely studied area of neuroscience. Many labs study contingency-based, cost-benefit decision-making in mazes that involve choice points. For example, effort-based decision-making involves weighing whether it is worth exerting greater effort for a more valuable outcome. A common rodent assay for effort-based decision-making is the barrier T-maze task in which animals choose whether to climb over a barrier for a large reward (high effort, high value reward; HE/HVR) vs. taking an unimpeded path for a smaller reward (low

effort, low value reward; LE/LVR) (Bailey et al., 2016). Well trained animals typically prefer HE/HVR choices, taking a direct route over the barrier with stereotyped trajectories. However, when reward or effort contingencies are adjusted animals demonstrate vicarious trial and error (VTE), thought to be a marker of deliberative (rather than habitual) decision-making. During VTE trials, animals may pause, look back-and-forth, or reverse an initial choice50. Several groups have identified neural signatures of VTE in hippocampus, striatum, and prefrontal cortex suggesting that animals may be playing out potential choices (i.e. vicariously) based on an internal model of maze contingencies (Redish et al., 2016). Simple, flexible, and automated analysis tools for detecting VTE and aligning this behavior with neural data would significantly enhance our understanding of deliberative decision-making.

We used BehaviorDEPOT to automatically detect VTE in a barrier T-maze task and to report the ultimate choice animals made during each effort-based decision-making trial. First, we trained a new DLC network to track mice as they navigated the T-maze. In one version of the task, mice decided whether to turn left to collect a small reward or to turn right and climb a wire mesh barrier for a large reward. We then changed the effort contingency by adding a second barrier to equalize effort across choices. We used the BehaviorDEPOT Analysis Module to perform automated analysis of the task. We defined 8 regions of interest (Approach, Choice, Left Effort, Left Reward, Left Food Cup, Right Effort, Right Reward, and Right Food Cup, Fig. 6A). We then used the stored tracking data to automatically detect trials, which we defined as the first frame when the animal entered the approach zone until the first frame when the animal entered the reward zone, and to report the outcome of each trial (left choice or right choice) (Fig. 6B–D).

To develop a VTE heuristic, we used the head angle data stored in the BehaviorDEPOT ‘Metrics’ data structure. For each trial, we analyzed the head angles when the mouse was in the choice zone and used these values to determine the number of head turns per trial. Manually annotated VTE trials tended to have 1 or more head turns, while non-VTE trials tended to have

0 head turns, so we defined VTE trials as having 1 or more head turns in the choice zone (Fig. 6E). We then used our BehaviorDEPOT VTE heuristic to detect the fraction of trials with VTE in T-maze sessions with 1 vs. 2 barriers, finding a significant increase in the occurrence of VTE trials when a second barrier was added. Importantly, the BehaviorDEPOT performance was highly consistent with a human rater (Fig. 6F).

Together, these analyses showcase the many functions of the Analysis Module and highlight the utility of the repository of postural and kinematic statistics that is automatically generated in BehaviorDEPOT. By calculating and storing information including velocity, angular velocity, head angle, and acceleration in a framewise manner, BehaviorDEPOT allows users to design automated analysis pipelines for a wide range of commonly studied cognitive tasks. Indeed, BehaviorDEPOT can be tailored to meet individual needs. In the following sections, we describe additional modules that help users develop custom heuristics and integrate them into the Analysis Module.

Developing and Optimizing Heuristics for Behavior Detection

To broaden the utility of BehaviorDEPOT, we created four additional modules that guide users through the process of developing their own heuristics. The Inter-Rater, Data Exploration, Optimization and Validation modules help researchers identify and validate the combinations of metrics that track best with their behaviors of interest. Reference annotations can come from human raters or other heuristics software.

The Inter-Rater Module

A major hurdle in developing classifiers or heuristics using supervised approaches is settling on a ground truth definition of the behavior of interest. The Inter-Rater Module compares annotations from multiple human raters and identified points of overlap and disagreement (Fig. 7A). In response to the initial output of the Inter-Rater Module, human raters can discuss the

points of disagreement and modify their manual ratings until they converge maximally. The resulting ‘ground truth’ definitions of behavior can be used to benchmark the performance of newly developed heuristics or to optimize existing ones.

Here we demonstrate the outputs of the Inter-Rater module using freezing and novel object exploration as examples. This module imports multiple human annotations and users can select a reference dataset (e.g. the most highly trained expert rater, Fig. 7B_1,C_1). The module compares each set of annotations to the reference, scoring the annotations frame-by-frame as true positive, true negative, false positive, or false negative for each rater. These values are first used to calculate percent overlap and percent error between all raters. Precision, recall, specificity, and F1 score are calculated and reported for each rater relative to the chosen reference (Fig. 7B_2,C_2). Additionally, visualizations of frame-by-frame percent agreement (Fig. 7B_3,C_3) and user-by-user disagreement (Fig. 7B_4,C_4) are automatically generated to assist identifying areas of conflict between users. The automated features of the Inter-Rater Module make it fast and easy to perform iterative comparisons of manual annotations, interleaved with human updates, until a satisfactory level of agreement is achieved. The Inter-Rater Module can function as an independent unit and can thus support heuristic development with any application.

The Data Exploration Module

For users who want to develop new heuristics, the Data Exploration Module helps to identify combinations of keypoint metrics that have high predictive value for behaviors of interest. Users can choose between two different exploration modes: broad or focused. In focused mode, researchers use their intuition about behaviors to select the metrics to examine. The user chooses two metrics at a time and the Data Exploration Module compares values between frames where behavior is present or absent and provides summary data. A generalized linear model (GLM) also estimates the likelihood that the behavior is present in a

frame across a range of threshold values for the two selected metrics (Fig. 8A), allowing users to optimize parameters in combination. Focused mode is fast and easy to use and users can iteratively test as many combinations of metrics as they like.

In broad mode, the module uses all available keypoint metrics to generate a GLM that can predict behavior as well as a rank-order list of metrics based on their predictive weights. Poorly predictive metrics are removed from the model if their weight is sufficiently small. Users also have the option to manually remove individual metrics from the model. Once suitable metrics and thresholds have been identified using either mode, users can plug any number and combination of metrics into a heuristics template script that we provide and incorporate their new heuristics into the Analysis Module. Detailed instructions for integrating new heuristics are available in our GitHub repository (https://github.com/DeNardoLab/BehaviorDEPOT/wiki/Customizing-BehaviorDEPOT).

We used focused mode to create our freezing heuristic. First, the Data Exploration Module imports the ‘Metrics’ and ‘Behavior’ data structures we produced using the Analysis Module along with reference annotations for the same videos. We used the annotations of an expert human rater for reference. In focused mode, users iteratively select combinations of two keypoint metrics (e.g., head velocity, tail angular velocity, etc.) and a behavior label from the human annotations file (e.g. ‘Freezing’). We reasoned that low velocity of certain bodyparts would correlate with freezing and thus examined the predictive value of several keypoint velocities. The module creates two data distributions: one containing video frames labeled with the chosen behavior and a second containing the remaining video frames. The larger set is randomly downsampled to ensure that each distribution contains equal numbers of frames and then a series of analyses quantify how reliably chosen metrics align with the behavior of interest. Boxplots (Fig. 8B) and histograms (Fig. 8C) identify features that reliably segregate with frames containing a behavior of interest. Indeed, we discovered that the linear velocity of

the back and angular velocity of the head tracked particularly well with freezing (Fig. 8B,C). The GLM revealed the combinations of threshold values that best predicted freezing (Fig. 8D).

In general, we found that metrics that are well-suited for behavior detection contrast with metrics on frames that do not contain the behavior and have a low standard deviation within the behavior set. Distributions of useful metrics also tend to differ substantially from the total set of frames, especially when compared to frames that do not contain the behavior. The GLM predictions are useful for determining which of the selected metrics best predict the behavior and whether they enhance the predictive value when combined. This module will broaden the utility of BehaviorDEPOT, allowing researchers to tailor its automated functions to fit their needs.

The Optimization Module

A major advantage of using heuristics to detect behaviors is that parameters can be quickly and easily tuned to optimize behavioral detection in out-of-sample data. Some users of the Optimization Module may have just developed a new heuristic in the Data Exploration Module. Others may want to optimize an existing heuristic for their experimental setup since camera position, framerate and resolution and lighting conditions may influence behavior detection thresholds. To use the module, researchers provide reference annotations and the outputs from the Analysis Module (‘Params’, ‘Behavior’ and ‘Metrics’). By sweeping through the parameter space for chosen metrics, the Optimization Module identifies the set of thresholds that maximize detection accuracy (Fig. 9A). Through the graphical interface, users can then update the heuristic threshold values and save the settings for future use. Commercially available freezing classifiers also allow users to adjust the thresholds for freezing detection to ensure that accurate classification can be achieved in a variety of experimental conditions. However, their algorithms are hidden and there is no way to precisely measure error rates. Our

Optimization Module adds a level of rigor to the optimization step by reporting heuristic performance as F1, precision, recall and specificity values.

We used the Optimization Module to tune our freezing heuristic for videos recorded in other laboratories. Two research groups provided videos of rats and mice, respectively, recorded using their own acquisition hardware and software. For each dataset, we trained keypoint tracking networks (Fig. 9$B_{1,2}$) and manually annotated freezing in a subset of the videos. We then analyzed behavior using the Analysis Module with the default settings of our freezing heuristic. Using the 'Parameters', 'Behavior', and 'Metrics' files produced by the Analysis Module, the Optimization Module iteratively swept through a range of threshold values for the four metrics that define the freezing heuristic: back velocity, head angular velocity (Fig. 9$C_{1,2}$), window width and count threshold in the convolution algorithm and reports performance for different combinations of values (Fig. 9$D_{1,2}$).

The Validation Module

The Validation Module can assess a heuristic's predictive quality by comparing automated behavioral detection to human annotations. The user must first generate a reference set of annotations (either manual or otherwise) and analyze the video using the heuristic of interest in the Analysis Module. In the validation module, the user is prompted to indicate which heuristic to evaluate and select a directory containing behavior videos and the output files from the Analysis Module (Metrics, Behavior, etc). For each video, the module will categorize each frame as true positive, false positive, true negative, or false negative, using the human data as a reference. Precision, recall, specificity, and F1 score are then calculated and visualized for each video. These statistics are also reported for the total video set by concatenating all data and recalculating performance (Fig. 9E). We validated the performance of the BehaviorDEPOT freezing heuristic on the rat (Fig. 9F) and mouse (Fig. 9G) videos acquired in external laboratories which we had optimized using the Optimization Module. In both cases, the optimal

combination of thresholds for (Fig. 9C,D) each video set achieved high F1 scores (>0.9), indicating that our chosen features for freezing detection are robust across a range of camera, keypoint tracking networks, experimental conditions, and rodent species.

Comparison of BehaviorDEPOT and JAABA

Finally, we benchmarked BehaviorDEPOT's performance against JAABA (Kabra et al., 2013). Like BehaviorDEPOT, JAABA is geared toward a non-coding audience, and its classifiers are based on an intuitive understanding of what defines behaviors. JAABA uses supervised machine learning to detect behaviors and has been widely adopted by the drosophila community with great success. However, fewer studies have used JAABA to study rodents, suggesting there may be some challenges associated with using JAABA for rodent behavioral assays. The rodent studies that used JAABA typically examined social behaviors or gross locomotion, usually in an open field or homecage (Sangiomo et al., 2020; Neunuebel et al., 2015; Phillips et al., 2019; Nomoto et al., 2015; van der Boom et al., 2017).

As the basis for its classifiers, JAABA uses a large feature set that it calculates based on animal poses. JAABA is built around trackers like MoTr (Ohayon et al., 2013) and Ctrax (Branson et al., 2009), which model animal position and orientation by fitting ellipses. We used MoTr and Ctrax to track animals in fear conditioning videos we had recorded previously. The segmentation algorithms performed poorly when rodents were in fear conditioning chambers which have high contrast bars on the floor but could fit ellipses to mice in an open field, in which the mouse is small relative to the environment and runs against a clean white background (Fig. 10A–B). Poor tracking in visually complex environments such as a fear conditioning chamber may explain, at least in part, why relatively few rodent studies have employed JAABA.

To circumvent these issues, we fit ellipses to the mice based on DLC keypoints (Fig. 10C). Briefly, we used the nose-to-tail distance to calculate the long axis and the hip-to-hip distance to calculate the short axis and used a MATLAB function to generate well-fit ellipses for

each video frame. We then imported the ellipse features (animal position (centroid), semi-axis lengths, and orientation) into JAABA. We first trained a freezing classifier using JAABA. Even when we gave JAABA more training data than we used to develop BehaviorDEPOT heuristics (6 videos vs. 3 videos), the BehaviorDEPOT heuristic for freezing had significantly higher recall and F1 scores when tested on a separate set of videos (Fig. 10D). We also trained a VTE classifier with JAABA. When we tested its performance on a separate set of videos, JAABA could not distinguish VTE vs. non-VTE trials. It labeled every trial as containing VTE (Fig. 10E), suggesting a well-fit ellipse is not sufficient to detect these fine angular head movements.

Another strength of BehaviorDEPOT relative to JAABA is that BehaviorDEPOT can quantify behaviors with reference to spatial or temporal cues of interest. JAABA does allow users to draw spatial ROIs but uses this information as the basis of behavioral classification in ways that cannot be detected or controlled by the user. These direct comparisons highlight the need for new behavioral analysis software targeted towards a noncoding audience, particularly in the rodent domain. BehaviorDEPOT can now fill this role.

DISCUSSION

Keypoint tracking algorithms and in vivo methods including optogenetics, fiber photometry, and miniscope recordings have become increasingly accessible and widely adopted. Because many labs with limited programming expertise want to employ these methods, we need user-friendly software programs that can automate analysis of naturalistic behaviors and facilitate precise alignment of neural and behavioral data.

BehaviorDEPOT is a general utility behavioral analysis software package based on keypoint tracking. Its graphical interface allows even inexperienced coders to run experiments, automatically detect behaviors, and analyze the results of popular assays including those run in operant chambers (e.g., fear conditioning) or spatial mazes (e.g., T-mazes or elevated plus mazes). Our built-in heuristic freezing detector has low error rates across a range of video

recording setups, including videos of both mice and rats wearing tethered headmounts. BehaviorDEPOT's flexible interface accommodates varied experimental designs including conditioned tones, optogenetics, and spatial ROIs. It also builds rich data structures that facilitate alignment of neural and behavioral data and we provide additional code in our GitHub repository for this purpose. The experiment module and the UCLA MiniCAM extend the utility of BehaviorDEPOT, together forming a fully open-source pipeline from data collection to analysis. While the Analysis Module supports many behavioral analyses 'out of the box', we created four independent modules so that researchers can create, test, and optimize new behavioral detection heuristics and then integrate them into the Analysis Module.

BehaviorDEPOT employs heuristics to measure human-defined behaviors based on keypoint tracking data. Keypoints can be used to simultaneously track location and classify fine-scale behaviors. As such, keypoint tracking is well suited for analysis of widely-used assays in which researchers have carefully defined behaviors based on the pose of the animal and its location in an arena. Assays including fear conditioning, avoidance, T-mazes, elevated plus maze are published in tens of thousands of studies each year. Yet most still rely on laborious manual annotation, expensive commercial software packages, or open-source software packages that can fail to detect fine movements and are error prone, especially in visually complex arenas. With BehaviorDEPOT, we were able to quickly and intuitively design heuristics that combine spatial tracking with detection of fine movements.

In contrast to methods that use supervised machine learning (Nilsson et al., 2020; Segalin et al., 2020; Hong et al., 2015; Bohnslav et al., 2021), BehaviorDEPOT's heuristics are easier to interpret and they can be easily tweaked to fit out-of-sample videos. Like any supervised method, BehaviorDEPOT heuristics are based on human definitions, so human bias is not completely absent from the analyses. However, the automation serves to standardize human-expert definitions and can enhance rigor and reproducibility. Moreover, when behaviors are clearly defined, developing reliable BehaviorDEPOT heuristics may require less human-

labeled data compared to a supervised machine learning approach. Other methods use unsupervised approaches to classify behavior based on keypoint tracking. While relatively free of human biases, programs like B-SOiD (Hsu et al., 2021) and MotionMapper (https://github.com/DeepLabCut/DLCutils/tree/master/DLC_2_MotionMapper) are geared toward analysis of even more subtle behaviors that are more challenging for humans to reliably label and may be out of reach technically for researchers that lack computational expertise. The graphical interface and intuitive design of BehaviorDEPOT heuristics ensure it will serve a broad audience.

BehaviorDEPOT does require users to first train keypoint tracking models. However, the accuracy, precision and flexibility achieved by these methods will make BehaviorDEPOT more broadly useful than classifiers based on more coarse detection methods (e.g. background subtraction) that are not robust to environmental complexity or subject appearance. Some freezing detectors use pixel change functions to detect periods of no movement and can operate in complex arenas like fear conditioning chambers. However, they often fail to detect freezing when animals are wearing head-mounts for optogenetics or neural recordings because tethered patch cords can move even when the animal is immobile. To circumvent this problem, ezTrack (Pennington et al., 2019), VideoFreeze (Anagnostaras et al., 2010), and ANYmaze allow researchers to crop the tether out of the video, but this requires side-view videos and thereby constrains concurrent spatial analyses. In contrast, keypoint tracking algorithms can be trained to detect animals in any experimental condition, so users can analyze videos they have already recorded. With keypoint tracking, researchers can track body parts that best fit their experimental design and can detect fine movements of individual body parts, allowing researchers to detect a wider array of behaviors and discover subtle phenotypes arising from manipulations.

To enhance the utility of BehaviorDEPOT, the Inter-Rater, Data Exploration, Optimization and Validation Modules help users develop new heuristics or optimize existing

ones for their experimental setups. An important step in supervised behavior classification is establishing a ground truth definition of behavior. This is typically achieved by training multiple human raters and through discussion, refining their annotations until they converge maximally. These reference annotations are then used to create classifiers. MARS includes a large dataset of human annotations for social behaviors and provides detailed quantitative descriptions of similarity and divergence between human raters (Segalin et al., 2021). While the MARS BENTO feature can import human annotations for visualization alongside behavior videos or automated annotations, our Inter-Rater Module has added functions to automatically calculate performance statistics with the click of a button. This makes it fast and easy to train novice manual raters or establish new ground truth definitions. Human annotations or ratings from another classifier program can be imported into the Data Exploration, Optimization, and Validation Modules and are compared to BehaviorDEPOT metrics or heuristic outputs for development and evaluation of heuristic performance.

Our heuristic for freezing detection operate on similar principles as commercial software that apply a motion threshold and a minimum duration threshold to detect bouts of freezing. However, BehaviorDEPOT has added functionality in that freezing detection can be integrated with spatial analyses so researchers can determine not only when an animal is freezing, but also where it is freezing. Another major limitation of commercial algorithms is that they are not well validated (Anagnostaras et al., 2000). Researchers typically use their intuition to set thresholds for freezing. BehaviorDEPOT's Optimization module allows users to adjust parameters and determine the combination of thresholds that produce the lowest error rates. We envision that new users will manually annotate a set of videos from their lab, analyze them with BehaviorDEPOT using the default heuristic settings, and then test the error rates using the Validation Module. If error rates are high, they can adjust threshold values with the Optimization Module. This process can be done for any behavior of interest. By making the optimization and validation process easy – it can be done with a few button clicks in the graphical interface –

BehaviorDEPOT will enhance the rigor of behavior classification and increase reproducibility across labs.

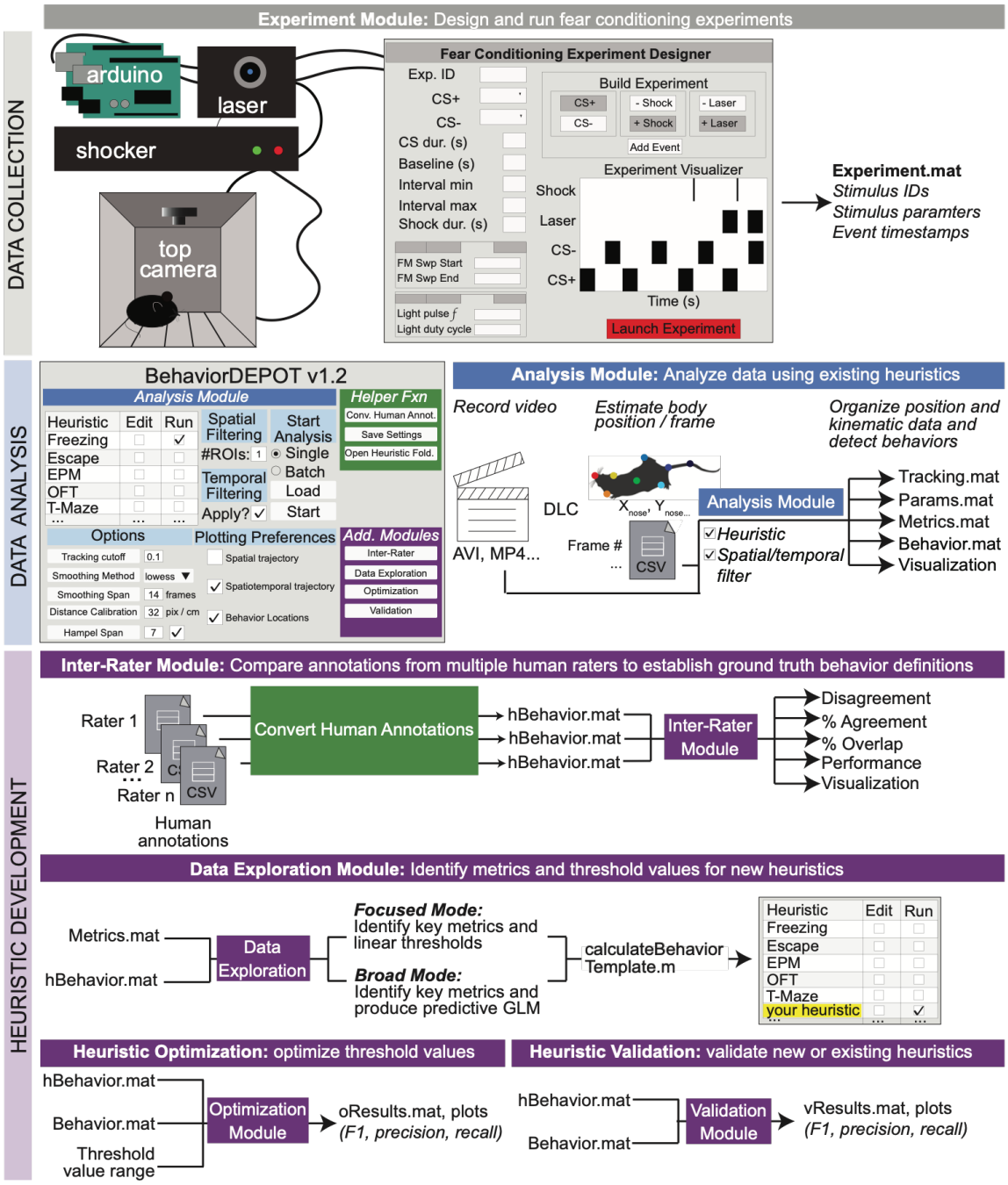

Figure 1. BehaviorDEPOT is a general-purpose behavioral analysis software comprising six modules.

The Experiment Module is a MATLAB application with a graphical interface that allows users to design and run fear conditioning experiments. The software uses Arduinos to interface with commercially available hardware (e.g., shockers and lasers) to control stimuli. The Analysis Module imports keypoint tracking data, calculates postural and kinematic metrics, detects behaviors, and analyzes the results of behavior experiments. Four additional modules help users develop custom heuristics. The Inter-Rater Module compares human annotations, helping researchers settle on 'ground truth' definitions of behavior. These human definitions serve as reference data for behavioral detection heuristics. The data exploration module identifies features of movement with the highest predictive value for specific behaviors. The optimization module identifies combinations of feature thresholds that maximize behavioral detection. The validation module reports the accuracy of heuristics.

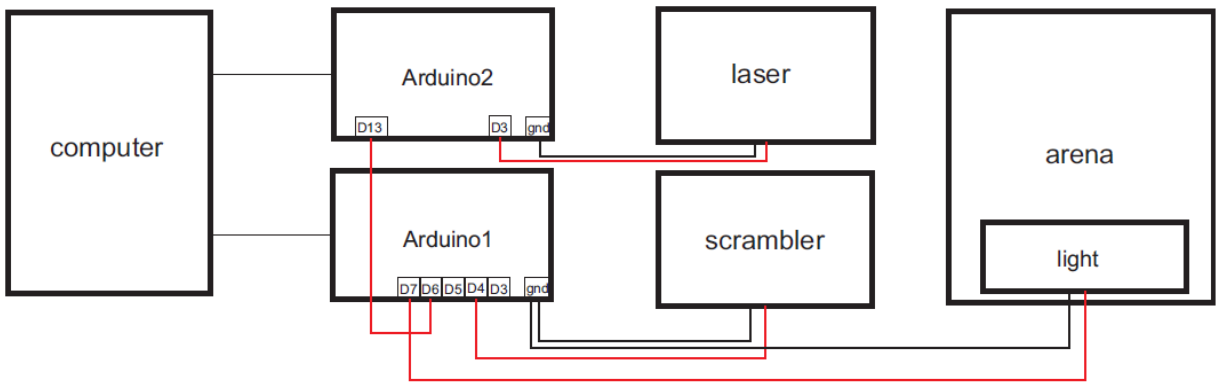

Figure 1-S1. Example arrangement of Arduino interface between computer, fear conditioning, and optogenetics hardware.
The Experiment Module controls two Arduinos that control delivery of the scrambled shocker, and a light (for use as a conditioned cue), and the laser for optogenetics, respectively. MATLAB software triggers the conditioned tone.

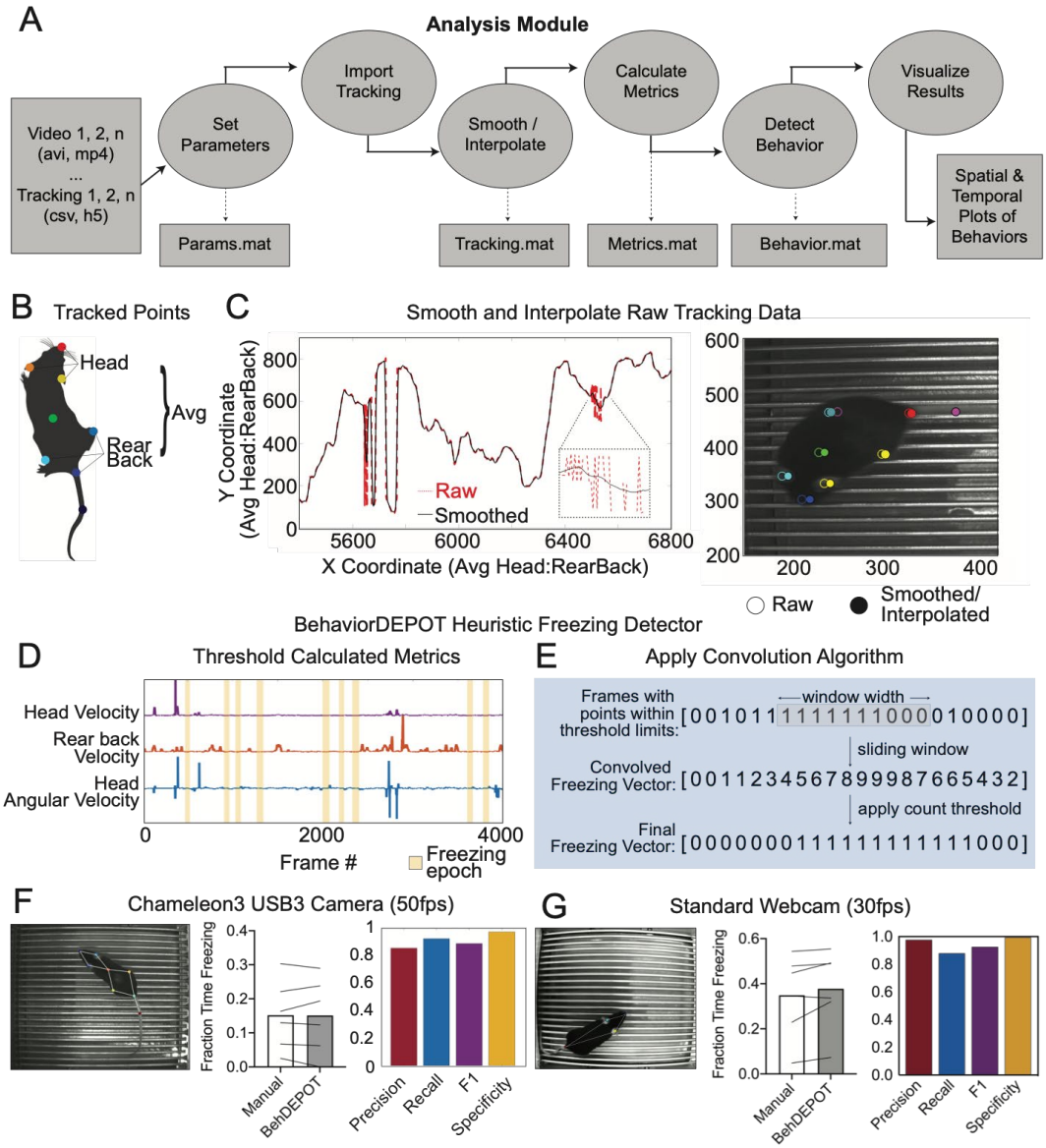

Figure 2. The Analysis Module.
A) The Analysis Module workflow. Videos and accompanying pose tracking data are the inputs. Pose tracking and behavioral data is vectorized and saved in MATLAB structures to facilitate subsequent analyses.
B) Metrics based on individual tracked points and weighted averages are calculated and stored in BehaviorDEPOT data matrices.
C) Visualization of the effects of the LOWESS smoothing and interpolation algorithms for the weighted average of head and rear back (left) and for all tracked points in a representative example frame (right).
D) Visualization of metrics that form the basis of the BehaviorDEPOT freezing heuristic. Colored lines represent framewise calculated values for each metric. Yellow bars indicate freezing epochs.
E) Visualization of the convolution algorithm employed by the BehaviorDEPOT freezing heuristic. A sliding window of a specified width produces a convolved freezing vector in which each value represents the number of freezing frames visible in the window at a given frame. An adjustable count threshold converts the convolved freezing vector into the final binary freezing vector.
F) Evaluation of freezing heuristic performance on videos recorded at 50 fps with a high resolution, high framerate camera (*P*=0.95, paired t-test, N=6; *Precision*: 0.86, Recall: 0.92, F1: 0.89, Specificity: 0.97).
G) Evaluation of freezing heuristic performance on videos recorded at 30fps with a standard webcam (*P*=0.10, paired t-test, N=6; Precision: 0.98, Recall: 0.88, F1: 0.93, Specificity: 0.99).

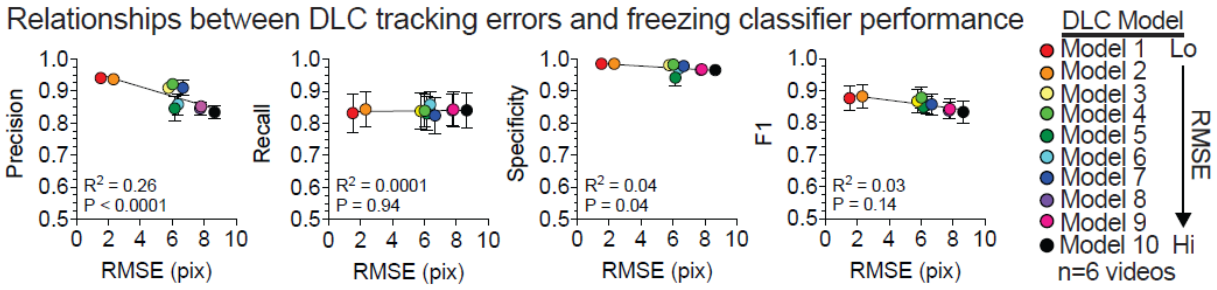

Figure 2-S1. Performance of the freezing heuristic based on DLC mean tracking error.
Heuristic performance statistics plotted against root mean squared error (RMSE) of the DLC model. N=6 videos were tested to generate average heuristic performance for each model. Error bars, S.E.M. R and P values indicate summary statistics for simple linear regression.

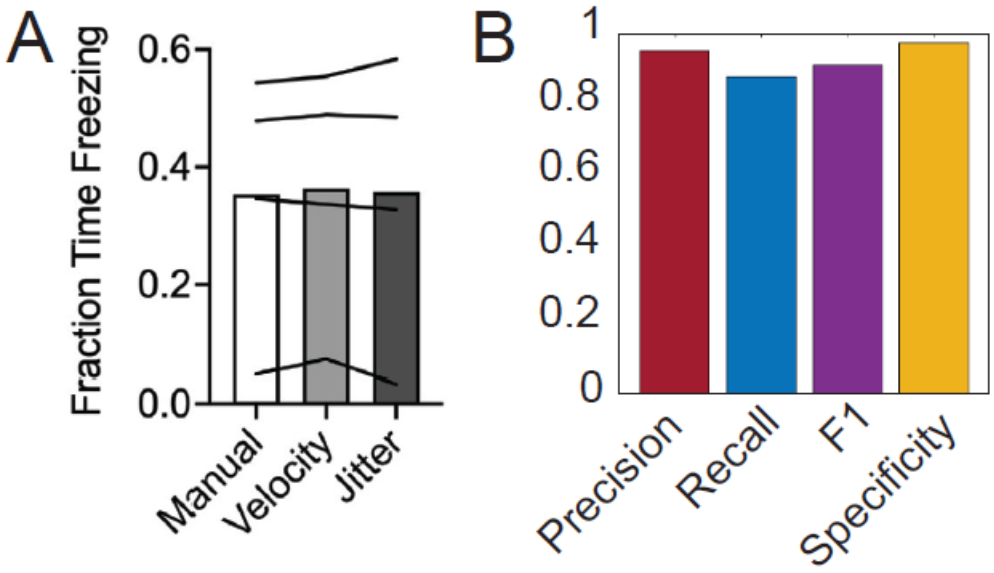

Figure 2-S2. Performance of the 'Jitter' Freezing Heuristic on Webcam videos.
(A) Human vs. velocity vs. jitter freezing annotations ($F(1.4,4.2)=0.32$, $P=0.67$, RM one-way ANOVA). (B) Evaluation of freezing heuristic performance on videos recorded at 30fps with a standard webcam (Precision: 0.95, Recall: 0.88, F1: 0.97, Specificity: 0.91).

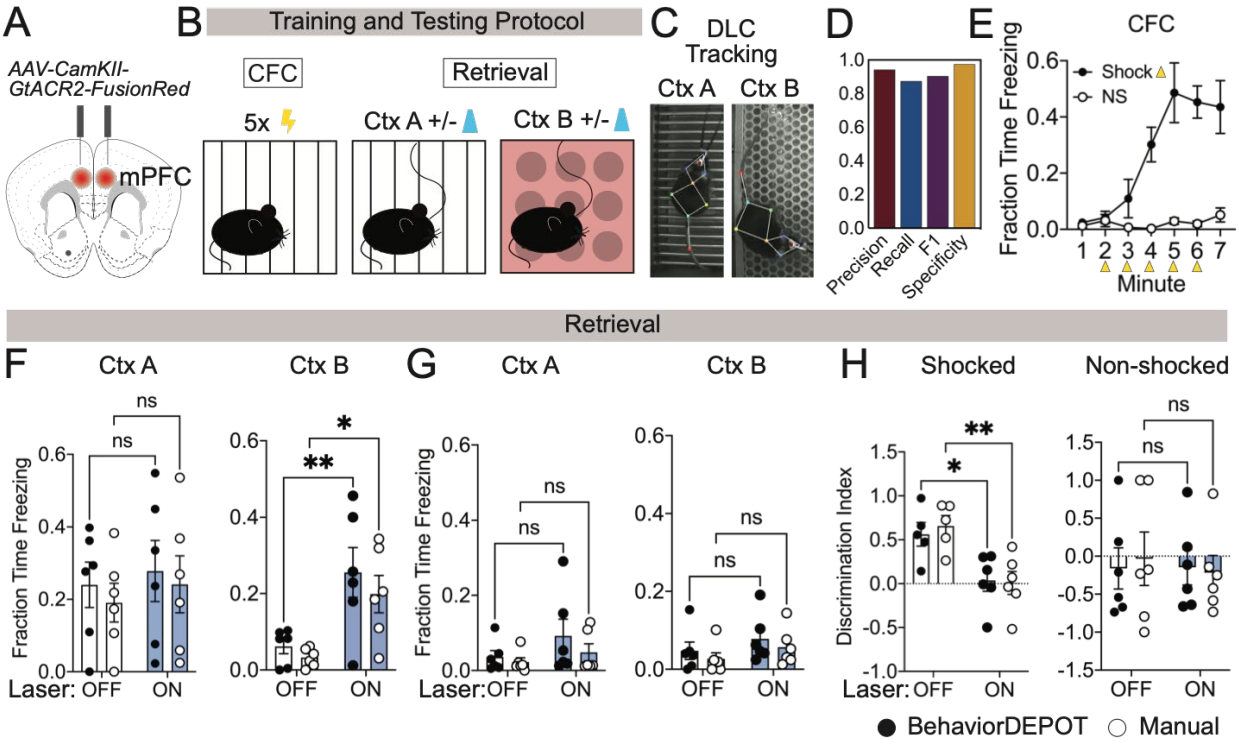

Figure 3. Use Case 1: Optogenetics.
A) AAV1-CamKII-GtACR2-FusionRed was injected bilaterally into medial prefrontal cortex (mPFC).
B) Behavioral protocol. Mice underwent contextual fear conditioning on day 1. On day 2, mice were returned to the conditioned context or a novel context in a counterbalanced fashion and received 2x2 min 473nm laser stimulation separated by 2 min laser off intervals.
C) Example DLC tracking of mice attached to patch cords in different contexts.
D) Performance of freezing heuristic (Precision: 0.94, Recall: 0.87, F1: 0.91, Specificity: 0.98).
E) Quantification of contextual freezing during training analyzed with BehaviorDEPOT.
F–G. Comparing human annotations to BehaviorDEPOT freezing heuristic.
F) Shocked mice: freezing in context A (left) and context B (right) with and without mPFC silencing (CtxA: $F_{laser}(1,10)=0.42$, $P=0.53$; $F_{rater}(1,10)=0.35$, $P=0.57$; Off vs. On: $P_{BD}=0.91$, $P_{Manual}=0.86$; CtxB: $F_{laser}(1,10)=26.51$, $P=0.0004$; $F_{rater}(1,10)=0.08$, $P=0.78$; Off vs. On: $P_{BD}=0.008$, $P_{Man}=0.02$; Two-way repeated measures ANOVA and Sidak's test, N=6 mice per group).
G) Non-shocked controls: freezing in context A (left) and context B (right) with and without mPFC silencing (Ctx A: $F_{laser}(1,10)=3.60$, $P=0.09$; $F_{rater}(1,10)=0.79$, $P=0.39$; Off vs. On: $P_{BD}=0.30$, $P_{Manual}=0.76$; CtxB: $F_{laser}(1,10)=1.486$, $P=0.25$; $F_{rater}(1,10)=1.59$, $P=0.24$; Off vs. On: $P_{BD}=0.52$, $P_{Manual}=0.54$; Two-way repeated measures ANOVA, N=6 mice per group).
H) Discrimination index = (FreezeA - FreezeB) / (FreezeA + FreezeB) for shocked mice ($F_{laser}(1,10)=17.54$, $P=0.002$; $F_{rater}(1,8)=0.09$, $P=0.77$; Mixed-effects analysis, On vs. Off: $P_{BD}=0.02$, $P_{Manual}=0.004$, Sidak's test, N=5–6 per group) and non-shocked controls ($F_{laser}(1,10)=0.07$, $P=0.80$; $F_{rater}(1,8)=0.02$, $P=0.90$; Two-way ANOVA; On vs. Off: P_{BD}=,0.99 $P_{Manual}=0.87$, Sidak's test, N=6 per group). Error bars represent S.E.M.

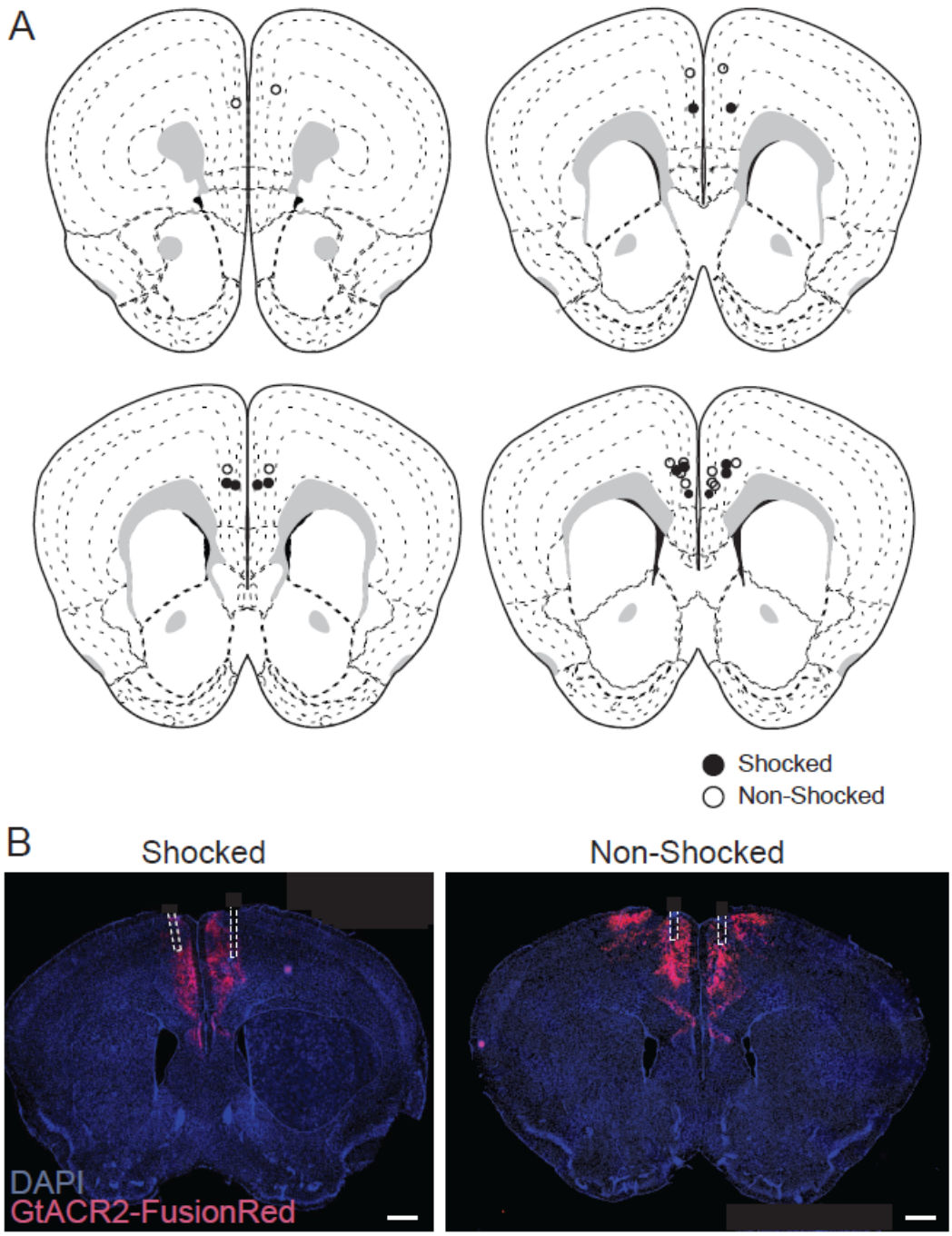

Figure 3-S1. Histology for optogenetics viral injections and fiber implants.
(A) Optic fiber cannula placements for experiment described in Figure 3.
(B) StGtACR2 -FusionRed expression and bilateral fiber placement for representative shocked and non-shocked mice. Scale bar, 500 μm.

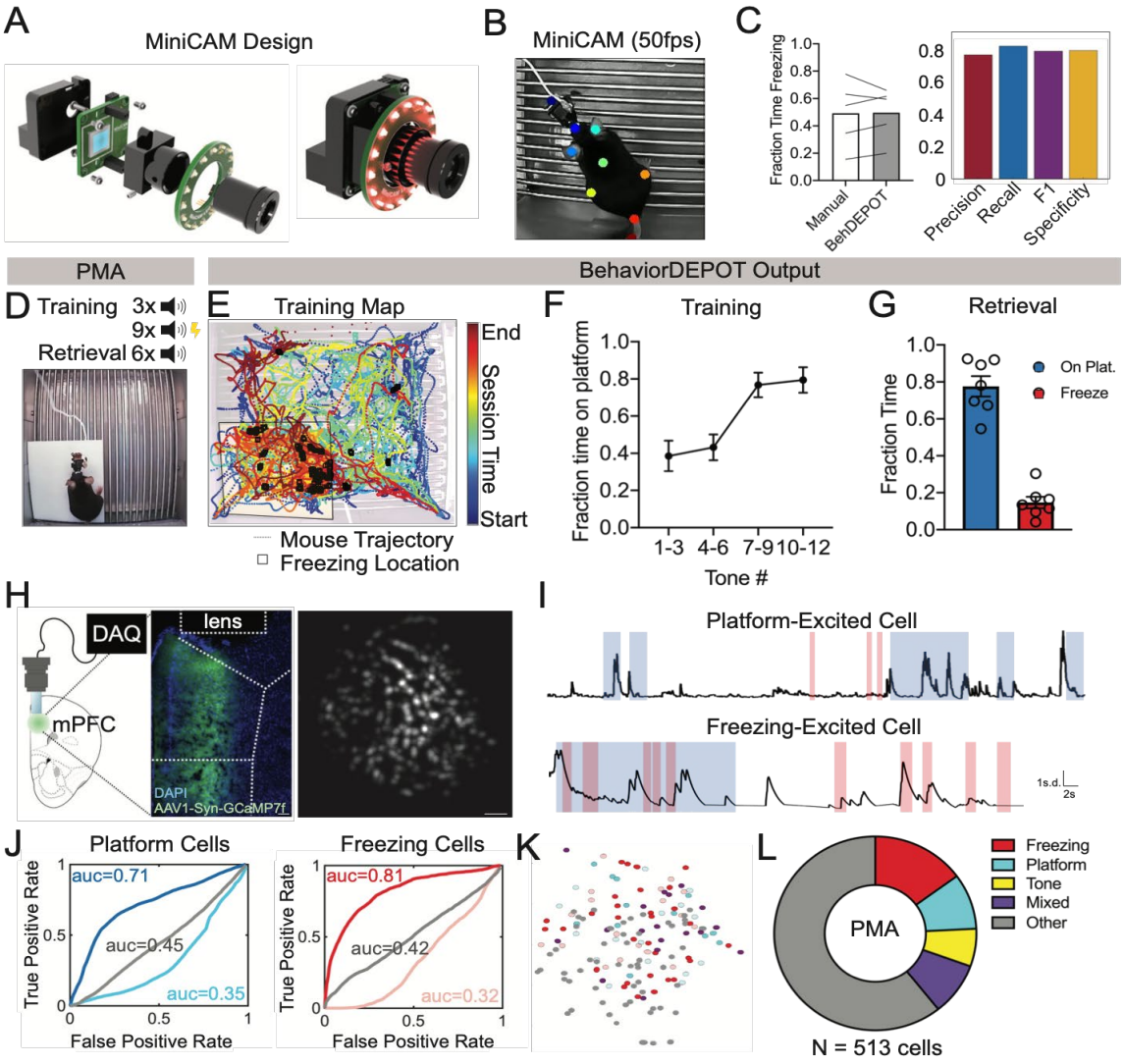

Figure 4. Use Case 2: Mice wearing miniscopes.
A) Design for MiniCAM, an open-source camera designed to interface with miniscopes and pose tracking.
B) Still frame from MiniCAM recording of mouse wearing a V4 miniscope. DLC tracked points are labeled with rainbow dots.
C) Performance of freezing heuristic on videos of mouse wearing miniscope recorded with MiniCAM (Precision: 0.85; Recall: 0.93; F1 Score: 0.89; Specificity: 0.84).
D) Task design.
E) Sample BehaviorDEPOT output for mouse wearing miniscope during PMA. Map displays animal position over time as well as freezing locations (black squares).
F) Temporal alignment of time on the platform (blue), time freezing (black), and tones.
G) Summary data for training and retrieval.
H) GCaMP7-exressing mPFC neurons imaged through a V4 miniscope.
I) Example Ca^{2+} traces from platform (top) and tone (bottom) modulated cells during time on the platform (blue) or time freezing (pink).
J) Receiver operating characteristic (ROC) curves that were calculated for platform-modulated cells (excited cell: auc=0.71; suppressed cell: auc=0.35, unmodulated cell: auc=0.45) and freezing-modulated cells (excited cell: auc=0.81; suppressed cell: auc=0.32; unmodulated cell: auc=0.42).
K) Example field of view showing locations of freezing- and platform-modulated mPFC neurons.
L) Proportion of modulated cells of each functional type from 513 cells recorded across 3 mice. Scale bars, 100um. Error bars represent S.E.M.

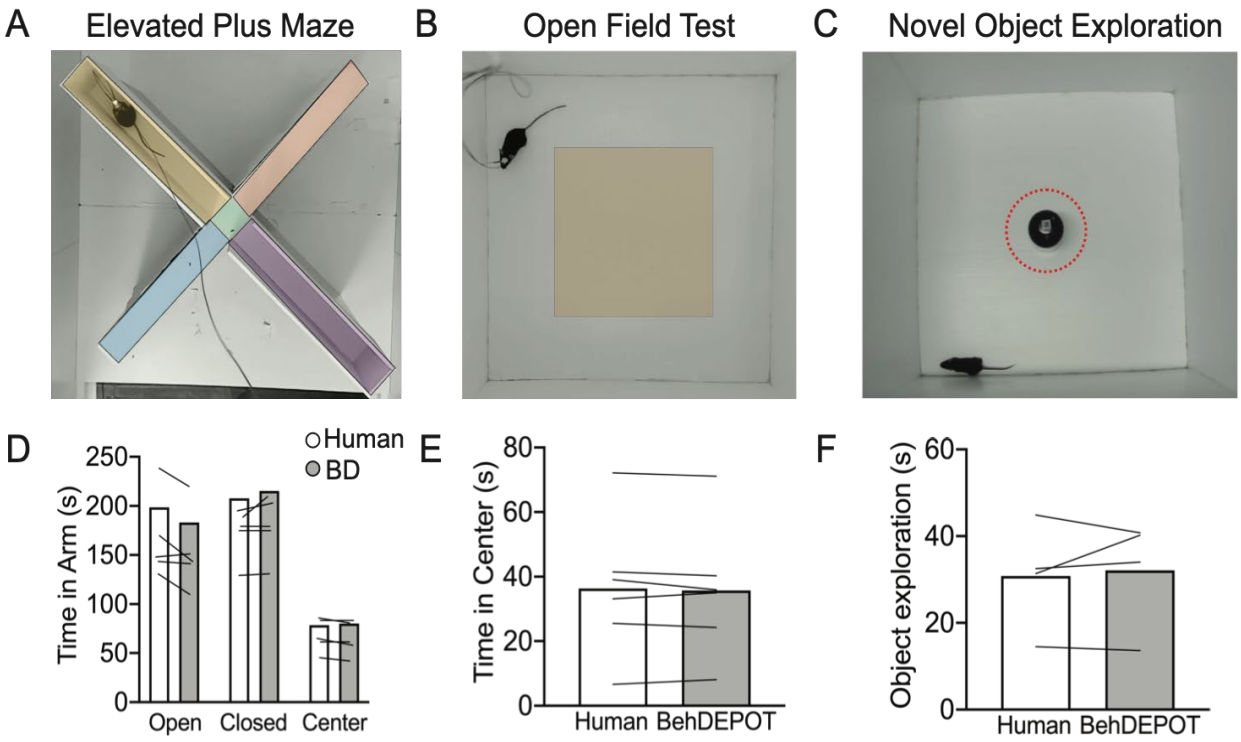

Figure 5. Use cases 3–5: EPM, OFT, NOE

A-C) Screens shot from Analysis Module showing user-defined ROIs in the EPM, OFT and NOE

D) Statistical comparison of human vs. BehaviorDEPOT ratings for time in each arm (F_{Rater} (1, 4) = 2.260, P=0.21, F_{Arm}(2,8)=12.69, P=0.003, Two-way ANOVA; Human vs BD: P_{Open}=0.15, P_{Closed}=0.66, P_{Center}=0.99, Sidak post-hoc test, N=5 mice).

E) Statistical comparison of human vs. BehaviorDEPOT ratings for time in center (P=0.50, paired t-test, N=6 mice)

F) Statistical comparison of human vs. BehaviorDEPOT ratings for time in center P=0.66, paired t-test, N=4 mice)

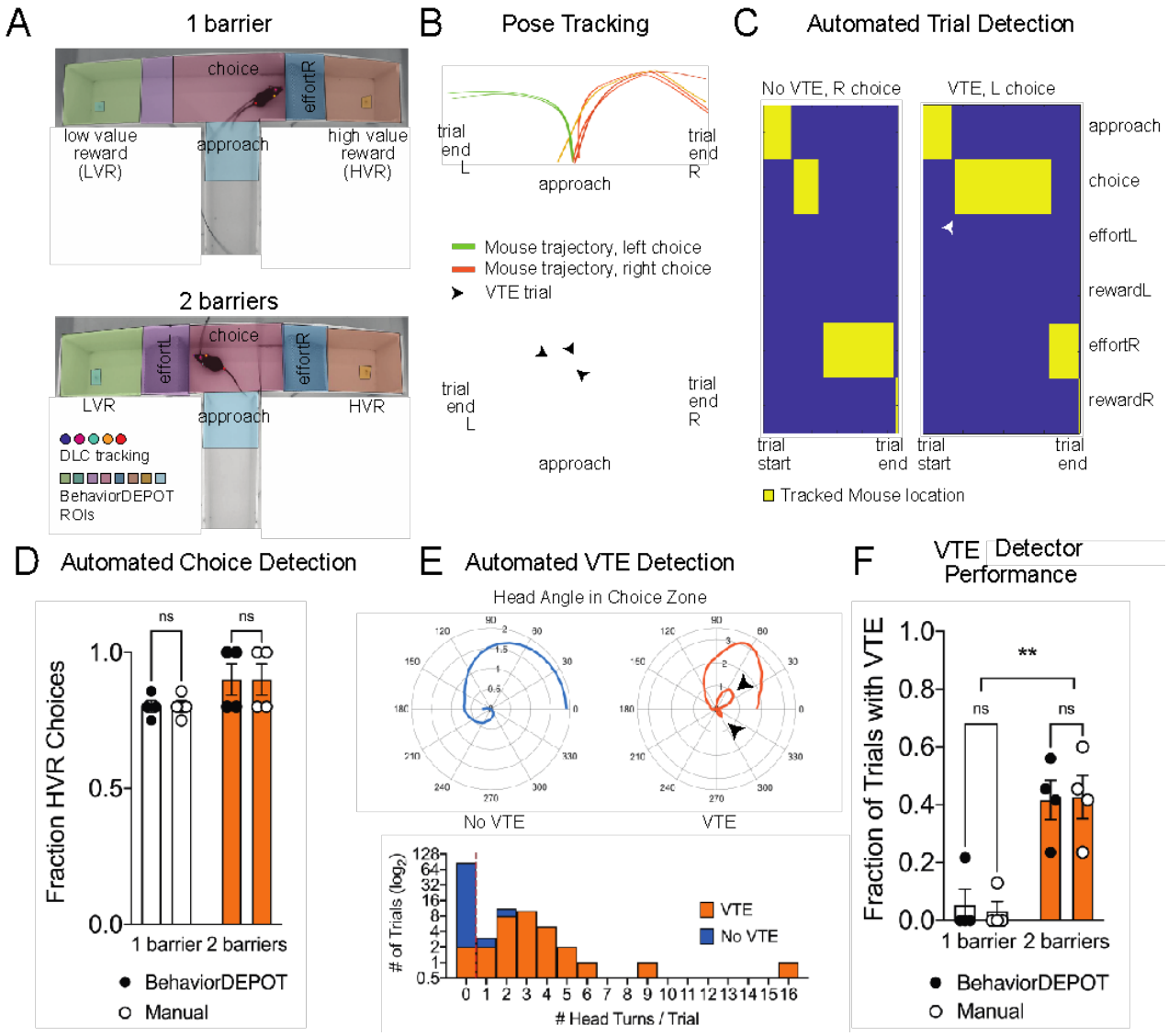

Figure 6. Use Case 6: Automated analysis of an effort-based decision-making T-maze task

A) Screen shots showing DLC tracking in a 1-barrier (top) and 2-barrier (bottom) T-maze and ROIs used for analysis in BehaviorDEPOT.

B) Sample mouse trajectories in a 1-barrier (left) and 2-barrier (right) T-maze. Lines represent individual trials for 1 mouse. Blue lines represent right choices, orange lines represent left choices, and thick lines indicate vicarious trial and error (VTE).

C) Illustration of automated trial definitions.

D) Automated choice detection using BehaviorDEPOT. BehaviorDEPOT indicated choice with 100% accuracy ($F_{Rater}(1,6)=6.84$, $P>0.99$, $F_{Barriers}(1,7)=4.02$, $P=0.09$; $F_{Subject}(6,7)=0.42$, $P=0.84$, 2-way ANOVA with Sidak post-hoc comparisons, 84 trials, N=4 mice).

E) Top: Polar plots show representative head angle trajectories when the mouse was in the choice zone during a trial without VTE (left) and with VTE (right). Bottom: Histogram of head turns per trial for trials without VTE (blue) and with VTE (orange). Red dotted line indicates selected threshold.

F) Fraction of trials with VTE during 1-barrier and 2-barrier sessions, comparing manual annotations to BehaviorDEPOT classification ($F_{RaterxBarriers}(1,6)=0.04$, $P=0.85$, $F_{Rater}(1,7)=0.03$, $P=0.85$; $F_{Barriers}(1,6)=22.9$, $P=0.003$, 2-way ANOVA with Sidak post-hoc comparisons, 102 trials, N=4 mice). Error bars represent S.E.M.

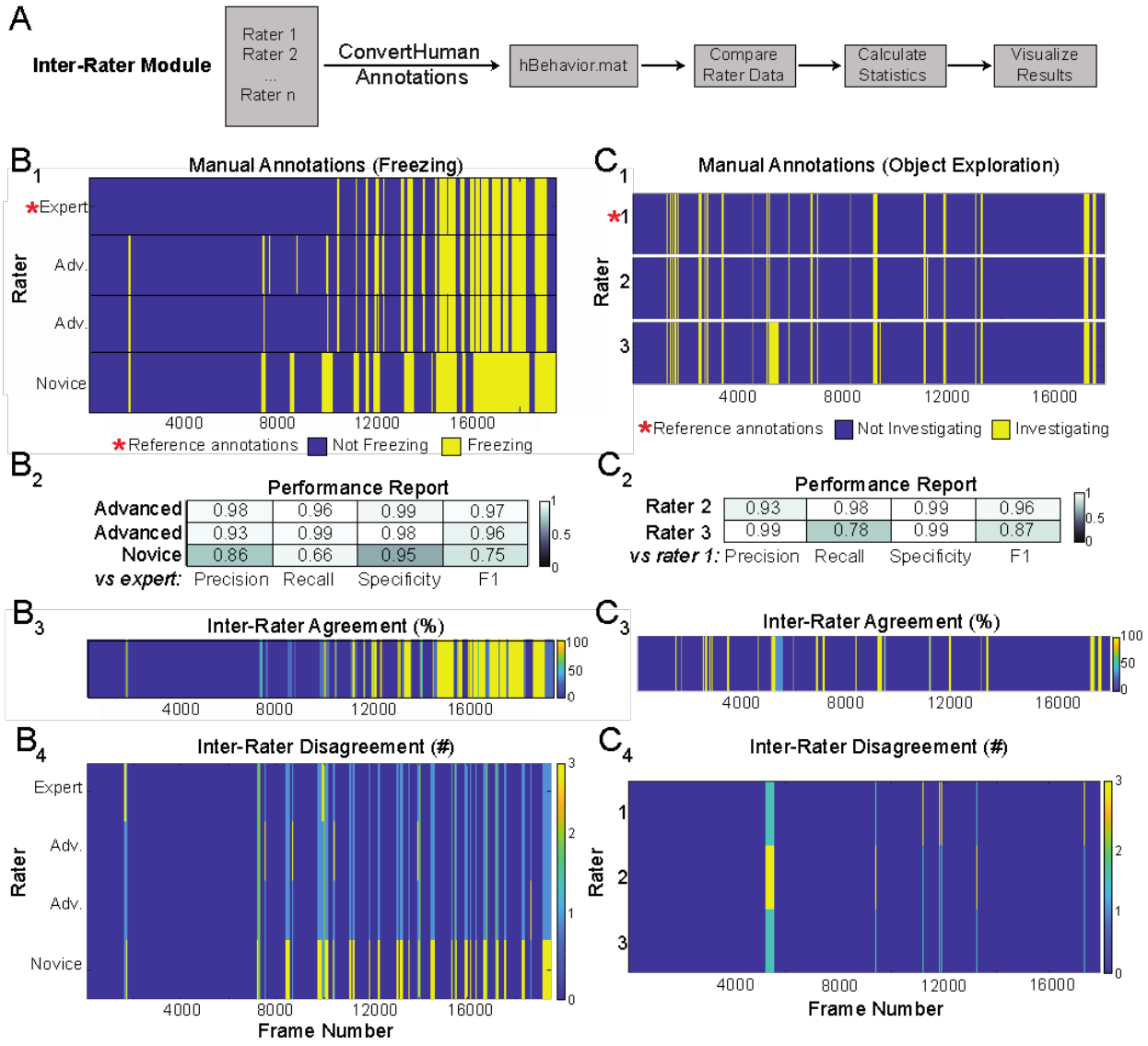

Figure 7. Sample Outputs of the Inter-Rater Module.
A) The Inter-Rater Module imports reference annotations, converts them to a BehaviorDEPOT friendly format, aligns annotations and reports statistics about agreement between raters.
B_1) Alignment of freezing annotations from four raters with different levels of annotation experience.
B_2) Summary report of inter-rater error rates for freezing.
B_3) Visualizations of framewise agreement levels for multiple raters for freezing.
B_4) Visualizations of framewise disagreements for multiple raters for freezing.
C_1) Alignment of NOE annotations from four raters with different levels of annotation experience.
C_2) Summary report of inter-rater error rates for NOE.
C_3) Visualizations of framewise agreement levels for multiple raters for NOE.
C_4) Visualizations of framewise disagreements for multiple raters for NOE.

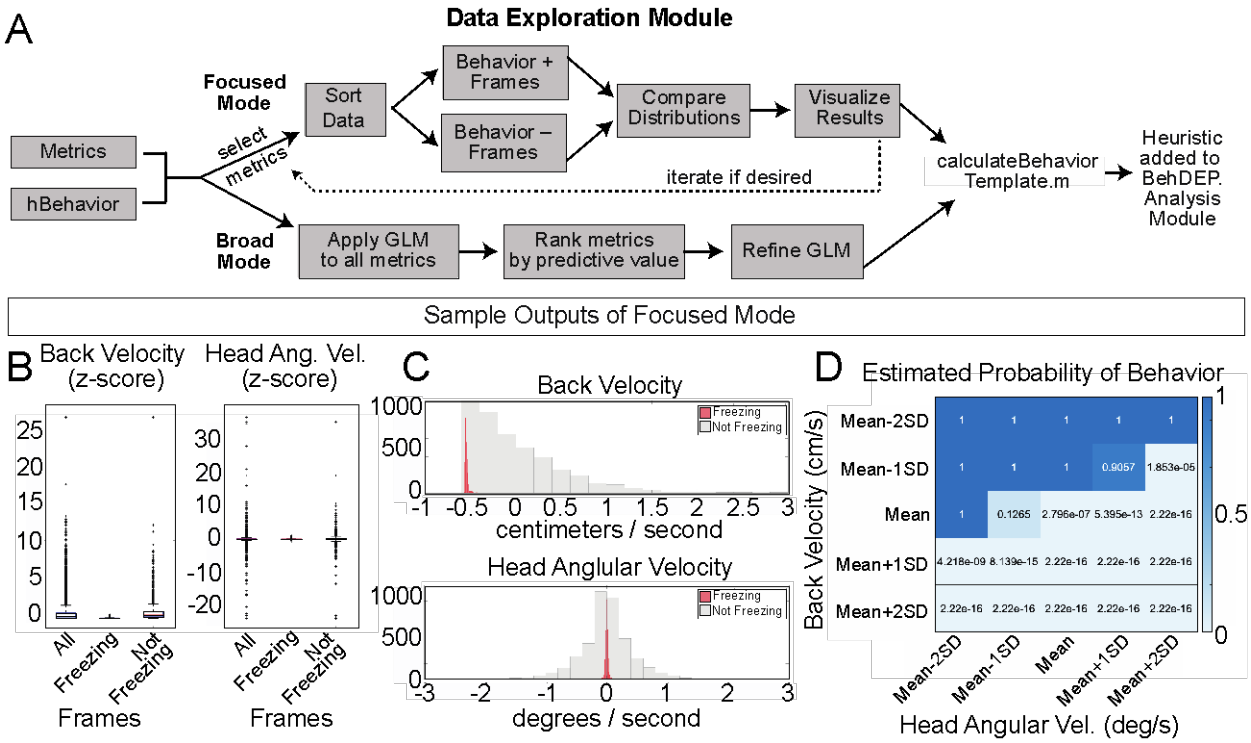

Figure 8. The Data Exploration Module.
A) The Data Exploration Module takes in tracked metrics from the Analysis Module along with reference annotations. It sorts the data, separating frames containing the behavior of interest from those without and then visualizes and compares the distribution of values for metrics of interest.
B) Distributions of Z-scored values for head velocity (left) and change in head angle (right) are distinct for freezing vs. not freezing frames. Box plots represent median, 25th, and 75th percentile. Error bars extend to the most extreme point that is not an outlier
C) Histograms showing distribution of values for back velocity (top) and head angular velocity (bottom) for freezing (red) vs. not-freezing (grey) frames.
D) A generalized linear model (GLM) computes the predictive power of given metrics for frames containing the behavior of interest.

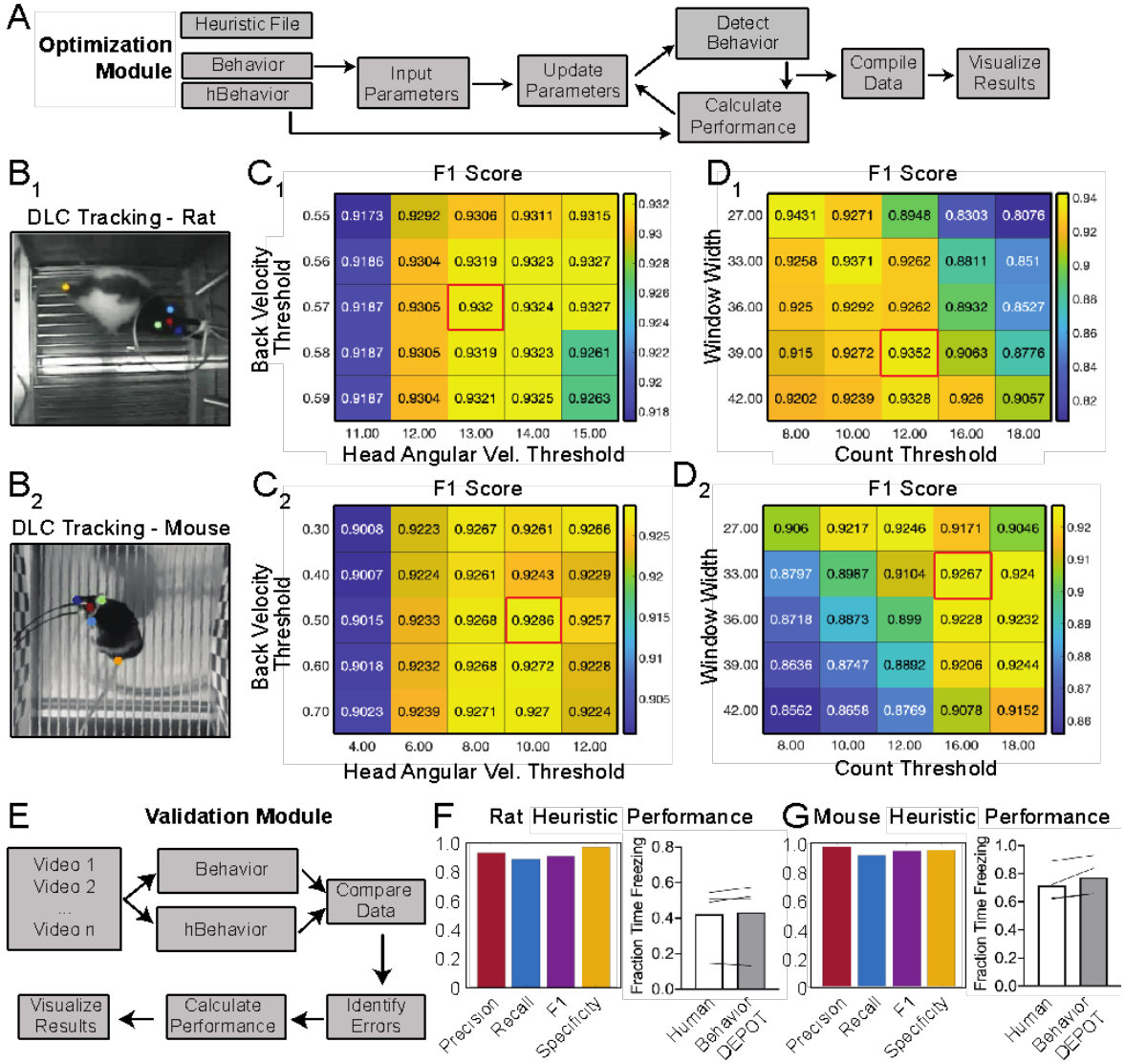

Figure 9. Analysis of External Data using Optimization and Validation Modules.
A) Optimization Module workflow. This module sweeps through a range of thresholds for statistics calculated based on tracked points and then compares the resulting behavior detection to human annotations.
$B_{1,2}$) DLC tracking in rat and mouse freezing in videos obtained from other laboratories.
$C_{1,2}$) Heatmaps showing F1 scores following iterative sweeps through a range of thresholds for two metrics: back velocity and angular velocity of the head. Red box marks highest F1 score.
$D_{1,2}$) F1 scores from a subsequent sweep through two additional value ranges for window width and count threshold from the smoothing algorithm. Red box marks highest F1 score.
E) Validation Module workflow.
F) The BehaviorDEPOT heuristic performed robustly on videos of rats recorded in a different lab (Precision = 0.93; Recall = 0.88; F1=0.91; Specificity = 0.96). BehaviorDEPOT freezing detection was comparable to highly trained human raters (N=4 videos, *P*=0.89, Mann-Whitney U).
G) The BehaviorDEPOT heuristic performed robustly on videos of mice recorded in a different lab (Precision = 0.98; Recall = 0.92; F1=0.95; Specificity = 0.95). BehaviorDEPOT freezing detection was comparable to highly trained human raters (N=4 videos, *P*=0.49, Mann-Whitney U).

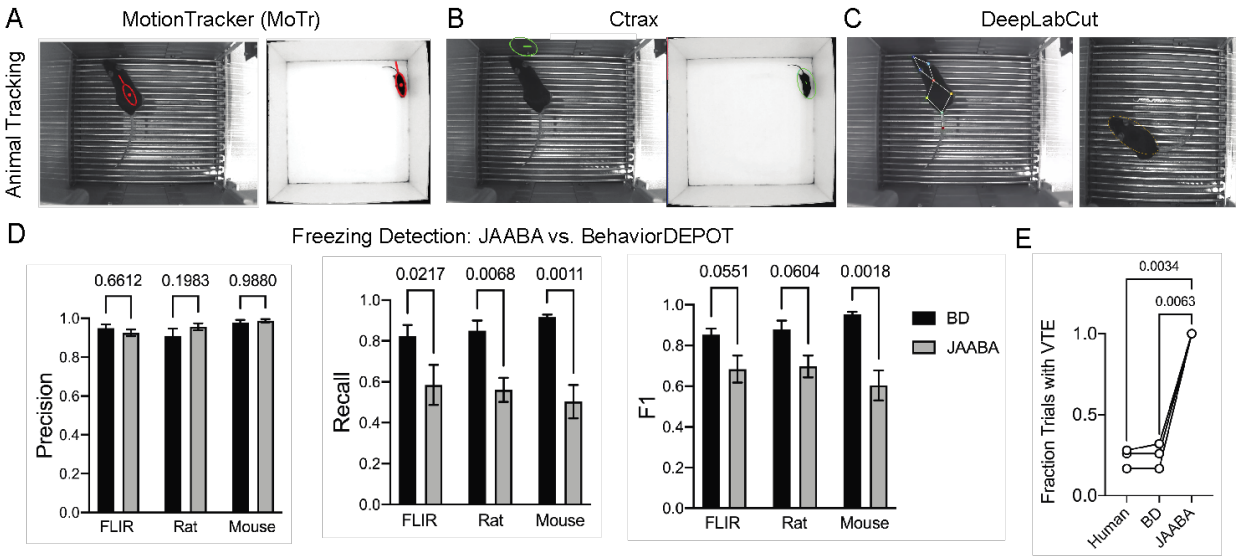

Figure 10. Comparisons with JAABA

A) MoTr tracking in a standard fear conditioning chamber and an open field.

B) Ctrax tracking in a standard fear conditioning chamber and an open field.

C) DLC raw tracking (left) and ellipse calculated based on keypoints (right) in a standard fear conditioning chamber.

D) Quantification of freezing detection errors for BehaviorDEPOT and JAABA (Precision: $F_{Classifier}(1,12)$=0.58, P=0.46; Recall: $F_{Classifier}(1,11)$=51.27, P<0.001; F1: $F_{Classifier}(1,11)$=51.27, P<0.001, 2-way ANOVA with Sidak's multiple comparison test, N=4–6 per group).

E) Comparison of VTE detection by human, BehaviorDEPOT and JAABA ($F_{Classifier}(1.072,2.143)$=340.2, P=0.0021, Repeated measures one-way ANOVA with Tukey multiple comparison's test, N=3).

METHODS

Animals

Female and male C57B1/6J mice (JAX Stock No. 000664) aged 10–16 weeks were group housed (2–5 per cage) and kept on a 12hr light cycle. Following behavior conditioning, animals were individually housed until the memory retrieval sessions. All animal procedures followed animal care guidelines approved by the University of California, Los Angeles Chancellor's Animal Research Committee.

Contextual fear conditioning

Mice were handled for 5 days preceding the behavioral testing procedure. The conditioning chamber consisted of an 18cm x 18cm x 30cm cage with a grid floor wired to a scrambled shock generator (Lafayette Instruments) surrounded by a custom-built acoustic chamber. The chamber was scented with 50% Windex. Mice were placed in the chamber and then after a 2-minute baseline period, received 5 0.75mA footshocks spaced 1 minute apart. Mice were removed 1 minute after the last shock. Non-shocked control animals freely explored the conditioning chamber but never received any shocks. The following day, mice were returned to the conditioning chamber and a novel context (different metal floor, scented with 1% acetic acid), separated by a 1-hour interval. Context presentation order on day 2 was counterbalanced across mice.

Platform-mediated avoidance

PMA used the fear conditioning chamber described above, except 25% of the floor was covered with a thin acrylic platform (3.5x4x0.5 inches). During training, mice were presented with 3 baseline 30s 4kHz tones (CS), followed by 9 presentations of the CS that co-terminated with a 2s footshock (0.13mA). The following day, mice were presented with 6 CS in the absence of shocks.

Viruses

AAV1-syn-jGCaMP7f.WPRE (ItemID: 104488-AAV1) were purchased from Addgene and diluted to a working titer of $8.5x10^{12}$ GC/ml, and AAV1-CamKIIa-stGtACR2-FusionRed (ItemID: 105669-AAV1) were purchased from Addgene and diluted to a working titer of $9.5x10^{11}$ GC/ml.

AAV injection with Optogenetic Cannula Implant

Adult wildtype C57/Bl6 mice were anesthetized with isoflurane and secured to a stereotaxic frame. Mice were placed on a heating blanket and artificial tears kept their eyes moist throughout the surgery. After exposing the skull, we drilled a burr hole above mPFC in both hemispheres (AP+1.8, ML+/-0.3 from bregma). A Hamilton syringe containing AAV-CaMKIIa-stGtACR2-WPRE was lowered into the burr hole and 400nL of AAV was pressure injected into each site (DV -2.25mm and -2.50mm from bregma) at 100nL/min using a microinjector (Kopf, 693A). The syringe was left in place for 10 minutes to ensure the AAV did not spill out of the target region. After injecting the AAV, chronic fiber-optic cannula (0.37NA, length = 2mm, diameter = 200um) were implanted bilaterally above the injection site and secured to the skull with Metabond (Parkell, S371, S396, S398). After recovery, animals were housed in a regular 12hr light/dark cycle with food and water ad libitum. Carprofen (5mg/kg) was administered both during surgery and for 2d after surgery together with amoxicillin (0.25 mg/mL) in the drinking water for 7d after surgery.

Optogenetics

Animals were habituated to the patch-cord for 3 days in advance of optogenetic stimulation. A patch-cord was connected to the fiber-optic cannula and animals were allowed to explore a clean cage for 5 minutes. On the testing day, optical stimulation through the fiber-optic connector was administered by delivering light through a patch-cord connected to a 473-nm

laser (SLOC, BL473T8-100FC). Stimulation was delivered continuously with 2.5mW power at the fiber tip.

Miniscope Surgery and Baseplating

For miniscope recordings, all mice underwent two stereotaxic surgeries (Cai et al., 2016; Dana et al., 2019). First, adult WT mice were anesthetized with isoflurane and secured to a stereotaxic frame. Mice were placed on a heating blanket and artificial tears kept their eyes moist throughout the surgery. After exposing the skull, a burr hole was drilled above PL in the left hemisphere (+1.85, -0.4, -2.3 mm from bregma). A Hamilton syringe containing AAV1-Syn-jGCaMP7f-WPRE was lowered into the burr hole and 400nL of AAV was pressure injected using a microinjector (Kopf, 693A). The syringe was left in place for 10 minutes to ensure the AAV did not spill out of the target region and then the skin was sutured. After recovery, animals were housed in a regular 12hr light/dark cycle with food and water ad libitum. Carprofen (5mg/kg) was administered both during surgery and for 2d after surgery together with amoxicillin (0.25 mg/mL) for 7d after surgery. Two weeks later, mice underwent a GRIN lens implantation surgery. After anesthetizing the animals with isoflurane (1–3%) and securing them to the stereotaxic frame, the cortical tissue above the targeted implant site was carefully aspirated using 27-gauge and 30-gauge blunt needles. Buffered ACSF was constantly applied throughout the aspiration to prevent tissue desiccation. The aspiration ceased after full termination of bleeding, at which point a GRIN lens (1mm diameter, 4mm length, Inscopix 1050-002176) was stereotaxically lowered to the targeted implant site (-2.0 mm dorsoventral from skull surface relative to bregma). Cyanoacrylate glue was used to affix the lens to the skull. Then, dental cement sealed and covered the exposed skull, and Kwik-Sil covered the exposed GRIN lens. Carprofen (5 mg/kg) and dexamethasone (0.2 mg/kg) were administered during surgery and for 7d after surgery together with amoxicillin (0.25 mg/mL) in the drinking water. 2 weeks after implantation, animals were anesthetized again with isoflurane (1–3%) and a miniscope attached

to an aluminum baseplate was placed on top of the GRIN lens. After searching the field of view for in-focus cells, the baseplate was cemented into place, and the miniscope was detached from the baseplate. A plastic cap was locked into the baseplate to protect the implant from debris.

Miniscope Recordings

Mice were handled and habituated to the weight of the microscope for 4 days before behavioral acquisition. On the recording day, a V4 miniscope was secured to the baseplate with a set screw and the mice were allowed to acclimate in their home cage for 5 minutes. Imaging through the miniscope took place throughout the entire PMA training (~30 min) and retrieval session the following day. Behavior was simultaneously recorded with a UCLA MiniCAM.

Miniscope data processing and analysis

Frames in which animals were freezing and/or on the safety platform were determined using BehaviorDEPOT. Cell footprints and Ca2+ fluorescence timeseries were extracted from miniscope recordings using MIN1PIPE. We identified 513 neurons across 3 mice. Custom MATLAB software was used to align data from the behavior camera and the miniscope camera. To identify neurons that were active during freezing or when the animal was on the safety platform, we plotted receiver operating characteristic curves (ROC) for individual neurons and measured the area under the curve (AUC). ROCs plot the true positive rate (true positive/(true positive + false negative)) against the false positive rate (false positive/(false positive + true negative)) over a range of probability thresholds. Neurons with high AUC values therefore predict the behavioral variable of interest with a high true positive rate and low false positive rates over a large range of thresholds. To determine if a neuron significantly encoded a particular behavioral event, we generated a null distribution of AUCs by circularly shuffling event timing and recalculating the AUC over 1000 permutations. Neurons were considered significantly activated during a behavior if their AUC was greater than 97.5% of AUCs in the null

distributions and significantly suppressed if their AUC value was in the lowest 2.5% of all AUCs in the null distribution.

Histology

Mice were transcardially perfused with phosphate-buffered saline (PBS) followed by 4% paraformaldehyde (PFA) in PBS. Brains were dissected, post-fixed in 4% PFA for 12–24h and placed in 30% sucrose for 24–48 hours. They were then embedded in Optimum Cutting Temperature (OCT, Tissue Tek) and stored at -80°C until sectioning. 60um floating sections were collected into PBS. Sections were washed 3x10min in PBS and then blocked in 0.3% PBST containing 10% normal donkey serum (JacksonImmunoresearch, 17-000-121) for 2h. Sections were then stained with rabbit anti-RFP (Rockland 600-41-379 at 1:2000) in 0.3% PBST containing 3% donkey serum overnight at 4°C. The following day, sections were washed 3x5min in PBS and then stained with secondary antibody (JacksonImmunoresearch Cy3 donkey anti-rabbit IgG(H+L) 711-165-152, 1:1000) in 0.3% PBST containing 5% donkey serum for 2 hours at room temperature. Sections were then washed 5 min with PBS, 15 min with PBS+DAPI (Thermofisher Scientific, D1306, 1:4000), and then 5 min with PBS. Sections were mounted on glass slides using FluoroMount-G (ThermoFisher, 00-4958-02) and then imaged at 10x with a Leica slide scanning microscope (VT1200S).

Open Field Test

For the open field test, a 50 cm x 50 cm arena with 38 cm high walls was used. The total area of the arena was 2,500 cm2 and the center was determined to be one fourth of this, 625 cm2 or a 25 cm x 25 cm square. Mice were placed into the room 20 minutes prior to test for habituation. At the beginning of the test mice were placed in the arena facing the wall and allowed to explore for 10 minutes. Arena was cleaned with 70% ethanol between animals. The total time spent in

the center was determined using the OFT heuristic in BehaviorDEPOT and a 2-minute epoch was compared to human annotations.

Elevated Plus Maze

The EPM consisted of a cross-shaped platform 38 cm off the ground with four arms, two that are enclosed by walls 20 cm in height. Mice were placed into the room 20 minutes prior to test for habituation. For the test, mice were placed in the center of the platform (5 cm x 5cm) facing a closed arm and allowed to explore for 8 minutes. The EPM was cleaned in between animals with 70% ethanol. The number of entries into the open arms and the time spent in the open arms were determined using the EPM heuristic in BehaviorDEPOT and compared to human annotations for six full-length videos.

Novel Object Exploration

The NOE used the same arena as OF and mice were placed into the room 20 minutes before testing took place. The objects used were an empty isoflurane bottle (6.5 cm x 6.5 cm x 10 cm) and an ice pack (6 cm x 6.5 cm x 15 cm). At the beginning of each session the object, cleaned with 70% ethanol, was placed into the center of the arena. The mouse was placed facing a wall into the arena and allowed to explore for 10 min. The arena and objects were cleaned in between animals. The time spent exploring the novel object was defined by a human annotator as when the mouse's head was oriented toward the object with the nose within 2 cm of the object. If the mouse was on top of the object this was not included. These human annotations were compared to the output of BehaviorDEPOT using the NOE heuristic.

Effort-based decision-making

For T-maze experiments, mice were food deprived to ~85% of the ad libitum initial weight (3–4 days) and habituated to handling and maze exploration. Reward pellters were chopped Reese's

peanut butter chips (~0.01g each). One arm of the maze was designated as high value reward ('HVR', 3 pellets), the other low value reward ('LVR', 1 pellet). Mice were trained to perform effort-reward decision-making via a sequential process. Once mice learned to choose the HVR arm (>80%), a 10cm wire-mesh barrier was inserted to block that arm. Training was complete when mice achieved >70% success high effort/HVR choices on 2 consecutive days. Forced trials were used to encourage sampling of the barrier arm during training. Once mice achieved stable performance, a second barrier was interested in the LVR arm to equalize effort between choices.

Behavior Video Recordings

Behavioral videos were acquired using one of the following 3 setups:

1) 50fps using a Chameleon3 3.2 megapixel monochrome USB camera fitted with a Sony 1/1.8 sensor (FLIR systems, CM3-U3-31S4M-CS) and a 1/1.8 lens with a 4.0-13mm variable focal length (Tamron, M118VM413IRCS). We recorded 8-bit videos with a 75% M-JPEG compression.

2) 30fps using a ELP 2.8-12mm Lens Varifocal Mini Box 1.3 megapixel USB Camera.

3) 50fps using a UCLA MiniCAM 5 megapixel CMOS sensor (MT9P031I12STM-DP, ON Semiconductor)

Manual annotation of behavior

Two-minute samples of each video recording were manually annotated by 1–3 highly trained individuals for freezing behavior using QuickTime7, FIJI (FFMPEG plugin), or MATLAB. One-minute intervals were chosen from the beginning and end of the video recordings to capture diverse behaviors. In some cases, the entire video was annotated. Freezing was defined as the absence of movement except for respiration. Novel object exploration was defined as when the mouse's head was oriented toward the object with the nose within 2 cm of the object. If the

mouse was on top of the object this was not included. Time in zones of the EPM and OFT was defined by when the middle of the back crossed the threshold between zones. VTE was defined as when the animal was in the choice zone and swept its head back and forth across ~180°. Annotations were iteratively refined after discussion between users until they converged maximally and then each heuristic was developed based on the annotations of one human expert.

Design of behavior detection heuristics development and test sets

To develop heuristics, videos were randomly assigned to heuristic development and test sets. Dividing up the dataset by video rather than by frame ensures that highly correlated temporally adjacent frames are not sorted into training and test sets, which can cause overestimation of accuracy. Since the videos in the test set were separate from those used to develop the heuristics, our validation data reflects the accuracy levels users can expect from BehaviorDEPOT. Heuristic performance was assessed using precision (true positive frames / true positive frames+false positive frames), recall (true positive frames / true positive frames + false negative frames), F1 score (2*(precision*recall / precision + recall)) and specificity (true negative frames / true negative frames + false positive frames).

Heuristic development

Heuristic parameters for freezing, NOE and VTE were chosen based on human definitions of these behaviors and examined in held-out videos. For freezing, we explored linear and angular velocity metrics for various keypoints, finding that angular velocity of the head and linear velocity of a back point tracked best with freezing. Common errors in our heuristics were identified as short sequences of frames at the beginning or end of a behavior bout. This may reflect failures in human detection. Other common errors were sequences of false positive or false negative frames that were shorter than a typical behavior bout. We included the convolution algorithm to

correct these short error sequences, finding empirically that window widths that are the length of the smallest bout of 'real' behavior and count thresholds approximately one third of the window width yielded the best results.

Statistical analyses

Statistical analyses were performed in MATLAB or GraphPad Prism

The BehaviorDEPOT Pipeline

Overview of Functions

The Analysis Module imports video recordings of behavior and accompanying DLC keypoint tracking data and exports four data structures (Tracking, Params, Metrics, Behavior) as well as trajectory maps. If using the spatial functions to analyze EPM, OFT, etc., the Analysis Module also outputs a data summary file that reports time spent in each zone as well as entries and exits. The four heuristic development modules import these data structures along with reference annotations for a video of interest and reports performance metrics (precision, recall, F1, specificity) in graphical and text formats. Reference annotations can come from human raters or another classifier software. A list of the inputs and outputs of each module can be found in Supplementary File 3.

Computer workstation specs

We trained networks in DLC and analyzed videos using two different custom-built workstations (Intel Core i9-9900K processor (8x 3.60GHz/16MB L3 Cache), 2x16GB DDR4-3000 RAM, NVIDIA GeForce RTX 2070 SUPER - 8GB GDDR6; AMD RYZEN 9 3950x processor (16x3.5GHz/64MB L3 Cache), 16GB DDR4 RAM, Gigabyte GeForce RTX 2060 SUPER 8GB WINDFORCE OC). BehaviorDEPOT can run on any personal computer and does not require a GPU.

Installation of BehaviorDEPOT

Detailed instructions on BehaviorDEPOT installation can be found on GitHub: https://github.com/DeNardoLab/BehaviorDEPOT. Briefly, after installing a recent version of MATLAB (2018+), BehaviorDEPOT can be downloaded from GitHub and installed with a single click as either a MATLAB application or as a standalone EXE file. The app can be found in the 'APPS' tab of MATLAB. If users would like to read or modify the underlying code, they can hover their computer mouse over the app and then click the link to the file location in the resulting pop-up window. Updates to the application will be added to the GitHub repository as they come available. We welcome feedback and bug reports on the BehaviorDEPOT GitHub page and encourage users to watch the page to be aware of any new releases.

DeepLabCut Training and Model Availability

For pose estimation, we found that dedicated models for a given video recording setup produced the lowest error rates for keypoint estimations. It is easy to train keypoint tracking models and worth the initial time investment. To expedite this process for others, our models are available for download from GitHub via a link embedded in the BehaviorDEPOT Wiki page (https://github.com/DeNardoLab/BehaviorDEPOT/wiki/Pretrained-DLC-Models). Depending on the users' setup, our models may be used 'out of the box' or may require some additional training. For high resolution, high framerate cameras (Chameleon-3 camera or MiniCAM) we trained models to track 8 or 9 keypoints (nose, ears, hips, midback, tailbase, mid-tail, and head implant when present). Our webcam videos and the videos we acquired from outside labs had lower resolution, lower framerates and therefore more blur in the images, so we trained models to detect 4 or 5 keypoints that were easiest to detect by eye (nose, ears, tailbase and head implant when present). We trained models in DeepLabCut for 1–1.65 million iterations on sets of ~400 video frames. In our DLC training sets, frame rates ranged from 30–75fps, resolution

ranged from 7-32pixels/cm. DLC training errors ranged from 0.74–2.76 pixels and DLC test error rates ranged from 1.44–5.93 pixels (Supplementary File 4). While we do not know the upper limit for DLC tracking errors that can be tolerated by our freezing detection heuristic, our data indicate that heuristic performance is robust to a large range of camera types and DLC models.

DLC Post-processing

BehaviorDEPOT imports keypoint tracking data in the form of a csv or h5 file containing framewise estimates of X-Y coordinates and confidence level for each estimate. After importing the tracking data, BehaviorDEPOT rejects points that were tracked with low confidence ($p<0.1$), removes outliers using a hampel transformation, smooths the remaining points using a LOWESS (or other user selected) algorithm, and then fills in missing points using spline interpolation. Users can update the confidence threshold in the GUI and the source code can be found in smoothTracking_custom.m. Raw and smoothed tracking data is stored in the data structure 'Tracking' for future reference.

Metric Calculations

To increase the diversity of metrics that can be used to build heuristics, BehaviorDEPOT also calculates additional keypoints defined as the weighted averages of multiple body parts. The raw and smoothed tracking data for calculated points are included in the 'Tracking' structure generated by BehaviorDEPOT (Supplementary File 1). For each keypoint, BehaviorDEPOT calculates the linear (cm/s) and angular (deg/s) velocity, acceleration cm/s2), and linear (cm) and angular (deg) distance moved since the previous frames. All of these data, along with distance travelled throughout the entire section are stored in the 'Metrics' MATLAB structure (Supplementary File 2) that is saved automatically for future reference. Metrics and Tracking are then imported by heuristics and spatial tracking functions.

Behavior Analysis Functions

Velocity-based freezing heuristic

This heuristic imports the Metrics structure and identifies frames in which the linear velocity of the back is below a specified threshold value (default is 0.59cm/sec) and angular velocity of the head is below a specified threshold value (15deg/sec). If it meets these requirements, a frame will be labeled as 'freezing'. To smooth over falsely non-contiguous freezing bouts, a sliding window of a specified width produces a convolved freezing vector in which each value represents the number of freezing frames visible in the window at a given frame. An adjustable count threshold then converts the convolved freezing vector into the final binary freezing vector. Finally, the heuristic rejects freezing bouts that are shorter than a user-defined minimum duration. The default value is 0.9 seconds, a definition that draws on published literature56 and was tested empirically to give the most cohesiveness with human raters. Freezing data is saved framewise as a binarized vector that is the length of the video (Behavior.Freezing.Vector) and boutwise, indicating the start and stop frames of each freezing bout (Behavior.Freezing.Bouts), the length of each bout (Behavior.Freezing.Length) as well as the total number of bouts (Behavior.Freezing.Count).

Jitter-based freezing detection Heuristic

To ensure that BehaviorDEPOT will be able to detect freezing for a wide variety of videos and DLC networks, we generated a second freezing heuristic with a different design. As an alternative to the heuristic based on velocity thresholds, we generated a second freezing heuristic that uses a MATLAB changepoint function to find frames at which the mean of the data changes most significantly and then separate frames into groups that minimize the sum of the residual (squared) error from the local mean. The heuristic imports the velocities of the head, nose and tail from the Metrics structure. Users set the error term, which is calculated based on

the estimated max linear velocity for freezing. This minimum residual threshold is ultimately determined by the DLC tracking error, or the ‘jitter’ of keypoint estimates.

Novel Object Exploration Heuristic

The object exploration heuristic was developed to automate quantification of object investigation. Animal pose and behavior criteria corresponding to object investigation were developed from multiple sources (Ennaceur et al.,1988; Leger et al., 2013; Vogel-Ciernia, A. & Wood. M.A., 2014; Zeidler et al., 2020). Key features of behavioral criteria were replicated in the heuristic: A) nose within an extended boundary from the object (customizable but tested with 2cm radius), B) head oriented directly toward the object (as determined by a line from between the ears extending out past the nose), C) an exclusionary criteria for climbing on or over the object, created by establishing a smaller boundary within the original object perimeter (customizable but tested at 2cm from object edge) that rejects any instance in which the nose, ears, or tailbase is within the boundary. To achieve these features, tracking of ears, nose, and tailbase is required. The object exploration heuristic was manually fit to two different exploration sessions using two different objects: a rectangular, blue, plastic object with a flat top that encouraged climbing (6.5 x 5.5 x 8.5 cm) and a round, dark, glass bottle with a curved top that discouraged climbing (5.5 cm diameter, 13 cm height). The heuristic was validated using BehaviorDEPOT Inter-Rater and Validation modules, comparing the precision, recall, specificity, and F1 scores between heuristic output to an expert human rater across four new videos that were not used to develop the heuristic.

EPM Analysis Function

The Elevated Plus Maze analysis function prompts users to define task-relevant ROIs (open arms, closed arms, and center), then calculates the number of entries, total time spent, and percentage time spent in each ROI. The heuristic outputs boutwise and framewise information

about when the subject was in each ROI, as well as a report summarizing the results of the session.

Open Field Test Analysis Function

This function prompts the user to define the arena perimeter and the center region. It then calculates the number of entries, total time spent, and percentage time spent in each ROI along with a summary report.

T-Maze Analysis Function

To analyze T-maze data, we first analyzed the behavior videos using the Analysis Module, drawing 8 ROIs (approach, choice, effortR, effortL, rewardR, rewardL, foodCupL and foodCupR). The VTE heuristic imports data structures produced by the Analysis Module (Params, Metrics, Behavior) and extracts trials. Trial start is defined as when the midback point enters the approach zone and trial end is defined as when the midback point enters the reward zone. For each trial, the heuristic determines the choice the animal made based whether it entered the left reward or the right reward zone.

VTE Heuristic

Instances of vicarious trial and error are characterized by sweeps of the head and longer times in the choice zone. The VTE heuristic identifies sequences of frames in the choice zone when the head angles span 180 degrees. It imports outputs from the Analysis Module (Metrics, Params, and Behavior) and uses the intersection of Metrics.degHeadAngle and the Choice zone ROI to and detect ranges of head angles when the animal was in the choice zone. If the opposing head angles are detected within the choice zone in a single trial, this is counted as a head turn. Trials in which the animal spends at least 0.6s in the choice zone and has at least 1 head turn aligned best with human annotations of VTE so the heuristic uses those values and

the minimum criterion for VTE detection. This code is available for download from our GitHub repository.

Heuristic Development Modules

The Inter-Rater Module

This module compares annotations from any number of raters. Human annotations can be generated using any software of the experimenters choosing and organized in a 3-column csv file (column 1: bout start, column 2: bout stop, column 3: behavior label). The csv file can be converted to a BehaviorDEPOT-friendly MATLAB table using the helper function ‘Convert Human Annotations’ which is accessible via BehaviorDEPOT’s graphical interface. The Inter-Rater Module imports the resulting ‘hBehavior.mat’ files and provides visual summaries of rater agreement and disagreement, and reports precision, recall, F1 and specificity in both heatmap and tabular (iR_Results.mat) formats.

The Data Exploration Module

The data exploration module imports the data structures produced by the Analysis Module (Tracking, Params, Metrics, Behavior) and accompanying references annotations as a ‘hBehavior.mat’ table, which can be generated using the helper function from the graphical interface. Although this function is called ‘convertHumanAnnotations’, it can be used to convert boutwise annotations from any source into a MATLAB table that can be imported by BehaviorDEPOT. In focused mode, researchers can use their intuition or established definitions of behavior to select pairs of metrics to explore. The module reports metric values in behavior containing and behavior-lacking frames in the form of histograms and box plots and a text file (Results.txt) containing descriptive statistics for the plots. A GLM model is also produced which reports the predictive value of combinations of threshold levels for the two metrics. Users can iteratively examine as many metrics as they please. Once they have settled on features and

threshold values, users can use our template script to incorporate the new heuristic into the analysis module.

The broad exploration mode allows researchers to explore the predictive quality of different metrics in an unbiased way. It incorporates all metrics into a GLM and then rejects those with very low predictive value. The resulting refined GLM can be incorporated into the Analysis Module using our heuristic template file.

Optimization and Validation Modules

The optimization and validation modules import the data structures produced by the Analysis Module and reference annotations in 'hBehavior.mat' format. They output heatmaps and results tables reporting precision, recall, F1 and specificity values.

The Experiment Module

The Fear Conditioning Experiment Designer is a MATLAB-based GUI to design and execute cued fear conditioning experiments. It uses an Arduino interface to control commercially available, transistor-transistor logic (TTL)-based equipment. Stimuli are designed to be either auditory or visual. Auditory stimuli can be pure tones or frequency modulated (FM) sweeps. The FM sweeps can be customized for start frequency, end frequency, and sweep duration. Both pure tones and FM sweeps are generated via sine waves in MATLAB, then played through the computer or attached speaker using the sound function. Visual stimuli are generated by sending a timed TTL pulse corresponding to the light pattern. Pure light turns on the TTL for length of the stimulus; pulsed light turns on and off the TTL at a user specific frequency with a user specified duty cycle.

The user builds an experiment in event blocks. Each event can include any permutation of the conditioned stimuli (CS+ or CS-), the shock, and the laser. If a shock is triggered, it is designed to co-terminate with the conditioned stimulus (CS). If a laser is triggered, it occurs for the

duration of the CS. Inter-block intervals are randomly chosen between the minimum and maximum values input by the user.

Once the user sets up the event blocks and launches the experiment, a baseline period prior to starting the events begins (if instructed). Afterward, the first event is implemented. This is handled by cycling through a matrix of the events. Each event combination is given a unique identifier, and each identifier has its own implementation function. Within each function, the event is triggered (sound generation or TTL-adjusting), and the timestamp is logged. Timestamps record the system block to the millisecond. For blocks with multiple events (e.g. laser-TTL plus tone plus shock), these are handled sequentially. The pause function is used to time the period between event-on and event-off times.

A countdown of events is shown on screen as each event is being done and completed. Once all events have completed, a file is saved (as 'NAME_YYYY-MM-DD-HH-MM-SS') containing the complete set of experimental information, including identities and parameters of the stimuli, the events and their associated timestamps, and a log of the events delivered in that session.

MiniCAM Instructions and Installation

Descriptions of fabrication and use of MinCAMs can be found on GitHub: https://github.com/Aharoni-Lab/MiniCAM.

REFERENCES

Anagnostaras, S. G., Craske, M. G. & Fanselow, M. S. Anxiety: at the intersection of genes and experience. Nat. Neurosci. 2, 780–782 (1999). doi.org/10.1038/12146

Anagnostaras, S. G., Josselyn, S. A., Frankland, P. W. & Silva, A. J. Computer-assisted behavioral assessment of Pavlovian fear conditioning in mice. Learn. Mem. 7, 58–72 (2000). doi.org/10.1101/lm.7.1.58

Anagnostaras, S. G., Wood, S. C., Shuman, T., Cai, D. J., Leduc, A. D., Zurn, K. R., Zurn, J. B., Sage, J. R., & Herrera, G. M. (2010). Automated assessment of pavlovian conditioned freezing and shock reactivity in mice using the video freeze system. Frontiers in Behavioral Neuroscience, 4, 158. https://doi.org/10.3389/fnbeh.2010.00158

Bailey, M. R., Simpson, E. H. & Balsam, P. D. Neural substrates underlying effort, time, and risk-based decision making in motivated behavior. Neurobiol. Learn. Mem. 133, 233–256 (2016). doi.org/10.1016/j.nlm.2016.07.015

Barretto, R. P. J., Messerschmidt, B. & Schnitzer, M. J. In vivo fluorescence imaging with high-resolution microlenses. Nat. Methods 6, 511–512 (2009). doi.org/10.1038/nmeth.1339

Bohnslav, J. P. et al. DeepEthogram, a machine learning pipeline for supervised behavior classification from raw pixels. Elife 10, (2021). doi.org/10.7554/eLife.63377

Branson, K., Robie, A. A., Bender, J., Perona, P. & Dickinson, M. H. High-throughput ethomics in large groups of Drosophila. Nat. Methods 6, 451–457 (2009). doi.org/10.1038/nmeth.1328

Bravo-Rivera, C., Roman-Ortiz, C., Montesinos-Cartagena, M. & Quirk, G. J. Persistent active avoidance correlates with activity in prelimbic cortex and ventral striatum. Front. Behav. Neurosci. (2015) doi:10.3389/fnbeh.2015.00184.

Cai, D. J., Aharoni, D., Shuman, T., Shobe, J., Biane, J., Song, W., Wei, B., Veshkini, M., La-Vu, M., Lou, J., Flores, S. E., Kim, I., Sano, Y., Zhou, M., Baumgaertel, K., Lavi, A., Kamata, M., Tuszynski, M., Mayford, M., … Silva, A. J. (2016). A shared neural

ensemble links distinct contextual memories encoded close in time. Nature, 534(7605), 115–118. https://doi.org/10.1038/nature17955

Cleveland, W. S. LOWESS: A Program for Smoothing Scatterplots by Robust Locally Weighted Regression. Am. Stat. 35, 54 (1981). doi.org/10.2307/2683591

Corcoran, K. A. & Quirk, G. J. Activity in prelimbic cortex is necessary for the expression of learned, but not innate, fears. J. Neurosci. 27, 840–844 (2007). doi.org/10.1523/JNEUROSCI.5327-06.2007

Dana, H., Sun, Y., Mohar, B., Hulse, B. K., Kerlin, A. M., Hasseman, J. P., Tsegaye, G., Tsang, A., Wong, A., Patel, R., Macklin, J. J., Chen, Y., Konnerth, A., Jayaraman, V., Looger, L. L., Schreiter, E. R., Svoboda, K., & Kim, D. S. (2019). High-performance calcium sensors for imaging activity in neuronal populations and microcompartments. Nature Methods, 16(7), 649–657. https://doi.org/10.1038/s41592-019-0435-6

Diehl, M. M., Iravedra-Garcia, J. M., Morán-Sierra, J., Rojas-Bowe, G., Gonzalez-Diaz, F. N., Valentín-Valentín, V. P., & Quirk, G. J. (2020). Divergent projections of the prelimbic cortex bidirectionally regulate active avoidance. eLife, 9, e59281. https://doi.org/10.7554/eLife.59281

Ennaceur, A. & Delacour, J. A new one-trial test for neurobiological studies of memory in rats. 1: Behavioral data. Behav. Brain Res. 31, 47–59 (1988). doi.org/10.1016/0166-4328(88)90157-x

Fanselow, M. S. & Bolles, R. C. Naloxone and shock-elicited freezing in the rat. J. Comp. Physiol. Psychol. 93, 736–744 (1979). doi.org/10.1037/h0077609

Fanselow, M. S. Shock-induced analgesia on the formalin test: effects of shock severity, naloxone, hypophysectomy, and associative variables. Behav. Neurosci. 98, 79–95 (1984). doi.org/10.1037//0735-7044.98.1.79

Frankland, P. W., Bontempi, B., Talkton, L. E., Kaczmarek, L. & Silva, A. J. The Involvement of the Anterior Cingulate Cortex in Remote Contextual Fear Memory. Science. 304, 881–883 (2004). doi.org/10.1126/science.1094804

Geuther, B. Q., Deats, S. P., Fox, K. J., Murray, S. A., Braun, R. E., White, J. K., Chesler, E. J., Lutz, C. M., & Kumar, V. (2019). Robust mouse tracking in complex environments using neural networks. Communications Biology, 2, 124. https://doi.org/10.1038/s42003-019-0362-1

Geuther, B. Q., Peer, A., He, H., Sabnis, G., Philip, V. M., & Kumar, V. (2021). Action detection using a neural network elucidates the genetics of mouse grooming behavior. eLife, 10, e63207. https://doi.org/10.7554/eLife.63207

Ghosh, K. K., Burns, L. D., Cocker, E. D., Nimmerjahn, A., Ziv, Y., Gamal, A. E., & Schnitzer, M. J. (2011). Miniaturized integration of a fluorescence microscope. Nature Methods, 8(10), 871–878. https://doi.org/10.1038/nmeth.1694

Giustino, T. F. & Maren, S. The Role of the Medial Prefrontal Cortex in the Conditioning and Extinction of Fear. Front. Behav. Neurosci. 9, 1–20 (2015). doi.org/10.3389/fnbeh.2015.00298

Graving, J. M., Chae, D., Naik, H., Li, L., Koger, B., Costelloe, B. R., & Couzin, I. D. (2019). DeepPoseKit, a software toolkit for fast and robust animal pose estimation using deep learning. eLife, 8, e47994. https://doi.org/10.7554/eLife.47994

Grossen, N. E. & Kelley, M. J. Species-specific behavior and acquisition of avoidance behavior in rats. J. Comp. Physiol. Psychol. 81, 307–310 (1972). doi.org/10.1037/h0033536

Hampel, F. R. The Influence Curve and its Role in Robust Estimation. J. Am. Stat. Assoc. 69, 383–393 (1974). doi.org/10.1080/01621459.1974.10482962

Hong, W., Kennedy, A., Burgos-Artizzu, X. P., Zelikowsky, M., Navonne, S. G., Perona, P., & Anderson, D. J. (2015). Automated measurement of mouse social behaviors using depth sensing, video tracking, and machine learning. Proceedings of the National Academy of

Sciences of the United States of America, 112(38), E5351-5360. https://doi.org/10.1073/pnas.1515982112

Hsu, A. I. & Yttri, E. A. B-SOiD, an open-source unsupervised algorithm for identification and fast prediction of behaviors. Nat. Commun. 12, 1–13 (2021). doi.org/10.1038/s41467-021-25420-x

Jercog, D., Winke, N., Sung, K., Fernandez, M. M., Francioni, C., Rajot, D., Courtin, J., Chaudun, F., Jercog, P. E., Valerio, S., & Herry, C. (2021). Dynamical prefrontal population coding during defensive behaviours. Nature, 595(7869), 690–694. https://doi.org/10.1038/s41586-021-03726-6

Kabra, M., Robie, A. A., Rivera-Alba, M., Branson, S. & Branson, K. JAABA: interactive machine learning for automatic annotation of animal behavior. Nat. Methods 10, 64–67 (2013). doi.org/10.1038/nmeth.2281

La-Vu, M., Tobias, B. C., Schuette, P. J. & Adhikari, A. To Approach or Avoid: An Introductory Overview of the Study of Anxiety Using Rodent Assays. Front. Behav. Neurosci. 14, (2020). doi.org/10.3389/fnbeh.2020.00145

Ledoux, J. E. Emotion circuits in the brain. Annu. Rev. Neurosci. 155–184 (2000). doi.org/10.1146/annurev.neuro.23.1.155

Leger, M., Quiedeville, A., Bouet, V., Haelewyn, B., Boulouard, M., Schumann-Bard, P., & Freret, T. (2013). Object recognition test in mice. Nature Protocols, 8(12), 2531–2537. https://doi.org/10.1038/nprot.2013.155

Lu, J., Li, C., Singh-Alvarado, J., Zhou, Z. C., Fröhlich, F., Mooney, R., & Wang, F. (2018). MIN1PIPE: A Miniscope 1-Photon-Based Calcium Imaging Signal Extraction Pipeline. Cell Reports, 23(12), 3673–3684. https://doi.org/10.1016/j.celrep.2018.05.062

Luo, L., Callaway, E. M. & Svoboda, K. Genetic Dissection of Neural Circuits: A Decade of Progress. Neuron (2018) doi:10.1016/j.neuron.2018.03.040.

Mahn, M., Gibor, L., Patil, P., Cohen-Kashi Malina, K., Oring, S., Printz, Y., Levy, R., Lampl, I. & Yizhar, O. High-efficiency optogenetic silencing with soma-targeted anion-conducting channelrhodopsins. Nat. Commun. 9, 4125 (2018). doi.org/10.1038/s41467-018-06511-8

Mathis, A., Mamidanna, P., Cury, K.M., Abe, T., Murthy, V. N., Mathis, M.W. & Bethge, M. DeepLabCut: markerless pose estimation of user-defined body parts with deep learning. Nat. Neurosci. 21, (2018). doi.org/10.1038/s41593-018-0209-y

Neunuebel, J. P., Taylor, A. L., Arthur, B. J. & Egnor, S. E. R. Female mice ultrasonically interact with males during courtship displays. Elife 4, e06203 (2015). doi.org/10.7554/eLife.06203

Nilsson, S. R. O. et al. Simple Behavioral Analysis (SimBA) – an open source toolkit for computer classification of complex social behaviors in experimental animals. bioRxiv 2020.04.19.049452 (2020) doi:10.1101/2020.04.19.049452.

Noldus, L. P. J. J., Spink, A. J. & Tegelenbosch, R. A. J. Ethovision Video Tracking System. Behav. Res. Methods, Instruments, Comput. 33, 398–414 (2001). doi.org/10.1016/S0031-9384(01)00530-3

Nomoto, K. & Lima, S. Q. Enhanced Male-Evoked Responses in the Ventromedial Hypothalamus of Sexually Receptive Female Mice. Curr. Biol. 25, 589–594 (2015). doi.org/10.1016/j.cub.2014.12.048

Ohayon, S., Avni, O., Taylor, A. L., Perona, P. & Roian Egnor, S. E. Automated multi-day tracking of marked mice for the analysis of social behaviour. J. Neurosci. Methods 219, 10–19 (2013). doi.org/10.1016/j.jneumeth.2013.05.013

Pennington, Z. T., Dong, Z., Feng, Y., Vetere, L. M., Page-Harley, L., Shuman, T., & Cai, D. J. (2019). ezTrack: An open-source video analysis pipeline for the investigation of animal behavior. Scientific Reports, 9(1), 19979. https://doi.org/10.1038/s41598-019-56408-9

Pereira, T. D., Aldarondo, D. E., Willmore, L., Kislin, M., Wang, S. S.-H., Murthy, M., & Shaevitz, J. W. (2019). Fast animal pose estimation using deep neural networks. Nature Methods, 16(1), 117–125. https://doi.org/10.1038/s41592-018-0234-5

Perusini, J.N. & Fanselow, M.S. Neurobehavioral perspectives on the distinction between fear and anxiety. Learn. Mem. 9, 417-425 (2015). doi: 10.1101/lm.039180.115

Phillips, M. L., Robinson, H. A. & Pozzo-Miller, L. Ventral hippocampal projections to the medial prefrontal cortex regulate social memory. Elife 8, e44182 (2019). doi.org/10.7554/eLife.44182

Pollack, G. A., Bezek, J. L., Lee, S. H., Scarlata, M. J., Weingast, L. T., & Bergstrom, H. C. (2018). Cued fear memory generalization increases over time. Learning & Memory (Cold Spring Harbor, N.Y.), 25(7), 298–308. https://doi.org/10.1101/lm.047555.118

Redish, A. D. Vicarious trial and error. Nat. Rev. Neurosci. 17, 147–159 (2016). doi.org/10.1038/nrn.2015.30

Sangiamo, D. T., Warren, M. R. & Neunuebel, J. P. Ultrasonic signals associated with different types of social behavior of mice. Nat. Neurosci. 23, 411–422 (2020). doi.org/10.1038/s41593-020-0584-z

Segalin, C., Williams, J., Karigo, T., Hui, M., Zelikowsky, M., Sun, J. J., Perona, P., Anderson, D. J., & Kennedy, A. (2021). The Mouse Action Recognition System (MARS) software pipeline for automated analysis of social behaviors in mice. eLife, 10, e63720. https://doi.org/10.7554/eLife.63720

Shuman, T., Aharoni, D., Cai, D. J., Lee, C. R., Chavlis, S., Page-Harley, L., Vetere, L. M., Feng, Y., Yang, C. Y., Mollinedo-Gajate, I., Chen, L., Pennington, Z. T., Taxidis, J., Flores, S. E., Cheng, K., Javaherian, M., Kaba, C. C., Rao, N., La-Vu, M., … Golshani, P. (2020). Breakdown of spatial coding and interneuron synchronization in epileptic mice. Nature Neuroscience, 23(2), 229–238. https://doi.org/10.1038/s41593-019-0559-0

Sierra-Mercado, D., Padilla-Coreano, N. & Quirk, G. J. Dissociable Roles of Prelimbic and Infralimbic Cortices, Ventral Hippocampus, and Basolateral Amygdala in the Expression and Extinction of Conditioned Fear. Neuropsychopharmacology 36, 529–538 (2011). doi.org/10.1038/npp.2010.184

Stout, J. J. & Griffin, A. L. Representations of On-Going Behavior and Future Actions During a Spatial Working Memory Task by a High Firing-Rate Population of Medial Prefrontal Cortex Neurons. Front. Behav. Neurosci. 14, 1–17 (2020). doi.org/10.3389/fnbeh.2020.00151

van den Boom, B. J. G., Pavlidi, P., Wolf, C. J. H., Mooij, A. H. & Willuhn, I. Automated classification of self-grooming in mice using open-source software. J. Neurosci. Methods 289, 48–56 (2017). doi.org/10.1016/j.jneumeth.2017.05.026

Vogel-Ciernia, A. & Wood, M. A. Examining object location and object recognition memory in mice. Curr. Protoc. Neurosci. 69, 8.31.1-17 (2014). doi.org/10.1002/0471142301.ns0831s69

Xu, W. & Südhof, T. C. A neural circuit for memory specificity and generalization. Science (80-.). 339, 1290–1295 (2013). doi.org/10.1126/science.1229534

Zeidler, Z., Hoffmann, K. & Krook-Magnuson, E. HippoBellum: Acute Cerebellar Modulation Alters Hippocampal Dynamics and Function. J. Neurosci. 40, 6910–6926 (2020). doi.org/10.1523/JNEUROSCI.0763-20.2020

Chapter 3: Transformations in prefrontal ensemble activity underlying rapid threat avoidance learning

ABSTRACT

Learning to respond adaptively to threatening cues is critical to survival. The medial prefrontal cortex (mPFC) is important for adaptive decision making, including about whether to approach or avoid stimuli in the environment. One subregion of mPFC, the prelimbic cortex (PL), is associated with integration of threatening cues and their aversive outcomes. Most studies have examined relationships between mPFC activity and avoidance behavior after learning has occurred, but little is known about when these changes emerge and how they contribute to learning at the behavioral level. In this study, we recorded from ensembles of PL neurons using calcium imaging via head-mounted miniscopes. We examined single neuron dynamics and population activity states that are associated with the emergence of rapidly learned threat avoidance. Over the course of learning, we observed enhanced modulation of PL activity that represented the intersections between threatening cues and a safe location. These changes were apparent in individual neurons and in PL population dynamics. We also discovered a learning-related divergence in PL population activity surrounding conditioned tones that is linked to the learning rate of individual animals. Together our findings revealed that representations of safe and threatening locations are amongst the first to emerge in PL during learning.

INTRODUCTION

To thrive in a dynamic environment, individuals must rapidly learn new associations between threatening cues and behaviors required to prevent aversive outcomes. Once individuals learn these associations, they must then carefully balance avoiding threats with seeking beneficial outcomes. Aversive learning must occur rapidly to ensure animals survive. But the neural computations that allow individuals to rapidly and flexibly associate environmental cues with behaviors that prevent aversive outcomes are poorly understood.

The medial prefrontal cortex (mPFC) plays a key role in emotional regulation and decision-making, including about whether to approach or avoid potentially threatening stimuli (Euston et al., 2012; Giustino & Maren, 2015; Mack et al., 2024). Activity in the prelimbic subregion of mPFC (PL) encodes threatening cues and threat-induced behaviors including freezing and threat avoidance (Burgos-Robles et al., 2009; Courtin et al., 2014; Moscarello & LeDoux, 2013; Jiao et al., 2015; Diehl et al., 2018; Cummings et al., 2020). Even after a single aversive stimulus, PL can integrate emotional and contextual information regardless of the resulting behavior (Zelikowsky et al., 2014). PL bidirectionally influences approach and avoidance behaviors through divergent outputs to the ventral striatum and basolateral amygdala, respectively (Diehl et al., 2020).

In well-trained mice, threat avoidance behavior is associated with inhibition of PL firing (Diehl et al., 2018), including in PL neurons that project to the basolateral amygdala (Kajs et. al., 2022). Population decoding approaches revealed that PL activity before avoidance actions accurately predicted whether mice would successfully avoid aversive outcomes (Jercog et al., 2021). While these studies show that PL is a key player in learned threat avoidance, how the necessary ensemble dynamics arise during learning is poorly understood.

We used miniscopes (Ghosh, et al. 2011; Cai et al., 2016) to record Ca^{2+} activity simultaneously from hundreds of PL neurons as mice successfully learned platform mediated avoidance (PMA), in which a conditioned tone prompts mice to navigate to a safety platform.

We compared PL ensemble activity across PMA training with PL activity in non-shocked control mice. During learning, we observed emergent changes in the encoding of the safety platform location. PL neurons that encoded avoidance actions were increasingly modulated by the presence of the threatening tone. By the first day of PMA training, a support vector machine trained on PL activity during conditioned tones could accurately decode trial outcomes. By combining a Rescorla-Wagner model of PMA behavior with analysis of PL population activity, we discovered that the distance between population vectors on successful vs. unsuccessful trials was highly correlated with the learning rates. These changes were not observed in non-shocked controls, indicating that avoidance learning generates novel PL representations of whether mice had taken avoidance vs. exploratory actions, and novel links between cues and actions.

RESULTS

Mice rapidly learn PMA

To examine neural correlates of avoidance learning, we used miniscopes to record Ca^{2+} activity from ensembles of PL neurons as animals learned PMA. We injected PL with an AAV vector encoding GCaMP7f under the control of the human synapsin promoter (Dana et al., 2019). We then implanted a GRIN lens above PL and installed a miniscope baseplate. Mice underwent an extensive habituation protocol before beginning PMA training (Figure 1A). All mice were trained for 2 days in PMA (Figure 1B). On day 1, animals were given 12 tone presentations. The first 3 tones were presented without co-terminating shocks to assess baseline tone responses from the recorded cells. The remaining 9 tones co-terminated with a mild 2-second foot shock. On day 2, all 12 tones were paired with shock. To determine whether observed changes in neural dynamics were due to learning vs. the passage of time or exposure to novel tones, we compared PL activity to non-shock control mice that underwent the same procedures without receiving any foot shocks.

We tracked mouse behavior using automated approaches (Figure 1C,D; Mathis et al., 2018; Gabriel et al., 2022) and quantified several behavioral metrics across days. We defined successful trials as those when mice entered the platform before the beginning of the shock and remained on the platform for the duration of the shock period (i.e., until the end of the tone). Experimental mice exhibited a steady increase in the proportion of successful trials on day 1 and exhibited significantly higher proportion of successful trials compared to non-shocked controls by the end of day 1 and for all of day 2 (Figure 1E). On day 1, during presentations of the tone, experimental and control mice spent a similar proportion of time on platform during the tone and a similar proportion of time freezing, with differences emerging by the end of day 1 (Figure 1F,G). Mice in both groups had a comparable latency to enter the platform (Figure 1S). To assess how learning impacted PL activity, we performed *in vivo* microendoscopic calcium imaging of PL neurons during both sessions (Figure 1H-J). After imaging, we extracted calcium signals associated with individual neurons using a constrained non-negative matrix factorization algorithm (Dong et al., 2022) and analyzed single neuron and population level activity patterns. We recorded a total of 1394 PL neurons across 9 shocked animals, and 967 PL neurons across 7 non-shocked animals.

Avoidance learning-dependent changes in single neuron encoding properties in PL

To determine whether and when individual PL neurons selectively encode features of PMA (tone, platform, freezing), we computed a receiver operating characteristic (ROC) curve for each neuron's response to each feature (Figure 2A,B; Li et al., 2017; Kingsbury et al., 2019) during three epochs: baseline period of day 1 (tones 1-3), end of day 1 (tones 9-12), and end of day 2 (tones 9-12). In both shocked and non-shocked mice, we observed neurons that were tuned to each feature we examined, with both excited cells exhibiting increased activity and inhibited cells exhibiting decreased activity during features of interest (Figure 2C).

To determine to what extent PL activity changes across learning, we calculated the mean activity levels for all cells in each category and compared across days in shocked vs. non-shocked control mice (Figure 2D). There were no significant differences in the amplitude of responses to tone onset or offset during either day of training for shocked or non-shocked mice (Figure $2D_1$). While we observed few differences in the cell activity during freezing onset, we observed a learning-dependent sharpening of freezing offset-related activity across days. In shocked mice, activity returned to baseline faster following freezing offset by the second day of PMA (Figure $2D_2$). While we observed no differences in activity during platform entries, we observed a large learning-dependent increase in activity during platform exits. On day 1 of PMA, in shocked mice, a subset of PL neurons ('platform exit' neurons) exhibited persistently elevated activity that lasted ~4 seconds following platform exits. In contrast, activity in the corresponding population of neurons in non-shocked mice rapidly decayed following platform exits (Figure $2D_3$). By day 2, shocked mice had significant ramping activity that preceded platform exits and reached a significantly higher peak compared to day 1 and to non-shocked controls (Figure $2D_3$). These data suggest that representations of spatial threat levels quickly emerge in the encoding properties of individual PL neurons during learning.

We next investigated whether the proportion of neurons encoding different features of PMA may change across learning. In each stage of learning, the fraction of behaviorally modulated cells in PL was similar between groups. In shocked animals, we observed a modest increase from 32 to 39% significantly modulated PL neurons. Non-shocked mice were similar, also showing a modest increase from 34 to 36% modulated PL neurons across days (black and grey circles, Figure 2E). However, we observed a large learning-dependent increase in the proportion of PL neurons that exhibited mixed selectivity, encoding multiple behavioral relevant features including the tone, the safety platform, and freezing behavior. By day 2 of PMA training, PL neurons that exhibited mixed selectivity represented 51% of the significantly modulated PL cells in shocked mice (i.e., ~20% of the overall recorded neurons) but only 25% of the

significantly modulated PL neurons in non-shocked mice (~9% overall recorded cells) (Figure 2E). Examining these mixed cells more closely, we determined that these differences were driven by cells tuned to both platform and freezing as well as cells responding to all three event types (Figure 2F).

PMA drives enhanced modulation of tone and platform responses

The increase in PL neurons exhibiting mixed-selectivity suggested to us that learning results in enhanced tuning of cells to threatening cues and the behavioral features of PMA. To test this, we quantified how strongly cells were modulated based on the intersection of avoidance actions and conditioned stimuli (Figure 3A,B). Cumulative frequency histograms of area under the ROC curve (auROC) values were constructed from responsive neurons for each animal and used to extract a measurement of overall modulation levels. These analyses include cells that significantly increased and decreased their activity – highly modulated cells exhibited larger increases or decreases in activity, respectively, during presentations of the tone. The modulation score is derived from the absolute value of the auROC, so neurons modulated in either direction will have a higher value.

On day 1, neurons encoding platform entries and exits had significantly increased modulation during tone periods compared to inter-trial intervals (ITIs) (Figure 3C,D). But this effect was evident in both shocked and non-shocked mice, suggesting it was not a feature of learning. During tone periods on day 2, activity during platform entries (towards safety) and especially during platform exits (towards threat) was more strongly modulated in shocked animals compared to controls (Figure 3C,D).

In a complementary set of analyses, we examined how strongly tone-evoked activity was modulated based on the animal's location. We separated tone onset and offset responses based on whether the animal was on or off the platform during the event. Non-shocked mice did not exhibit location-dependent modulation of tone-onset activity on either day. Shocked mice

exhibited no spatial modulation of the tone onset responses on day 1. But a difference emerged on day 2 wherein tone onset responses were more highly modulated when the animal was off the platform when threat levels were high (Figure 3E). In shocked mice, tone offset responses were significantly enhanced when animals were off the platform, which corresponded to failed trials in which the animal received a foot shock (Figure 3F).

Enhanced trial outcome decoding is facilitated by PMA modulated cells

As mice learn to avoid the shock, the tone becomes both a predictor of shock and a signal to avoid. Recent work showed that in well-trained mice, PL activity immediately preceding the avoidance movement in a shuttle box could predict whether animals would successfully avoid the foot shock (Jercog et al., 2021). Thus, we wondered if neural activity during the tone could be used to predict the outcome of that trial in the early stages of learning and if so, which neurons contributed to the predictive power. To assess the encoding of activity patterns related to learning, we trained support vector machines (SVMs; Awad & Khanna, 2015) to decode the activity from neurons for each animal. We first assessed the performance when all recorded cells were used for decoding using the F1 score, which reports the harmonic mean of precision and recall. We found significant improvements in outcome decoding as the tone progressed in shocked animals and this effect was absent in control animals (Figure 4A). Decoding performance during the pre-shock period (23-28s after tone onset) and during the shock period (27-32s after tone onset) was significantly enhanced for shocked mice.

We asked if behaviorally modulated cells identified by ROC analysis were major contributors to decoding performance. To assess the contribution of these cell groups, we repeated the decoding analysis again, using only cells that were significantly modulated by features of PMA in the ROC analyses (Figure 2). When we performed decoding using only these behaviorally modulated cells, we saw lower variance in decoder performance and more reliable differences between shocked and control groups (Figure 4B). Using the behaviorally

modulated subset of cells, the activity during the pre-shock period (23-28s after tone onset), the shock period (27-32s after tone onset), and the post-shock period (33-38s after tone onset) was significantly better able to decode the trial outcome compared to non-shocked controls (Figure 4B).

We also wondered if cells that were not behaviorally modulated would contribute less to decoding performance. We repeated the decoding a third time and only included the non-modulated cells in the decoding. Though there were trend-level differences between shocked and control group performance, there were no significant differences during any of the periods examined (Figure 4C).

Tone Onset Response is Enhanced in the Population Activity of Shocked Mice

In PL, aspects of cues and behaviors can be distinctly encoded in the activity of individual neurons vs. in the larger population. We investigated how PL population codes evolve across learning and how changes in population activity relate to learning rates. To do so, we used a dimensionality reduction algorithm, calcium imaging linear dynamical system (CILDS, Koh et al., 2023), to extract latent variables of population activity across learning and examined their relationships with learning rates that we estimated using a Rescorla-Wagner model of PMA behavior.

Using CILDS, we extracted 3 latent variables for each day of training and quantified the average framewise Euclidean distance for trial trajectories across time (Figure 5A,C). We hypothesized that patterns of activity would shift following salient behavioral events. We examined how population activity changed after the first foot shock of each session, after the first successful trial of each session, and after the trial that marked the beginning of a pattern of successful avoidance. To assess how much each event modified PL activity, we computed the distance between the population vector for the event trial and the previous trial (V_n-V_{n-1}) and compared it to the distance between the event trial and the subsequent trial (V_n-V_{n+1}). We

focused on activity during two key epochs: at the onset of the tone and in the pre-shock period (23-28s after tone onset) when we observed a significant increase in trial outcome decoding (Figure 4).

On the first day of PMA training, we analyzed population activity aligned to the onset of the conditioned tone. We observed no significant changes in population vectors after foot shocks or at the onset of a reliable avoidance strategy (Figure $5B_{1,2}$). On the other hand, when trials were anchored to the first shock received on day 2, we saw a pattern emerge in which similar pre-event activity gave way to a shift in population activity on the following trial (Figure $5B_3$). Tone-evoked population vectors in non-shocked control mice had no reliable differences at any point examined. This suggests that once an avoidance strategy is learned, but not before, experiencing a foot shock drives significant reorganization of cue-evoked population activity in PL.

During the pre-shock epoch (23-28s after tone onset), we observed no shifts in population activity following the foot shocks on either day of PMA (Figure $5D_{1,3}$). However, once the animal adopted a consistent avoidance strategy, the trial-to-trial Euclidean distances in the same epoch were lower than in non-shocked mice (Figure $5D_2$). On Day 2, most mice had higher inter-trial Euclidean distances around the trial when they experienced a foot shock, which represented a deviation from their previously learned behavioral strategy. This suggests that in the seconds preceding the foot shock, a reliable pattern of PL population activity arises as a function of learning and is associated with a reliable pattern of threat avoidance behavior.

Aspects of PL population activity during conditioned tones are correlated with individual learning rates

Our CILDS-based analyses suggested that changes in population activity during specific epochs of the conditioned tone are associated with different aspects of learning. When animals had learned the predictive relationships between cues, shocks, and avoidance actions and then

experienced a foot shock, we observed significant changes in PL population activity at the onset of the cue. On the other hand, we observed the most stable patterns of PL population activity during the pre-shock epoch when mice established a reliable avoidance strategy on the first day of PMA. We hypothesized that learning-driven changes in population activity may relate to learning rates in individual mice.

To investigate this, we developed a Rescorla-Wagner (RW) model (Rescorla & Wagner, 1972) of mouse behavior during PMA (Figure 6A) and used it to estimate individual learning rates. After model fitting, we realized that PMA learning was better modeled by a complementary set of learning rates, which modeled improvements due to received foot shocks versus avoided foot shocks (Figure 6B). We then calculated the Euclidean distance between the PL population vectors in different epochs of the tone on averaged shock vs. successful trials (Figure 6C). We examined the correlations between these Euclidean distances and the learning rate extracted from the RW model for each mouse. The Euclidean distance between shocked vs. successful trials was positively correlated with learning rates for the tone onset and shock epochs but not for the pre-shock epoch (Figure $6D_{1–3}$). These patterns held true on both days of PMA for shocked mice and were absent in non-shocked mice. This suggests that the ability of PL population activity at cue onset to distinguish between successful vs. shock trials is a signature of learning that persists to support the learned behavioral strategy.

DISCUSSION

Learning to connect predictive cues with adaptive actions is critical for survival, especially when cues predict threats. Most research on aversive learning has focused on conditioned fear or threat avoidance in well-trained animals. These studies revealed that PL neurons encode threat-predictive cues and threat avoidance behaviors and that PL activity is required to actively avoid signaled threats (Giustino & Maren, 2015; Diehl et al., 2020; Jercog et al., 2021). But how the underlying neural computations emerge during associative

learning remains poorly understood. What are the first changes to emerge in PL as animals begin learning to avoid signaled threats? Which changes in PL activity are related to learning vs. the implementation of new behavioral strategies?

Here we combined the PMA behavioral assay with miniscope recordings to identify the transformations in PL activity as animals learn to preemptively avoid signaled threats (Figure 1). We discovered distinct changes in PL single neuron and population activity patterns that emerged early in learning vs. later, once behavioral performance stabilized. We then uncovered how changes in PL population activity correspond to individual learning rates that we estimated using a Rescorla-Wagner model of PMA behavior.

Models of learned threat avoidance behaviors

Many previous studies of threat avoidance used two-way active avoidance, in which animals can avoid experiencing a signaled foot shock by shuttling to the opposite side of a chamber (Mowrer & Lamoreaux, 1946; Moscarello & LeDoux, 2013; Krypotos et al., 2015). While studies using this assay have revealed key neural mechanisms that drive cued threat avoidance behaviors, there is no consistently safe location in two-way active avoidance. In many versions of the assay, shuttling terminates the conditioned tone and the shock, though modifications to the task have been adapted to mitigate this issue (Bolles, Stokes, & Younger, 1966; Smith et al., 2002; Carmona et al., 2014). The ability to terminate the threat-predicting cue enables an unrealistic level of control over the environment.

Here we used PMA – in which there is a safe location and entering the safety platform does not terminate the conditioned tone or shock – to overcome some of these limitations and study threat avoidance under more naturalistic conditions. In PMA, mice rapidly learned the association between the tone and the shock, the location of the safety platform, and the association between conditioned cues and adaptive actions. They then improved their performance across 2 days of training (Figure 1). In PMA, mice can freely access the safety

platform during tones and ITIs, creating a unique opportunity to study how PL encodes the intersections of conditioned cues, safe locations, and threat-induced behaviors.

Learning-induced changes in PL single neuron encoding properties

Consistent with previous studies in well-trained animals (Giustino & Maren, 2015; Diehl et al., 2018; Jercog et al., 2021), we identified individual PL neurons that encoded the tone, the location of the safety platform, and freezing behavior events (Figure 2A,B). The overall proportion of significantly modulated neurons was similar in mice that learned PMA vs. non-shocked controls, indicating that changes in the number of behaviorally modulated PL neurons is not required for learning to avoid threats. On the other hand, we observed learning-induced changes in how PL encoded the intersection of cues and actions. Early in learning, on Day 1, a subset of PL neurons displayed an emergent, persistent increase in activity as animals exited the safety platform (Figure $2D_3$). These changes were absent in non-shocked mice, suggesting that representations of the spatial locations of threat and safety are some of the first to emerge in PL neurons as animals learn PMA.

We also found that learning increases the modulation of behavioral signals by conditioned cues. Our ROC analyses revealed a learning-dependent increase in the proportion of mixed selectivity PL neurons that encoded multiple features of PMA including the tone, the location of the platform, and freezing (Figure 2E,F). In line with this, as mice learned PMA, PL neurons encoding avoidance actions were increasingly modulated by the presence of conditioned cues and that tone-related activity was modulated by the location of the animal on or off the safety platform (Figure 3C-E). These changes were absent in non-shocked control mice, indicating that in PL, emergent modulation of the neural activity associated with avoidance behaviors by salient stimuli may be a key neural mechanism underlying the rapid linking of novel predictive cues with adaptive actions. As these changes did not emerge until the second day of PMA, these are likely a product of learning rather than a substrate for learning.

Learning-induced changes in PL population activity

Recent studies have revealed that some neural mechanisms underlying the defensive behavior system and other cognitive processes operate beyond the scale of single neurons, using activity patterns only present in latent activity of populations of neurons (Herry & Jercog, 2022; Sylte et al., 2024). In our data, the ability to decode the trial outcome from PL population activity during conditioned tones was already present on day 1. Consistent with previous studies (Jercog et al., 2021), we found that the activity at the onset of the conditioned tones was not an accurate predictor of trial outcome. Instead, activity immediately preceding the time of shock was a highly accurate predictor of trial outcome (Figure 4). Even though changes in individual neuron encoding properties largely emerged on day 2, decoding performance on day 1 was enhanced by using only the behaviorally modulated cells found by ROC analysis (Figures 2 and 4). This suggests that PL population activity reflects learned associations between cues, outcomes, and avoidance behaviors before learning-related changes are evident in the encoding properties of individual neurons.

Using dimensionality reduction, we identified latent variables that encode population-level activity. Using the distance between trials in latent space, we observed activity patterns that aligned with learning-relevant events. When we studied activity during the tone onset epoch, we observed that foot shocks only elicited large shifts in the population activity of subsequent trials on day 2, after mice had learned the relationships between tones, shocks, and avoidance actions (Figure 5B). This shift in tone-evoked activity may therefore reflect updating of predictive relationships between cues, actions, and outcomes following an aversive outcome. During the pre-shock epoch, we did not observe rapid shifts in population activity driven by salient events. Instead, we observed a transient stabilization of activity during pre-shock epoch on day 1 that was associated with the emergence of a reliable avoidance strategy (Figure 5D).

These findings indicate that PL population activity during different epochs has unique relationships to learning. Rapid shifts in population activity during the tone onset epoch may be

more associated with updating learned predictions after an aversive event. In contrast, PL activity during the pre-shock epochs may be more tightly tied to initial action-outcome learning. Consistent with this interpretation, studies in well trained mice also found epoch-specific functions of mPFC activity. For instance, inhibiting mPFC activity during the tone onset delayed avoidance while inhibition later in the tone decreased the probability of avoiding (Herry & Jercog, 2023).

Using R-W models of mouse behavior, we found significant positive correlations between the learning rates of individual mice and the extent to which PL population activity in the tone onset epoch distinguished between avoidance vs shock trials on both days of training (Figure $6D_1$). This was somewhat surprising as we could not decode the trial outcome from PL population activity in the same epoch (Figure 4). Nonetheless, our findings suggest that distinct patterns of cue-evoked PL population activity are associated with preemptive avoidance of predicted shocks. Further, during the pre-shock and shock periods, when decoding performance is high, we found only a significant positive correlation between the shock period of day 1 and learning rates (Figure $6D_{2\text{-}3}$). That we found few correlations during these periods where decoding performance is high is puzzling. This suggests that outcome-relevant activity during pre-shock and shock periods is relevant to learning, yet is not directly altered by it. During the tone onset, PL seems to encode associations between tones, shocks, and avoidance that are directly related to overall learning yet emerge before behavioral changes in learning.

PL subcircuits underlying aversive learning

While we recorded from the overall PL population, PL contains heterogenous neuronal classes with distinct connectivity and distinct functions (Gabbott et al., 2005; Collins et al., 2018; Anastasiades et al., 2019; Anastasiades & Carter, 2021). Previous studies have established that synchronization of firing patterns in mPFC and the basolateral amygdala (BLA) are associated with successful discrimination of threatening versus safe cues (Likhtik et al., 2014; Burgos-

Robles, et al., 2017). Bottom-up projections from BLA to mPFC provide threat representations to this region, which mPFC is thought to link with the initiation of avoidance strategies (Jercog et al., 2021). Top-down projections from mPFC to BLA enhance avoidance responses during threatening cues (Diehl et al., 2020). Using fiber photometry, previous studies showed that PL-BLA projection neurons exhibit learning-dependent increases in activity during conditioned tones and a small peak in activity that precedes avoidance actions and then rapidly declines (Kajs et al., 2022). Studies from our lab showed that in classes of PL neurons that project to contralateral PL or to the nucleus accumbens (NAc), the extent to which those neurons send collateral axons to BLA is positively correlated with the amplitude of the response to conditioned cues (Gongwer et al., 2023). Top down mPFC-BLA projection neurons exhibit preferential synaptic connectivity with bottom up BLA-mPFC neurons, forming reciprocal loops (Little & Carter, 2013; McGarry & Carter, 2017). Taken together with our studies, these data suggest that the learning-related evolution we observed in cue-evoked activity may represent an activity pattern that integrates bottom-up tone-shock representations from the amygdala with top-down signals in PL-BLA projection neurons that promote avoidance actions.

PL neurons that project to other brain regions have also been implicated in learning active avoidance strategies and may be important contributors to PL encoding patterns that we observed. One major target is the NAc, which is implicated in bidirectional control of PMA (Diehl et al., 2020). Activation of PL-NAc projections increases reward seeking behavior and reduces threat avoidance behavior during PMA (Diehl et al., 2020). But these projections contain functionally heterogeneous subpopulations. For instance, PL-NAc projection neurons that are active during aversive stimuli can suppress reward seeking in threatening situations (Kim et al., 2017). PL projections to contralateral PL (cPL) encode representations of threatening cues and threat avoidance behaviors, and projections to the ventral tegmental area (VTA) encode aversive stimuli as well as learned (but not innate) avoidance actions (Gongwer et al., 2023). mPFC projections to the dorsomedial striatum have learning-related increases in activity during

conditioned cues and avoidance actions during two-way active avoidance (Kajs et al, 2022). These studies suggest potential contributions of each of these projection types to PMA. PL-NAc neurons could contribute to modulation we observed during platform exits on day 2, either promoting risky exploration during the tone or reporting the impending danger indicated by the tone while off the safety platform (Figure 3D). PL-cPL projections may help synchronize PL activity across hemispheres or facilitate lateralized learning functions. Projections to the VTA could support activation of the DA system in response to aversive shocks and the tones that predict them. PL projections to dorsomedial striatum may facilitate activation of motor programs that lead to successful threat avoidance and could be contributing to enhanced modulation seen during platform entries that occur during the tone.

While previous studies used optogenetics and fiber photometry to identify unique functions of projection-defined PL populations, there is extensive heterogeneity within PL neurons that project to a given target (Gao et al., 2022). The question of which projection types are important to learning is complicated by the extensive collateralization of PL projections, with individual PL neurons projecting to distinct but overlapping subsets of 5–10 target regions. Future research should use miniscopes to record from projection-defined populations to better align functional and anatomical heterogeneity during aversive learning.

Potential mechanisms that drive learning

Dopamine (DA) is a neuromodulator that is strongly implicated in learning processes (Puig et al., 2014). Though DA has been well studied in the context of reward learning (Wise, 2004; Schultz, 2016), recent attention has been given to its role in aversive processing (Vander Weele et al., 2019). In fear conditioning, reductions in DA are associated with impaired fear learning (Fadok et al., 2009). Manipulation of DA neuron firing was sufficient to disrupt aversive learning (Zweifel et al, 2011). The main source of DA in cortical regions comes from afferent neurons located in the VTA, though other sources have been identified (Devoto et al., 2020).

Distinct circuits in the VTA are used for rewarding versus aversive processing, with neurons that project to mPFC more heavily associated with aversive processing (Lammel et al., 2011, 2012). DA may therefore be a critical substrate for aversive learning during PMA.

While DA release in mPFC has been linked to experience of rewarding, novel, and aversive stimuli (Bassareo et al., 2002), prefrontal DA appears to be distinctly sensitive to aversive stimuli and is important for maintenance of aversive memories (Abercrombie et al., 1989, Mantz et al., 1989; Lammel et al., 2011; Gonzalez et al., 2014). However, what contribution mPFC DA makes to aversive learning remains unclear. DA release has been found to enhance representations of aversive stimuli in mPFC-PAG projection neurons by altering the signal-to-noise in mPFC population activity (Vander Weele et al., 2018). Given mPFC DA can be released to both rewarding and aversive events, DA may preferentially target aversion-relevant projection neurons in PL and drive plasticity to enhance adaptive behavioral responses. Based on the sensitivity of mPFC DA to aversive events, we expect PL DA release is enhanced during foot shock delivery and may also be released during conditioned tones that predict shock. DA release may facilitate plasticity within mPFC subcircuits that enables the emergence of the activity states we observed that effectively link aversive cues to avoidance actions (Figures 3–6).

Responses to DA are mediated by 2 broad classes of receptors, D1-like (D1, D5) and D2-like (D2, D3, D4). In the prefrontal cortex, D1 receptors (D1Rs) are more frequently expressed than D2 receptors (D2Rs) in interneurons while pyramidal neurons can express either D1 or D2Rs (Santana et al., 2009). Within pyramidal neurons, D1Rs are primarily expressed in intratelencephalic (IT) mPFC neurons that project to the contralateral cortex, claustrum, striatum, and BLA with low expression in corticothalamic or pyramidal tract neurons (Anastasiades et al., 2019). Other studies have revealed potential links between anatomical projections and DA receptor subtypes. For instance, D4 receptor signaling in mPFC neurons that receive direct input from the BLA is critical for fear learning (Laviolette et al., 2005).

Overall, our findings and those from previous studies suggest that some signatures of learning we observed in PL are likely mediated by IT neurons, especially those involved in reciprocal communication with the amygdala. Furthermore, DA activity may drive mPFC circuit plasticity necessary to link predictive cues with avoidance actions. Future studies can examine the contributions of these anatomically and genetically defined cell populations and neuromodulatory signaling to the learning-related changes in PL activity patterns we describe here.

Altered mPFC activity and the balance of approach-avoidance in psychiatric disorders

We revealed how the relationships between cues, aversive outcomes, and the actions necessary to avoid them are encoded within patterns of mPFC activity, and how these patterns emerge with learning. Our study builds an important foundation for understanding how altered patterns of mPFC activity may give rise to maladaptive learning as well as understanding how current treatments for mental health disorders may influence mPFC activity. Thriving in a complex environment requires that individuals precisely balance avoiding threats with seeking beneficial outcomes. Disruptions in this balance are a feature of numerous psychiatric disorders. mPFC dysfunction is linked to anxiety and depression, which are characterized by excessive or inappropriate threat avoidance (Papaleo et al., 2012; Clauss et al., 2016; Wang et al, 2021; Mack et al., 2022). Dysfunction accompanying these disorders is frequently characterized by reductions in mPFC gray matter volume and hypoactivity during emotional processing (Ball et al., 2012; Zhao et al., 2014; Mochcovitch et al. 2014; Bittar & Labonté, 2021).

Elevated avoidance behaviors are also common in other disorders associated with mPFC dysfunction, such as schizophrenia and autism spectrum disorder (de la Asuncion, et al., 2015; Montaser et al., 2023). In contrast, bipolar and substance use disorders are associated with excessive reward seeking and risk-taking behaviors (Ball et al., 1994; Alloy et al., 2008; Chandler et al., 2009; Preuss et al., 2021). These disorders are also associated with changes in

mPFC: In addiction, mPFC activation is associated with cocaine craving and heroin relapse (Maas et al., 1998; Bossert et al., 2011). In bipolar patients, mPFC hypofunction was associated with global deficits in emotional cognition (Kjærstad et al., 2024).

Though avoidance studies often focus on encoding of danger, encoding of safety is also highly relevant to psychiatric disease. For instance, behaviors promoting safety can complicate treatment for anxiety and are often discouraged when they prevent interaction with threatening stimuli (Blakey & Abramowitz, 2016; Goetz et al., 2016). Here we find that representations of safe vs. threatening locations are some of the first to emerge during aversive learning. Understanding how mPFC representations of aversive cues, avoidance actions and safe locations emerge during learning can inform how imbalance in approach-avoidance conflicts arises in mPFC and how excessive safety seeking may influence the development and treatment of multiple psychiatric disorders.

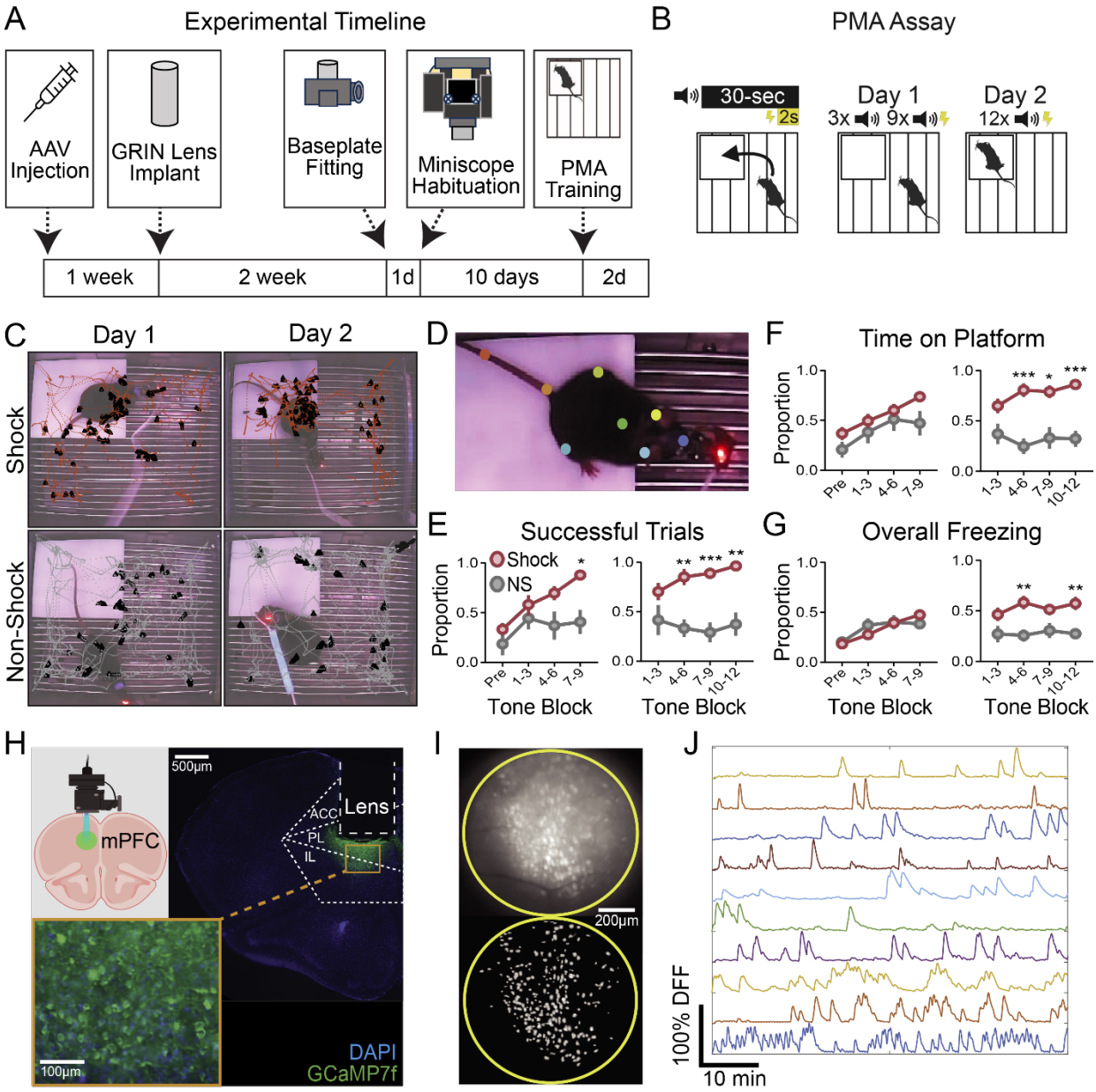

Figure 1: Experimental Design & PMA Behavior

A. Experimental timeline for miniscope surgeries and platform-mediated avoidance.

B. Design for PMA assay. Mice were presented with 3 baseline (no shock) tones and 9 tone-shock pairings on Day 1. On Day 2, all 12 tones are paired with footshocks.

C. Example maps of animal trajectory during training days 1 (left) and 2 (right). Trajectories (Shock: red; NonShock: gray) show each animal's location during tone periods for all trials across each session. Black triangles show the location of animal freezing.

D. Example frame from PMA showing custom DeepLabCut-based pose estimation of 8 points on a mouse wearing UCLA miniscope. Points tracked: nose, ears, mid-back, legs/hips, tailbase, and mid-tail.

(E-G) Line plots of behavior from PMA training Day 1 (left) and Day 2 (right) across Shock and NonShock groups for each tone block. Error bars show SEM. (Day 1: Shk: N=11, NS: N=9; Day 2: Shk: N=8, NS: N=8).

E. Successful trials (animal on platform during last 2s of tone). Day 1: $F_{time}(1.883, 33.90)=8.814$, $P=0.0010$; $F_{group}(1, 18)=7.372$, $P=0.0142$. Day 2: $F_{time}(2.311, 34.67)=0.7388$, $P=0.5034$; $F_{group}(1,15)=29.41$, $P<0.0001$.
F. Fraction of time spent on platform during each tone block. Day 1: $F_{time}(2.473, 44.51)=14.07$, $P<0.0001$; $F_{group}1, 18)=2.429$, $P=0.1365$. Day 2: $F_{time}(2.375, 35.62)=0.6540$, $P=0.5514$; $F_{group}(1, 15)=35.87$, $P<0.0001$.
G. Overall freezing during each tone block. Day 1: $F_{time}(2.346, 42.22)=15.02$, $P<0.0001$; $F_{group}(1, 18)=0.02244$, $P=0.8826$. Day 2: $F_{time}(2.174, 32.60)=0.5929$, $P=0.5720$; $F_{group}(1, 15)=13.98$, $P=0.0020$.
H. *(Upper left)* Miniscope experiment diagram showing virus and imaging targeting mPFC. *(Right)* Example image showing cell bodies, GCaMP7f expression, and GRIN lens placement. Approximate region boundaries show site of recording (scale bar: 500um). *(Bottom left)* Magnified recording region showing DAPI and GCaMP stained cell bodies (scale bar: 100um).
I. (*Top*) Maximum intensity projection of example miniscope window showing recorded neurons. (*Bottom*) Plot of extracted cell spatial footprints from the same miniscope window.
J. Example neural traces recorded from mPFC. Signal for each neuron is displayed in $\Delta F/F_o$. Full traces show 10 minutes of recording.

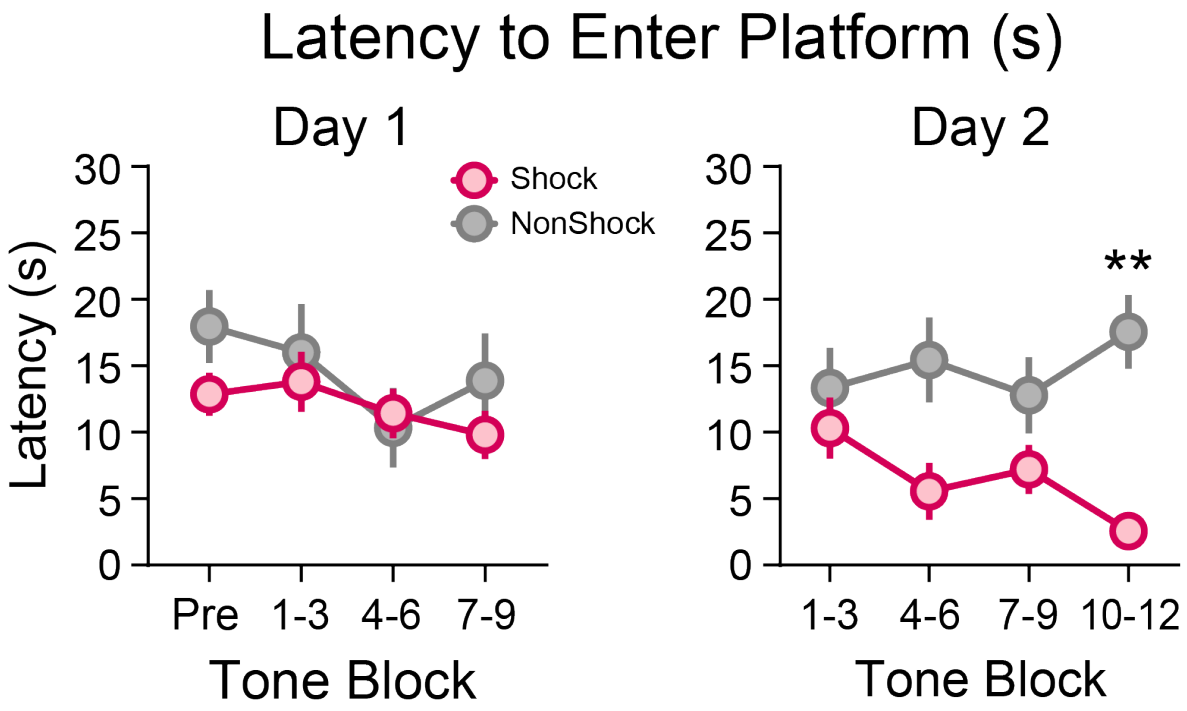

Figure 1S: Latency to Enter Platform Across Training
Line plots of latency to enter platform during Day 1 (*left*) and Day 2 (*right*) across Shock and NonShock groups. Day 1: $F_{time}(2.674, 48.12)=3.567$, $P=0.0247$; $F_{group}(1, 18)=0.7463$, $P=0.3990$. Day 2: $F_{time}(2.574, 38.61)=0.2622$, $P=0.8230$; $F_{group}(1, 15)=19.25$, $P=0.0005$. Error bars show SEM. (Shock: N=11, NS: N=9).

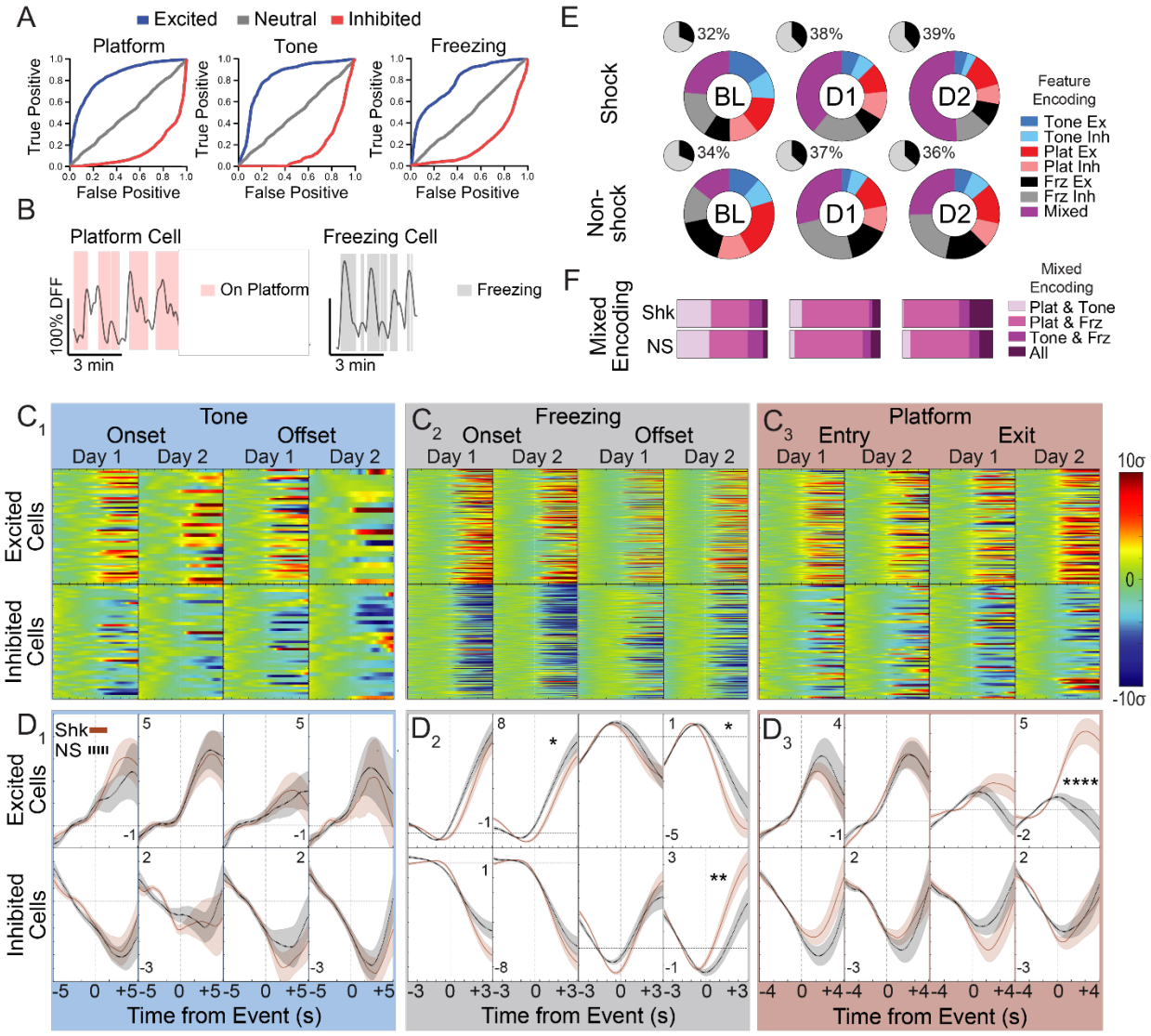

Figure 2: mPFC Modulation to PMA across Learning

A. Examples of excited (blue), suppressed (red), and neutral (gray) cells determined by ROC analysis for platform, tone, and freezing events.

B. Example traces from cells identified by ROC overlaid with behavior labels. Data are presented in $\Delta F/F_o$. Full traces show 3 min of recording.

C. Groups of modulated cells for tone, freezing, and platform event transitions separated by excited or inhibited response type. Heatmaps show responsive cells pooled across shock animals and are normalized to the period before each event. All heatmaps range from -10 to +10 z-scores.

D. Mean responses of modulated cells. Line plots show mean response to each feature pooled across groups and separated by response type (excited or inhibited). Each set of plots have y-axis limits labeled by min/max z-score. Error bars show SEM. Asterisks indicate significant difference in AUC by t-test. (*P=0.05, **P<0.01, ***P<0.001, ****P<0.0001).

E. Overall modulation responses for Shock and NonShock animals across PMA days 1 and 2. Black/gray pie charts show percent of recorded cells that were active at each time point. Multi-colored pie charts show modulated responses for tone, platform, and freezing cells. Time periods: BL (day 1, tones 1-3); D1 (day 1, tones 9-12); and D2 (day 2, tones 9-12). Cells analyzed: Shock (BL/D1: 1394, D2: 1031); NonShock (BL/D1: 847, D2: 967).

F. Breakdown of responses for mixed response cells. Bars show the behavior composition of mixed cells shown in E.

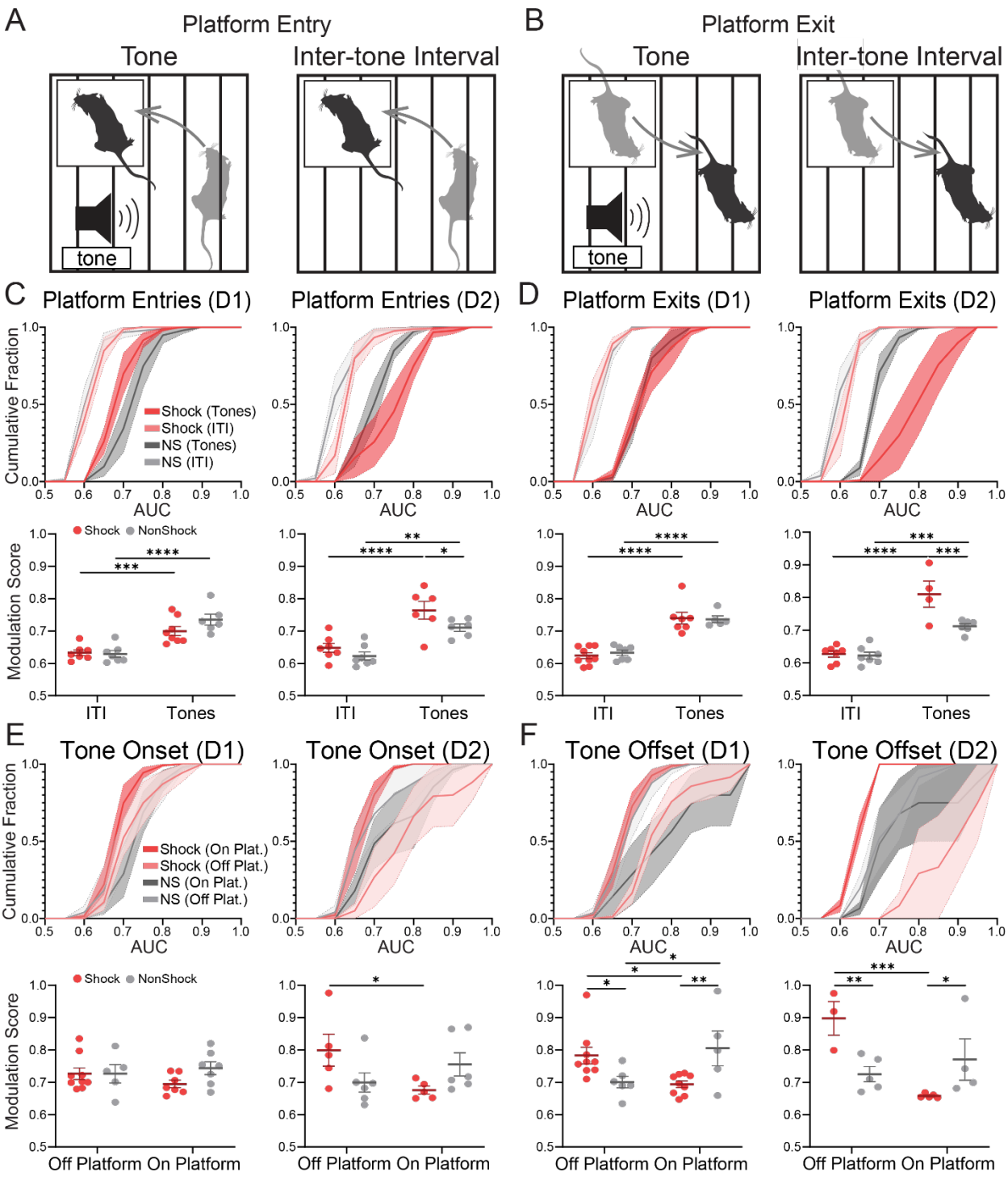

Figure 3: Enhanced mPFC Modulation During Tone and Platform Activity

A. Depiction of platform entries during tone and inter-tone intervals.

B. Depiction of platform exits during tone and inter-tone intervals.

(C-F) Cumulative frequency histograms of modulated cells identified by ROC analysis. Top plots depict mean group histogram with shaded SEM error. Bottom plots show quantification of modulation score and associated results from 2-way ANOVA. Multiple comparisons were corrected with Fisher's LSD.

C. Analysis of platform entries during tone or inter-trial interval (ITI) periods. D1: $F_{shock}(1,24)=1.534$, $P=0.2274$; $F_{tone}(1,24)=45.23$, $P<0.0001$; $F_{interaction}(1,24)=2.339$, $P=0.1392$; D2: $F_{shock}(1,22)=5.355$, $P=0.0304$; $F_{tone}(1,22)=35.87$, $P<0.0001$; $F_{interaction}(1,22)=0.7200$, $P=0.4053$. (Day 1: Shk: N=9; NS: N=7; Day 2: Shk: N=7, NS: N=7).
D. Analysis of platform exits during tone or ITI periods. D1: $F_{shock}(1,24)=0.05099$, $P=0.8233$; $F_{tone}(1,24)=78.37$, $P<0.0001$; $F_{interaction}(1,24)=0.2518$, $P=0.6204$; D2: $F_{shock}(1,20)=10.27$, $P=0.0044$; $F_{tone}(1,20)=72.03$, $P<0.0001$; $F_{interaction}(1,20)=8.404$, $P=0.0089$. (Day 1: Shk: N=9; NS: N=7; Day 2: Shk: N=6, NS: N=7).
E. Analysis of tone onset responses while on/off the platform. D1: $F_{shock}(1,24)=1.538$, $P=0.2269$; $F_{platform}(1,24)=0.1350$, $P=0.7165$; $F_{interaction}(1,24)=1.566$, $P=0.2228$; D2: $F_{shock}(1,18)=0.08758$, $P=0.7707$; $F_{platform}(1,18)=0.9529$, $P=3419$; $F_{interaction}(1,18)=6.751$, $P=0.0182$. (Day 1: Shk: N=8; NS: N=7; Day 2: Shk: N=7, NS: N=7).
F. Analysis of tone offset responses while on/off the platform. D1: $F_{shock}(1,25)=0.2890$, $P=0.5956$; $F_{platform}(1,25)=0.08148$, $P=0.7777$; $F_{interaction}(1,25)=12.93$, $P=0.0014$; D2: $F_{shock}(1,13)=0.6236$, $P=0.4439$; $F_{platform}(1,13)=6.513$, $P=0.0241$; $F_{interaction}(1,13)=13.98$, $P=0.0025$. (Day 1: Shk: N=9; NS: N=7; Day 2: Shk: N=5, NS: N=6).

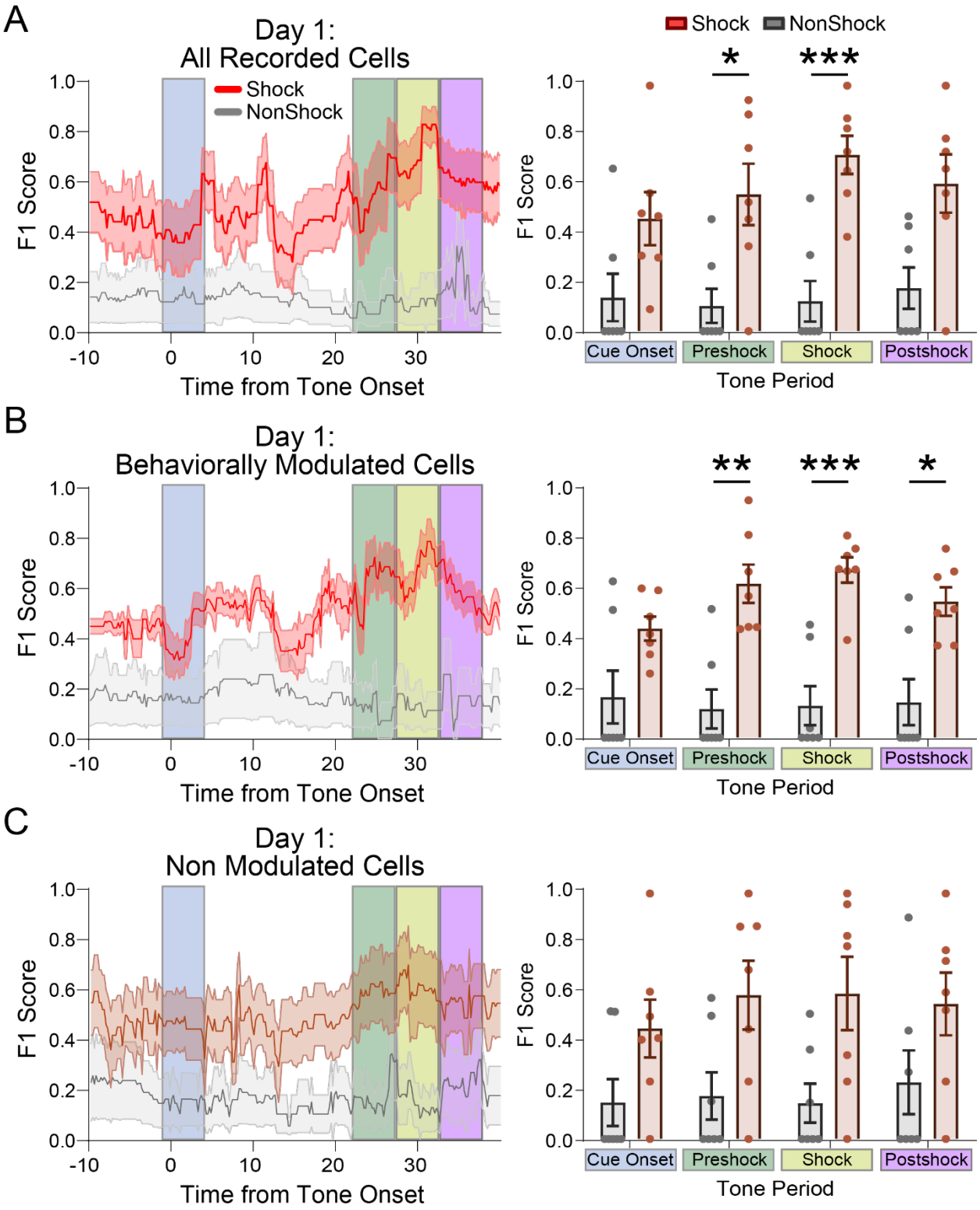

Figure 4: Population Decoding

A. (*Left*) Average performance for decoding of trial outcome analyzed per animal. Line plot shows the change in average decoding performance across the tone for Shock and NonShock animals with shaded SEM error bars. (*Right*) Performance for various tone periods and associated p-values from

2-way ANOVA. $F_{period}(2.313, 27.76)=1.302$, P=0.2908; $F_{group}(1, 12)=16.99$, P=0.0014; $F_{subject}(12, 36)=5.075$, P<0.0001. (Shk: N=7, NS: N=7).

B. Repeated decoding analysis using only cells identified by ROC as behaviorally-modulated (platform, tone, or freezing) during that session. $F_{period}(2.278, 27.33)=2.179$, P=0.1267; $F_{group}(1, 12)=20.46$, P=0.0007; $F_{subject}(12, 36)=11.21$, P<0.0001; $F_{period\ x\ group}(3, 36)=4.440$, P=0.0094.

C. Repeated decoding analysis using only cells identified by ROC as non-responsive to behavioral features. $F_{period}(1.913, 22.95)=0.9164$, P=0.4101; $F_{group}(1, 12)=5.988$, P=0.0308; $F_{subject}(12, 36)=12.14$, P<0.0001.

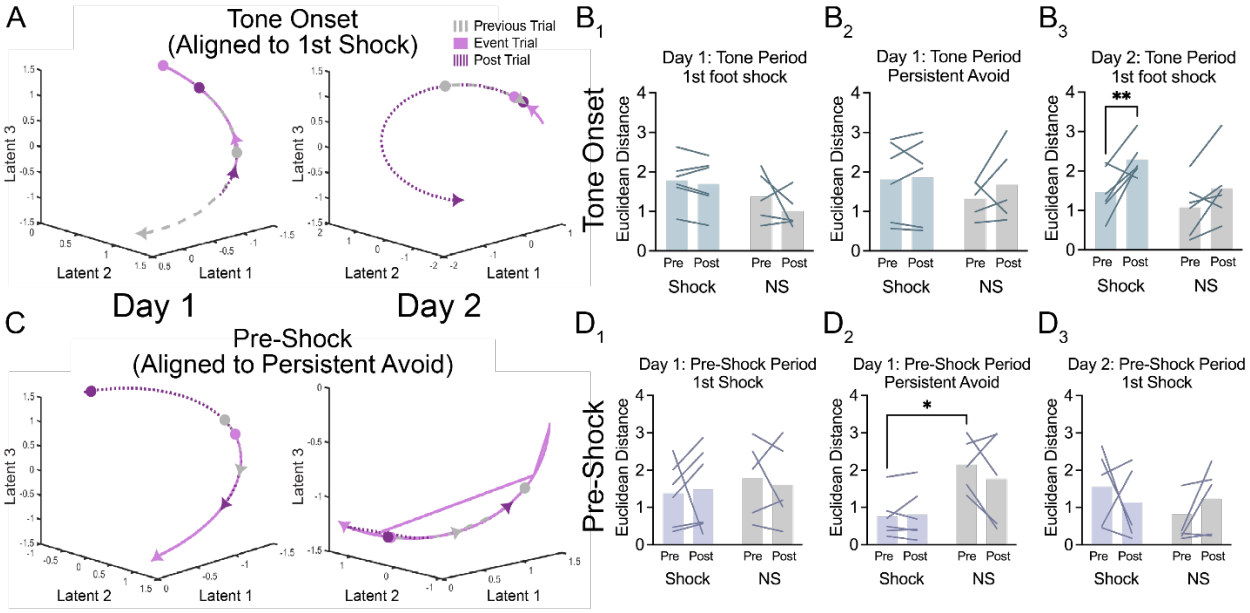

Figure 5: CILDS Population Analysis

A. Example trajectories of tone onset population response from trials before, during, and after the first shock received of days 1 and 2. Colored circle indicates the start of the trial. Arrow markers show the end of each trial. Each trajectory spans 5s.

B. Trial-by-trial latent distance measurements anchored to first shock received on days 1 and 2.
B_1) Day 1, 1st Shock: $F_{time}(1, 9)=1.766$, $P=0.2166$; $F_{group}(1, 9)=2.858$, $P=0.1252$; $F_{subject}(9, 9)=3.827$, $P=0.0292$. (Shk: N=6, NS: N=5).
B_2) Day 1, Persistent Avoid: $F_{time}(1, 9)=1.260$, $P=0.2907$; $F_{group}(1, 9)=0.4188$, $P=0.5337$; $F_{subject}(9, 9)=8.325$, $P=0.0021$. (Shk: N=6, NS: N=5).
B_3) Day 2, 1st Shock: $F_{time}(1, 9)=10.35$, $P=0.0105$; $F_{group}(1, 9)=10.73$, $P=0.0096$; $F_{subject}(9, 9)=1.774$, $P=0.2029$. (Shk: N=6, NS: N=5).

C. Example trajectories of tone onset population response from trials before, during, and after a pattern of avoidance emerged on days 1 and 2. Colored circle indicates the start of the trial. Arrow markers show the end of each trial. Each trajectory spans 5s.

D. Trial-by-trial latent distance measurements anchored to trial of persistent avoidance (no further shocks received that day).
D_1) Day 1, 1st Shock: $F_{time}(1, 10)=0.001046$, $P=0.9748$; $F_{group}(1, 10)=0.3049$, $P=0.5930$; $F_{subject}(10, 10)=2.618$, $P=0.0725$. (Shk: N=7, NS: N=5).
D_2) Day 1, Persistent Avoid: $F_{time}(1, 10)=0.9987$, $P=0.3412$; $F_{group}(1, 10)=4.661$, $P=0.0562$; $F_{subject}(10, 10)=6.700$, $P=0.0030$. (Shk: N=7, NS: N=5).
D_3) Day 2, 1st Shock: $F_{time}(1, 9)=1.706e\text{-}5$, $P=0.9968$; $F_{group}(1, 9)=0.6565$, $P=0.4387$; $F_{subject}(9, 9)=7.034$, $P=0.0039$. (Shk: N=5, NS: N=6).

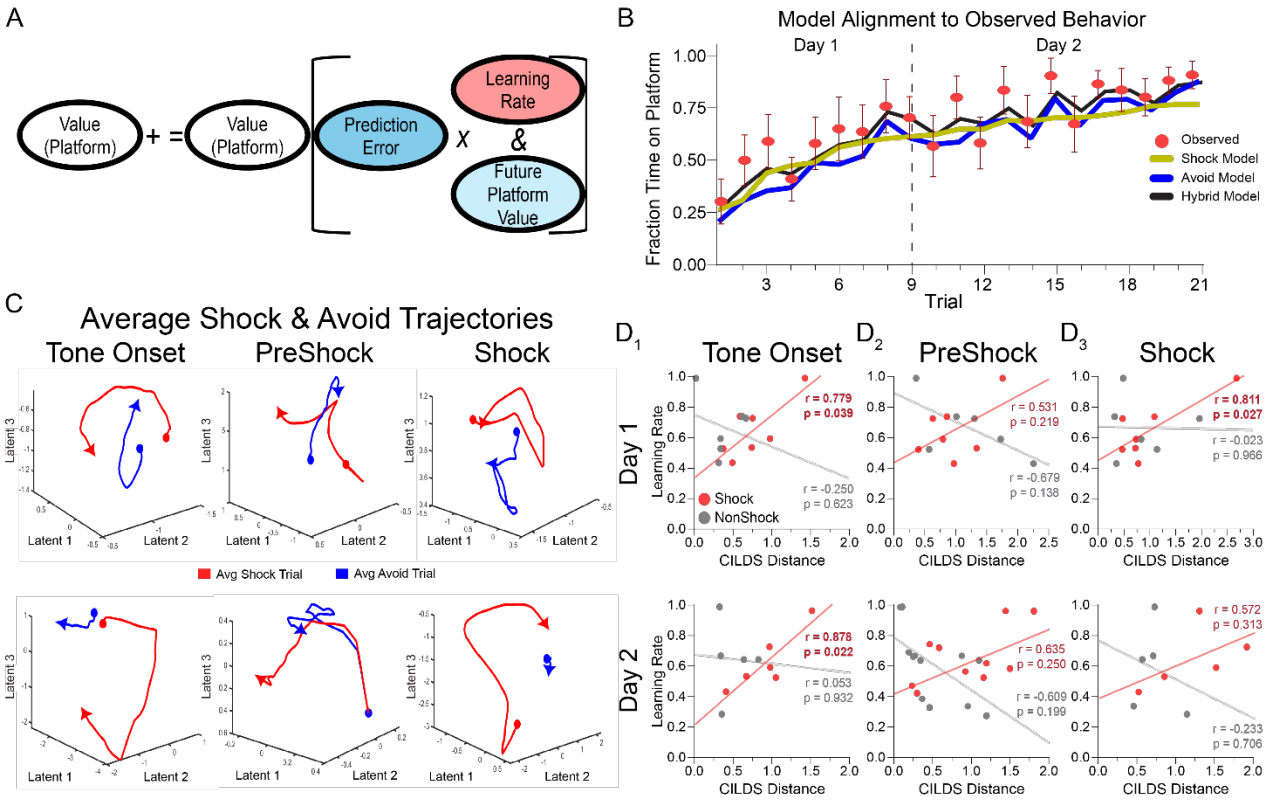

Figure 6: PMA Learning Rate Correlates with PL Population Responses

A. Schematic of Rescorla-Wagner model of PMA learning.

B. Line plot of observed behavior (red) and predictions from shock-based model (yellow), avoid-based model (blue), and hybrid model (black) during all trials across both days of learning for shocked animals. Error bars show SEM. N=9.

C. Example 3D trajectories of average shock (red) and average avoid (blue) responses to tone onset (*left*), pre-shock (*center*), and shock (*right*) periods across days in latent space.

D. Plots showing correlation between model learning rate and Euclidean distance between trial-averaged CILDS latent variable during tone onset, pre-shock, and shock periods for days 1 and 2 for shock and nonshock animals. R values and corresponding P values are reported on each plot. (Day 1, Shk: N=7, NS: N=6; Day 2: Shk: N=6, NS: N=6).

Data Table 1. Expanded ANOVA Results.

Two-way repeated measures ANOVA with Geisser-Greenhouse correction and post hoc Šídák's multiple comparisons test

Figure 1	Day	F_{trial}	DFn, DFd	p-value	F_{group}	DFn, DFd	p-value	$F_{interaction}$	DFn, DFd	p-value
1E: Successful Trials	1	8.814	1.883 , 33.90	0.0010	7.372	1, 18	0.0142	2.173	3, 54	0.1019
	2	0.7388	2.311 , 34.67	0.5034	29.41	1, 15	<0.0001	1.798	3, 45	0.1611
1F: Time on Platform	1	14.07	2.473 , 44.51	<0.0001	2.429	1, 18	0.1365	1.089	3, 54	0.3617
	2	0.654	2.375 , 35.62	0.5514	35.87	1, 15	<0.0001	1.970	3, 45	0.1320
1G: Overall Freezing	1	15.02	2.346 , 42.22	<0.0001	0.02244	1, 18	0.8826	1.960	3, 54	0.1309
	2	0.5929	2.174 , 32.60	0.5720	13.98	1, 15	0.0020	1.000	3, 45	0.4014
S1: Latency	1	3.567	2.674 , 48.12	0.0247	0.7463	1, 18	0.399	1.320	3, 54	0.2773
	2	0.2622	2.574 , 38.61	0.8230	19.25	1, 15	0.0005	2.503	3, 45	0.0713

Ordinary two-way ANOVA and Fishers LSD

Figure 3	Day	$F_{tone/platform}$	DFn, DFd	p-value	F_{group}	DFn, DFd	p-value	$F_{interaction}$	DFn, DFd	p-value
3C: Platform Entries	1	45.23	1, 24	<0.0001	1.534	1, 24	0.2274	2.339	1, 24	0.1392
	2	35.87	1, 22	<0.0001	5.355	1, 22	0.0304	0.7200	1, 22	0.4053
3D: Platform Exits	1	78.37	1, 24	<0.0001	0.05099	1, 24	0.8233	0.2518	1, 24	0.6204
	2	72.03	1, 20	<0.0001	10.27	1, 20	0.0044	8.404	1, 20	0.0089
3E: Tone Onset	1	0.1350	1, 24	0.7165	1.538	1, 24	0.2269	1.566	1, 24	0.2228
	2	0.9529	1, 18	0.3419	0.08758	1, 18	0.7707	6.751	1, 18	0.0182
3F: Tone Offset	1	0.08148	1, 25	0.7777	0.2890	1, 25	0.5956	12.93	1, 25	0.0014
	2	6.513	1, 13	0.0241	0.6236	1, 13	0.4439	13.98	1, 13	0.0025

Two-way repeated measures ANOVA with Geisser-Greenhouse correction and post hoc Šídák's multiple comparisons test

Figure 4	Day	F_{period}	DFn, DFd	p-value	F_{group}	DFn, DFd	p-value	$F_{interaction}$	DFn, DFd	p-value
4A: All Cells	1	1.302	2.313 , 27.76	0.2908	16.99	1, 12	0.0014	1.375	3, 36	0.2660
4B: BM Cells	1	2.179	2.278 , 27.33	0.1267	20.46	1, 12	0.0007	4.440	3, 36	0.0094
4C: Non Modulated Cells	1	0.9164	1.913 , 22.95	0.4101	5.988	1, 12	0.0308	0.6529	3, 36	0.5864
Figure 5	Day	F_{period}	DFn, DFd	p-value	F_{group}	DFn, DFd	p-value	$F_{interaction}$	DFn, DFd	p-value
$5B_1$: Tone Onset, 1st Shock	1	1.766	1, 9	0.2166	2.858	1, 9	0.1252	0.7370	1, 9	0.4129
$5B_2$: Tone Onset, Per Avoid	1	1.260	1, 9	0.2907	0.4188	1, 9	0.5337	0.7176	1, 9	0.4189
$5B_3$: Tone Onset, 1st Shock	2	10.35	1, 9	0.0105	10.73	1, 9	0.0096	1.451	1, 9	0.2590
$5C_1$: Pre-shock , 1st Shock	1	0.001046	1, 10	0.9748	0.3049	1, 10	0.5930	0.3306	1, 10	0.5780
$5C_2$: Pre-shock , Per Avoid	1	0.9987	1, 10	0.3412	4.661	1, 10	0.0562	1.265	1, 10	0.2870
$5C_3$: Pre-shock , 1st Shock	2	1.706e -5	1, 9	0.9968	0.6565	1, 9	0.4387	2.808	1, 9	0.1281
Figure 7	Day	$F_{trial\ block}$	DFn, DFd	p-value	F_{group}	DFn, DFd	p-value	$F_{interaction}$	DFn, DFd	p-value
7A: Preshock	1	1.157	1.937 , 27.12	0.3279	5.031	1, 14	0.0416	0.8794	3, 42	0.4595
7B: Preshock	2	0.7300	3, 36	0.5409	0.3317	1, 12	0.5753	0.6181	3, 36	0.6078

Data Table 1. Expanded ANOVA Results.

METHODS

Animals

Female and male C57B1/6 J mice (JAX Stock No. 000664) aged 10–16 weeks were group housed (2–5 per cage) and kept on a 12 hr light cycle. After GRIN lens implantation, all animals were single housed until the end of behavioral testing. Following the baseplate surgery, all animals were handled daily and habituated to the weight and feel of wearing the miniscope for 10 days. All animal procedures followed animal care guidelines approved by the University of California, Los Angeles Chancellor's Animal Research Committee.

Behavior video recordings

Behavioral videos were acquired at 30fps using a ELP 2.8–12 mm Lens Varifocal Mini Box 1.3 megapixel USB Camera.

Platform-mediated avoidance

For all PMA sessions, a conditioning chamber was used consisting of an 18cm x 18cm x 30 cm cage with a grid floor wired to a scrambled shock generator (Lafayette Instruments) surrounded by a custom-built acoustic chamber. The chamber was scented with 50% Windex. One corner was covered with a thin acrylic platform (3.5in x 4in x 0.5in), amounting to 25% of the chamber floor. During the first day of training, mice were presented with three baseline 30s 4 kHz tones (CS), followed by nine presentations of the CS that co-terminated with a 2s footshock (0.14mA). The following day, mice were presented with twelve CS that coterminated with a shock. For the remaining 3 sessions, mice were presented with nine CS in the absence of shock. During the no platform session (day 4), the acrylic platform was removed.

Viruses

AAV1-syn-jGCaMP7f.WPRE (ItemID: 104488-AAV1) was purchased from Addgene and diluted to a working titer of 8.5x1012 GC/ml.

Miniscope surgery and baseplating

For miniscope recordings, all mice underwent two stereotaxic surgeries (Cai et al., 2016). First, adult WT mice were anesthetized with isoflurane and secured to a stereotaxic frame (Kopf, 963). Mice were placed on a heating blanket and artificial tears kept their eyes moist throughout the surgery. After exposing the skull, a burr hole was drilled above PL in the left hemisphere (+1.85, –0.4, –2.1 mm from bregma). A Hamilton syringe containing AAV1-Syn-jGCaMP7f-WPRE was lowered into the burr hole and 600 nL of AAV was pressure injected using a microinjector (WPI, UMP3T-1). The syringe was left in place for 10 min to ensure the AAV did not spill out of the target region and then the skin was sutured. After recovery, animals were housed in a regular 12 hr light/dark cycle with food and water ad libitum. Carprofen (5 mg/kg) was administered both during surgery and for 2 days after surgery together with amoxicillin (0.25 mg/mL) for 7 days after surgery. One week later, mice underwent a GRIN lens implantation surgery. After anesthetizing the animals with isoflurane (1–3%) and securing them to the stereotaxic frame, a 1mm craniotomy was made above the virus site, and the cortical tissue above the targeted implant site was carefully aspirated using 27-gauge and 30-gauge blunt needles. Buffered ACSF was constantly applied throughout the aspiration to prevent tissue desiccation. The aspiration ceased after full termination of bleeding, at which point a GRIN lens (1 mm diameter, 4 mm length, Inscopix 1050–002176) was stereotaxically lowered to the targeted implant site (–2.0 mm dorsoventral from skull surface relative to bregma). Cyanoacrylate glue was used to affix the lens to the skull. Then, dental cement sealed and covered the exposed skull, and Kwik-Sil covered the exposed GRIN lens. Carprofen (5 mg/kg)

and dexamethasone (0.2 mg/kg) were administered during surgery and for 7 days after surgery together with amoxicillin (0.25 mg/mL) in the drinking water. Two weeks after implantation, animals were anesthetized again with isoflurane (1–3%), and a miniscope attached to an aluminum baseplate was placed on top of the GRIN lens. After searching the field of view for in-focus cells, the baseplate was cemented into place, and the miniscope was detached from the baseplate. A plastic cap was locked into the baseplate to protect the implant from debris and allow the baseplate to set.

Miniscope recordings

Mice were handled and habituated to the weight of the microscope for 10 days before behavioral acquisition. On the recording day, a V4 miniscope was secured to the baseplate with a set screw and the mice were allowed to acclimate in their home cage for 5 min. Imaging through the miniscope took place throughout the entire PMA training (~30 min) and retrieval (~18 min) sessions on following days. Behavior was simultaneously recorded using miniscope recording software to synchronize the data streams (https://github.com/Aharoni-Lab/Miniscope-DAQ-QT-Software).

Miniscope data processing

Frames in which animals were freezing and/or on the safety platform were determined using BehaviorDEPOT. Cell footprints and Ca2+ fluorescence timeseries were extracted from miniscope recordings using Minian (https://github.com/denisecailab/minian). We identified 1394 neurons across 9 mice in Shock animals and 847 neurons across 7 mice in NonShock animals. Custom MATLAB software was used to align data from the behavior camera and the miniscope camera.

ROC Analysis

To identify neurons that were active during freezing or when the animal was on the safety platform, we plotted receiver operating characteristic curves (ROC) for individual neurons and measured the area under the curve (AUC). ROCs plot the true positive rate (true positive/(true positive +false negative)) against the false positive rate (false positive/(false positive +true negative)) over a range of probability thresholds. Neurons with high AUC values therefore predict the behavioral variable of interest with a high true positive rate and low false positive rates over a large range of thresholds. To determine if a neuron significantly encoded a particular behavioral event, we generated a null distribution of AUCs by circularly shuffling event timing and recalculating the AUC over 1000 permutations. Neurons were considered significantly activated during a behavior if their AUC was greater than 97.5% of AUCs in the null distributions and significantly suppressed if their AUC value was in the lowest 2.5% of all AUCs in the null distribution.

Frequency Distributions of auROC Values

To identify differences in response modulation to intersections of tone and platform activity, Per animal, auROC values for all cells responding to a particular feature were collected and inhibited values (AUC=0-0.5) were converted into a fixed range using the formula: 1-AUC. These auROC values were then used to construct cumulative frequency histograms for each analysis. To measure modulation strength, we derived a modulation score from the AUC of each frequency histogram using the formula: Modulation Score = 1 – AUC.

Decoding Analysis

To determine how well the PL activity predicts avoidance in response to shock, we employed a radial basis function-kernel support vector machine (SVM) classifiers (Chang and Lin, 2002). We used the outcome of each trial successful avoidance (1) or no avoidance behavior (0) as

labels, excluding the first three trials on day one due to the absence of shock. We utilized the pattern of activity of the units in each trial as features. The activity of single units in each trial was binned in 0.2 seconds windows. To ascertain whether the activity from the PL cortex predicts avoidance behavior better before, during, or after the shock, we trained SVM and tested it in a free trial to predict the avoidance label using leave-one-trial-out cross-validation, with each time bin window stepping by 0.2 seconds. To maximize the decoder performance, we optimized the SVM parameters (*C, γ*) via grid search using five fold cross-validation for each time bin and each animal. We averaged the SVM performance over four epochs per mouse to compare the decoding performance between epochs and between groups (Shock, Non-shock): "Cue-onset" (0 - 5 s), "Pre-shock" (22 - 27 s), "Shock" (28 - 33 s), and "Post-shock" (34 - 38 s). SVM performance was calculated for each bin using the F1 score [F1 = 2(precision × recall) / (precision + recall)], where precision is calculated as the ratio of True positives to the sum of False positives and True positives; and recall is calculated as the ratio of True positives to the sum of False negatives and True positives.

Dimensionality Reduction of Recorded Neural Data

We used a dimensionality reduction pipeline for calcium imaging data, CILDS (https://github.com/kohth/cilds), to extract 3 latent variables from each session that were trained using neural data during 5s windows of the tone. Extracted latent variables were averaged by trial outcome or aligned trial-by-trial. Distance was assessed using the mean framewise Euclidean distance between each point in a set of compared trajectories for each animal.

Rescorla-Wagner Modeling

To correlate neural dynamics during PMA to mechanistic changes in subjects' behavior across learning, a Rescorla-Wagner learning model was fit to the proportion of trial time spent on the platform for each mouse across trials. The proportion of total trial time spent on the safety

platform during conditioned tones was modeled using a Rescorla-Wagner model (Rescorla & Wagner, 1972). We seeded the model with the proportion amount of baseline time animals spent on the platform prior to shock. Because mice in this task experience from a mixture of punishment (shock trials) and negative reinforcement (successful escapes to the platform), we used a version of model with two complimentary learning rates, $\alpha_{failure}$, which weights the rate of change in the platform value following an unsuccessful trial, and $\alpha_{success}$, which weights the rate of change in the platform value following a successful avoid. It is assumed that the subjects' behavioral expression of platform value is the proportion of trial time spent on the platform. Models were fit to individual subject data in Python using maximum likelihood estimation. The trial-by-trial change in the value of the platform was calculated as:

$$\Delta v_t = \begin{cases} \alpha_{success} * (R_t - v_t) & \text{if trial outcome was a success,} \\ \alpha_{failure} * (R_t - v_t) & \text{if trial outcome was a failure} \end{cases}$$

Where:

- $\alpha_{success} = 1 - \alpha_{failure}$
- Δv_t is the change in associative strength of the platform at trial t
- α is the learning rate (free parameter)
- R_t is the outcome at trial t
- v_t is associative strength at time t (initially the baseline probability of being on platform)

This is fit by minimizing a loss function $MSE = (1 / N) * \Sigma_i (v_i - data_i)^2$, where:

- MSE is the mean squared error
- N is the # of data points
- v_i is the model's predicted value at trial i
- $data_i$ is the observed data at trial i.

Histology

Mice were transcardially perfused with phosphate-buffered saline (PBS) followed by 4% paraformaldehyde (PFA) in PBS. Brains were dissected, post-fixed in 4% PFA for 12–24 hr and placed in 30% sucrose for 24–48 hr. They were then embedded in Optimum Cutting Temperature (OCT, Tissue Tek) and stored at –80 °C until sectioning. 60 µm floating sections were collected into PBS. Sections were washed 3x10 min in PBS and then blocked in 0.3% PBST containing 10% normal donkey serum (Jackson Immunoresearch, 17-000-121) for 2 hr.

Sections were then stained with chicken anti-GFP primary antibody (Aves 1020) in 0.3% PBST containing 3% donkey serum overnight at 4 °C. The following day, sections were washed 3x5 min in PBS and then stained with secondary antibody (goat anti-chicken 488) in 0.3% PBST containing 5% donkey serum for 2 hr at room temperature. Sections were then washed 5 min with PBS, 15 min with PBS + DAPI (Thermofisher Scientific, D1306, 1:4000), and then 5 min with PBS. Sections were mounted on glass slides using FluoroMount-G (ThermoFisher, 00-4958-02) and then imaged at 10x with a Leica slide scanning microscope (VT1200S).

Statistical analyses

Statistical analyses were performed in MATLAB or GraphPad Prism.

REFERENCES

Abercrombie, E. D., Keefe, K. A., DiFrischia, D. S., & Zigmond, M. J. (1989). Differential effect of stress on in vivo dopamine release in striatum, nucleus accumbens, and medial frontal cortex. *Journal of Neurochemistry*, *52*(5), 1655–1658. https://doi.org/10.1111/j.1471-4159.1989.tb09224.x

Alloy, L. B., Abramson, L. Y., Walshaw, P. D., Cogswell, A., Grandin, L. D., Hughes, M. E., Iacoviello, B. M., Whitehouse, W. G., Urosevic, S., Nusslock, R., & Hogan, M. E. (2008). Behavioral Approach System and Behavioral Inhibition System sensitivities and bipolar spectrum disorders: Prospective prediction of bipolar mood episodes. *Bipolar Disorders*, *10*(2), 310–322. https://doi.org/10.1111/j.1399-5618.2007.00547.x

Anastasiades, P. G., Boada, C., & Carter, A. G. (2019). Cell-Type-Specific D1 Dopamine Receptor Modulation of Projection Neurons and Interneurons in the Prefrontal Cortex. *Cerebral Cortex*, *29*(7), 3224–3242. https://doi.org/10.1093/cercor/bhy299

Anastasiades, P. G., & Carter, A. G. (2021). Circuit organization of the rodent medial prefrontal cortex. *Trends in Neurosciences*, *44*(7), 550–563. https://doi.org/10.1016/j.tins.2021.03.006

Awad, M., & Khanna, R. (2015). *Support Vector Machines for Classification* (pp. 39–66). https://doi.org/10.1007/978-1-4302-5990-9_3

Ball, S. A., Carroll, K. M., & Rounsaville, B. J. (1994). Sensation seeking, substance abuse, and psychopathology in treatment-seeking and community cocaine abusers. *Journal of Consulting and Clinical Psychology*, *62*(5), 1053–1057. https://doi.org/10.1037//0022-006x.62.5.1053

Ball, T. M., Ramsawh, H. J., Campbell-Sills, L., Paulus, M. P., & Stein, M. B. (2013). Prefrontal dysfunction during emotion regulation in generalized anxiety and panic disorders. *Psychological Medicine*, *43*(7), 1475–1486. https://doi.org/10.1017/S0033291712002383

Bassareo, V., De Luca, M. A., & Di Chiara, G. (2002). Differential Expression of Motivational Stimulus Properties by Dopamine in Nucleus Accumbens Shell versus Core and Prefrontal

Cortex. *The Journal of Neuroscience: The Official Journal of the Society for Neuroscience*, *22*(11), 4709–4719. https://doi.org/10.1523/JNEUROSCI.22-11-04709.2002

Bittar, T. P., & Labonté, B. (2021). Functional Contribution of the Medial Prefrontal Circuitry in Major Depressive Disorder and Stress-Induced Depressive-Like Behaviors. *Frontiers in Behavioral Neuroscience*, *15*, 699592. https://doi.org/10.3389/fnbeh.2021.699592

Blakey, S. M., & Abramowitz, J. S. (2016). The effects of safety behaviors during exposure therapy for anxiety: Critical analysis from an inhibitory learning perspective. *Clinical Psychology Review*, *49*, 1–15. https://doi.org/10.1016/j.cpr.2016.07.002

Bolles, R. C., Stokes, L. W., & Younger, M. S. (1966). Does CS termination reinforce avoidance behavior? *Journal of Comparative and Physiological Psychology*, *62*(2), 201–207. https://doi.org/10.1037/h0023678

Bossert, J. M., Stern, A. L., Theberge, F. R. M., Cifani, C., Koya, E., Hope, B. T., & Shaham, Y. (2011). Ventral medial prefrontal cortex neuronal ensembles mediate context-induced relapse to heroin. *Nature Neuroscience*, *14*(4), 420–422. https://doi.org/10.1038/nn.2758

Burgos-Robles, A., Kimchi, E. Y., Izadmehr, E. M., Porzenheim, M. J., Ramos-Guasp, W. A., Nieh, E. H., Felix-Ortiz, A. C., Namburi, P., Leppla, C. A., Presbrey, K. N., Anandalingam, K. K., Pagan-Rivera, P. A., Anahtar, M., Beyeler, A., & Tye, K. M. (2017). Amygdala inputs to prefrontal cortex guide behavior amid conflicting cues of reward and punishment. *Nature Neuroscience*, *20*(6), 824–835. https://doi.org/10.1038/nn.4553

Burgos-Robles, A., Vidal-Gonzalez, I., & Quirk, G. J. (2009). Sustained conditioned responses in prelimbic prefrontal neurons are correlated with fear expression and extinction failure. *The Journal of Neuroscience: The Official Journal of the Society for Neuroscience*, *29*(26), 8474–8482. https://doi.org/10.1523/JNEUROSCI.0378-09.2009

Cai, D. J., Aharoni, D., Shuman, T., Shobe, J., Biane, J., Song, W., Wei, B., Veshkini, M., La-Vu, M., Lou, J., Flores, S. E., Kim, I., Sano, Y., Zhou, M., Baumgaertel, K., Lavi, A., Kamata, M., Tuszynski, M., Mayford, M., … Silva, A. J. (2016). A shared neural ensemble links

distinct contextual memories encoded close in time. *Nature*, *534*(7605), 115–118. https://doi.org/10.1038/nature17955

Carmona, G. N., Nishimura, T., Schindler, C. W., Panlilio, L. V., & Notkins, A. L. (2014). The Dense Core Vesicle Protein IA-2, but not IA-2β, is Required for Active Avoidance Learning. *Neuroscience*, *269*, 35–42. https://doi.org/10.1016/j.neuroscience.2014.03.023

Cervin, M., Perrin, S., Olsson, E., Claesdotter-Knutsson, E., & Lindvall, M. (2020). Incompleteness, harm avoidance, and disgust: A comparison of youth with OCD, anxiety disorders, and no psychiatric disorder. *Journal of Anxiety Disorders*, *69*, 102175. https://doi.org/10.1016/j.janxdis.2019.102175

Chandler, R. K., Fletcher, B. W., & Volkow, N. D. (2009). Treating Drug Abuse and Addiction in the Criminal Justice System: Improving Public Health and Safety. *JAMA : The Journal of the American Medical Association*, *301*(2), 183–190. https://doi.org/10.1001/jama.2008.976

Clauss, J. A., Benningfield, M. M., Rao, U., & Blackford, J. U. (2016). Altered Prefrontal Cortex Function Marks Heightened Anxiety Risk in Children. *Journal of the American Academy of Child and Adolescent Psychiatry*, *55*(9), 809–816. https://doi.org/10.1016/j.jaac.2016.05.024

Collins, D. P., Anastasiades, P. G., Marlin, J. J., & Carter, A. G. (2018). Reciprocal Circuits Linking the Prefrontal Cortex with Dorsal and Ventral Thalamic Nuclei. *Neuron*, *98*(2), 366-379.e4. https://doi.org/10.1016/j.neuron.2018.03.024

Courtin, J., Chaudun, F., Rozeske, R. R., Karalis, N., Gonzalez-Campo, C., Wurtz, H., Abdi, A., Baufreton, J., Bienvenu, T. C. M., & Herry, C. (2014). Prefrontal parvalbumin interneurons shape neuronal activity to drive fear expression. *Nature*, *505*(7481), 92–96. https://doi.org/10.1038/nature12755

Cummings, K. A., & Clem, R. L. (2020). Prefrontal somatostatin interneurons encode fear memory. *Nature Neuroscience*, *23*(1), 61–74. https://doi.org/10.1038/s41593-019-0552-7

Dana, H., Sun, Y., Mohar, B., Hulse, B. K., Kerlin, A. M., Hasseman, J. P., Tsegaye, G., Tsang, A., Wong, A., Patel, R., Macklin, J. J., Chen, Y., Konnerth, A., Jayaraman, V., Looger, L. L., Schreiter, E. R., Svoboda, K., & Kim, D. S. (2019). High-performance calcium sensors for imaging activity in neuronal populations and microcompartments. *Nature Methods*, *16*(7), 649–657. https://doi.org/10.1038/s41592-019-0435-6

de la Asuncion, J., Docx, L., Sabbe, B., Morrens, M., & de Bruijn, E. R. A. (2015). Abnormal emotion processing, but intact fairness and intentionality considerations during social decision-making in schizophrenia. *Frontiers in Psychology*, *6*, 1058. https://doi.org/10.3389/fpsyg.2015.01058

Devoto, P., Sagheddu, C., Santoni, M., Flore, G., Saba, P., Pistis, M., & Gessa, G. L. (2020). Noradrenergic Source of Dopamine Assessed by Microdialysis in the Medial Prefrontal Cortex. *Frontiers in Pharmacology*, *11*, 588160. https://doi.org/10.3389/fphar.2020.588160

Diehl, M. M., Bravo-Rivera, C., Rodriguez-Romaguera, J., Pagan-Rivera, P. A., Burgos-Robles, A., Roman-Ortiz, C., & Quirk, G. J. (2018). Active avoidance requires inhibitory signaling in the rodent prelimbic prefrontal cortex. *eLife*, *7*, e34657. https://doi.org/10.7554/eLife.34657

Diehl, M. M., Iravedra-Garcia, J. M., Morán-Sierra, J., Rojas-Bowe, G., Gonzalez-Diaz, F. N., Valentín-Valentín, V. P., & Quirk, G. J. (2020). Divergent projections of the prelimbic cortex bidirectionally regulate active avoidance. *eLife*, *9*, e59281. https://doi.org/10.7554/eLife.59281

Dong, Z., Mau, W., Feng, Y., Pennington, Z. T., Chen, L., Zaki, Y., Rajan, K., Shuman, T., Aharoni, D., & Cai, D. J. (2022). Minian, an open-source miniscope analysis pipeline. *eLife*, *11*, e70661. https://doi.org/10.7554/eLife.70661

Euston, D. R., Gruber, A. J., & McNaughton, B. L. (2012). The role of medial prefrontal cortex in memory and decision making. *Neuron*, *76*(6), 1057–1070. https://doi.org/10.1016/j.neuron.2012.12.002

Fadok, J. P., Dickerson, T. M. K., & Palmiter, R. D. (2009). Dopamine is necessary for cue-dependent fear conditioning. *The Journal of Neuroscience: The Official Journal of the Society for Neuroscience*, *29*(36), 11089–11097. https://doi.org/10.1523/JNEUROSCI.1616-09.2009

Gabbott, P. L. A., Warner, T. A., Jays, P. R. L., Salway, P., & Busby, S. J. (2005). Prefrontal cortex in the rat: Projections to subcortical autonomic, motor, and limbic centers. *The Journal of Comparative Neurology*, *492*(2), 145–177. https://doi.org/10.1002/cne.20738

Gabriel, C. J., Zeidler, Z., Jin, B., Guo, C., Goodpaster, C. M., Kashay, A. Q., Wu, A., Delaney, M., Cheung, J., DiFazio, L. E., Sharpe, M. J., Aharoni, D., Wilke, S. A., & DeNardo, L. A. (2022). BehaviorDEPOT is a simple, flexible tool for automated behavioral detection based on markerless pose tracking. *eLife*, *11*, e74314. https://doi.org/10.7554/eLife.74314

Gao, L., Liu, S., Gou, L., Hu, Y., Liu, Y., Deng, L., Ma, D., Wang, H., Yang, Q., Chen, Z., Liu, D., Qiu, S., Wang, X., Wang, D., Wang, X., Ren, B., Liu, Q., Chen, T., Shi, X., … Yan, J. (2022). Single-neuron projectome of mouse prefrontal cortex. *Nature Neuroscience*, *25*(4), 515–529. https://doi.org/10.1038/s41593-022-01041-5

Ghosh, K. K., Burns, L. D., Cocker, E. D., Nimmerjahn, A., Ziv, Y., Gamal, A. E., & Schnitzer, M. J. (2011). Miniaturized integration of a fluorescence microscope. *Nature Methods*, *8*(10), 871–878. https://doi.org/10.1038/nmeth.1694

Giustino, T. F., & Maren, S. (2015). The Role of the Medial Prefrontal Cortex in the Conditioning and Extinction of Fear. *Frontiers in Behavioral Neuroscience*, *9*, 298. https://doi.org/10.3389/fnbeh.2015.00298

Goetz, A. R., Davine, T. P., Siwiec, S. G., & Lee, H.-J. (2016). The functional value of preventive and restorative safety behaviors: A systematic review of the literature. *Clinical Psychology Review*, *44*, 112–124. https://doi.org/10.1016/j.cpr.2015.12.005

Gongwer, M. W., Klune, C. B., Couto, J., Jin, B., Enos, A. S., Chen, R., Friedmann, D., & DeNardo, L. A. (2023). Brain-Wide Projections and Differential Encoding of Prefrontal

Neuronal Classes Underlying Learned and Innate Threat Avoidance. *Journal of Neuroscience*, *43*(32), 5810–5830. https://doi.org/10.1523/JNEUROSCI.0697-23.2023

Gonzalez, M. C., Kramar, C. P., Tomaiuolo, M., Katche, C., Weisstaub, N., Cammarota, M., & Medina, J. H. (2014). Medial prefrontal cortex dopamine controls the persistent storage of aversive memories. *Frontiers in Behavioral Neuroscience*, *8*, 408. https://doi.org/10.3389/fnbeh.2014.00408

Herry, C., & Jercog, D. (2022). Decoding defensive systems. *Current Opinion in Neurobiology*, *76*, 102600. https://doi.org/10.1016/j.conb.2022.102600

Herry, C., & Jercog, D. (2023). Stable coding of aversive associations in medial prefrontal populations. *Comptes Rendus Biologies*, *346*, 127–138. https://doi.org/10.5802/crbiol.126

Ironside, M., Amemori, K.-I., McGrath, C. L., Pedersen, M. L., Kang, M. S., Amemori, S., Frank, M. J., Graybiel, A. M., & Pizzagalli, D. A. (2020). Approach-Avoidance Conflict in Major Depressive Disorder: Congruent Neural Findings in Humans and Nonhuman Primates. *Biological Psychiatry*, *87*(5), 399–408. https://doi.org/10.1016/j.biopsych.2019.08.022

Jercog, D., Winke, N., Sung, K., Fernandez, M. M., Francioni, C., Rajot, D., Courtin, J., Chaudun, F., Jercog, P. E., Valerio, S., & Herry, C. (2021). Dynamical prefrontal population coding during defensive behaviours. *Nature*, *595*(7869), 690–694. https://doi.org/10.1038/s41586-021-03726-6

Jiao, X., Beck, K. D., Myers, C. E., Servatius, R. J., & Pang, K. C. H. (2015). Altered activity of the medial prefrontal cortex and amygdala during acquisition and extinction of an active avoidance task. *Frontiers in Behavioral Neuroscience*, *9*, 249. https://doi.org/10.3389/fnbeh.2015.00249

Kajs, B. L., Loewke, A. C., Dorsch, J. M., Vinson, L. T., & Gunaydin, L. A. (2022). Divergent encoding of active avoidance behavior in corticostriatal and corticolimbic projections. *Scientific Reports*, *12*(1), 10731. https://doi.org/10.1038/s41598-022-14930-3

Kim, C. K., Ye, L., Jennings, J. H., Pichamoorthy, N., Tang, D. D., Yoo, A.-C. W., Ramakrishnan, C., & Deisseroth, K. (2017). Molecular and Circuit-Dynamical Identification of Top-Down Neural Mechanisms for Restraint of Reward Seeking. *Cell*, *170*(5), 1013-1027.e14. https://doi.org/10.1016/j.cell.2017.07.020

Kingsbury, L., Huang, S., Wang, J., Gu, K., Golshani, P., Wu, Y. E., & Hong, W. (2019). Correlated Neural Activity and Encoding of Behavior across Brains of Socially Interacting Animals. *Cell*, *178*(2), 429-446.e16. https://doi.org/10.1016/j.cell.2019.05.022

Kjærstad, H. L., de Siqueira Rotenberg, L., Macoveanu, J., Coello, K., Faurholt-Jepsen, M., Bjertrup, A. J., Knudsen, G. M., Fisher, P. M., Vinberg, M., Kessing, L. V., Lafer, B., & Miskowiak, K. W. (2024). Stable neural underpinnings of emotional cognition subgroups in patients newly diagnosed with bipolar disorder: A prospective fMRI study. *Bipolar Disorders*. https://doi.org/10.1111/bdi.13444

Koh, T. H., Bishop, W. E., Kawashima, T., Jeon, B. B., Srinivasan, R., Mu, Y., Wei, Z., Kuhlman, S. J., Ahrens, M. B., Chase, S. M., & Yu, B. M. (2023). Dimensionality reduction of calcium-imaged neuronal population activity. *Nature Computational Science*, *3*(1), 71–85. https://doi.org/10.1038/s43588-022-00390-2

Krypotos, A.-M., Effting, M., Kindt, M., & Beckers, T. (2015). Avoidance learning: A review of theoretical models and recent developments. *Frontiers in Behavioral Neuroscience*, *9*, 189. https://doi.org/10.3389/fnbeh.2015.00189

Lammel, S., Ion, D. I., Roeper, J., & Malenka, R. C. (2011). Projection-specific modulation of dopamine neuron synapses by aversive and rewarding stimuli. *Neuron*, *70*(5), 855–862. https://doi.org/10.1016/j.neuron.2011.03.025

Lammel, S., Lim, B. K., Ran, C., Huang, K. W., Betley, M. J., Tye, K. M., Deisseroth, K., & Malenka, R. C. (2012). Input-specific control of reward and aversion in the ventral tegmental area. *Nature*, *491*(7423), 212–217. https://doi.org/10.1038/nature11527

Laviolette, S. R., Lipski, W. J., & Grace, A. A. (2005). A subpopulation of neurons in the medial prefrontal cortex encodes emotional learning with burst and frequency codes through a dopamine D4 receptor-dependent basolateral amygdala input. *The Journal of Neuroscience: The Official Journal of the Society for Neuroscience*, *25*(26), 6066–6075. https://doi.org/10.1523/JNEUROSCI.1168-05.2005

Li, Y., Mathis, A., Grewe, B. F., Osterhout, J. A., Ahanonu, B., Schnitzer, M. J., Murthy, V. N., & Dulac, C. (2017). Neuronal Representation of Social Information in the Medial Amygdala of Awake Behaving Mice. *Cell*, *171*(5), 1176-1190.e17. https://doi.org/10.1016/j.cell.2017.10.015

Likhtik, E., Stujenske, J. M., Topiwala, M. A., Harris, A. Z., & Gordon, J. A. (2014). Prefrontal entrainment of amygdala activity signals safety in learned fear and innate anxiety. *Nature Neuroscience*, *17*(1), 106–113. https://doi.org/10.1038/nn.3582

Little, J. P., & Carter, A. G. (2013). Synaptic mechanisms underlying strong reciprocal connectivity between the medial prefrontal cortex and basolateral amygdala. *The Journal of Neuroscience: The Official Journal of the Society for Neuroscience*, *33*(39), 15333–15342. https://doi.org/10.1523/JNEUROSCI.2385-13.2013

Maas, L. C., Lukas, S. E., Kaufman, M. J., Weiss, R. D., Daniels, S. L., Rogers, V. W., Kukes, T. J., & Renshaw, P. F. (1998). Functional Magnetic Resonance Imaging of Human Brain Activation During Cue-Induced Cocaine Craving. *American Journal of Psychiatry*, *155*(1), 124–126. https://doi.org/10.1176/ajp.155.1.124

Mack, N. R., Bouras, N. N., & Gao, W.-J. (2024). Prefrontal regulation of social behavior and related deficits: Insights from rodent studies. *Biological Psychiatry*, S0006-3223(24)01146-6. https://doi.org/10.1016/j.biopsych.2024.03.008

Mantz, J., Thierry, A. M., & Glowinski, J. (1989). Effect of noxious tail pinch on the discharge rate of mesocortical and mesolimbic dopamine neurons: Selective activation of the

mesocortical system. *Brain Research*, *476*(2), 377–381. https://doi.org/10.1016/0006-8993(89)91263-8

Mathis, A., Mamidanna, P., Cury, K. M., Abe, T., Murthy, V. N., Mathis, M. W., & Bethge, M. (2018). DeepLabCut: Markerless pose estimation of user-defined body parts with deep learning. *Nature Neuroscience*, *21*(9), 1281–1289. https://doi.org/10.1038/s41593-018-0209-y

McGarry, L. M., & Carter, A. G. (2017). Prefrontal Cortex Drives Distinct Projection Neurons in the Basolateral Amygdala. *Cell Reports*, *21*(6), 1426–1433. https://doi.org/10.1016/j.celrep.2017.10.046

Mochcovitch, M. D., da Rocha Freire, R. C., Garcia, R. F., & Nardi, A. E. (2014). A systematic review of fMRI studies in generalized anxiety disorder: Evaluating its neural and cognitive basis. *Journal of Affective Disorders*, *167*, 336–342. https://doi.org/10.1016/j.jad.2014.06.041

Montaser, J., Umeano, L., Pujari, H. P., Nasiri, S. M. Z., Parisapogu, A., Shah, A., & Khan, S. (2023). Correlations Between the Development of Social Anxiety and Individuals With Autism Spectrum Disorder: A Systematic Review. *Cureus*, *15*(9), e44841. https://doi.org/10.7759/cureus.44841

Moscarello, J. M., & LeDoux, J. E. (2013). Active avoidance learning requires prefrontal suppression of amygdala-mediated defensive reactions. *The Journal of Neuroscience: The Official Journal of the Society for Neuroscience*, *33*(9), 3815–3823. https://doi.org/10.1523/JNEUROSCI.2596-12.2013

Mowrer, O. H., & Lamoreaux, R. R. (1942). Avoidance conditioning and signal duration—A study of secondary motivation and reward. *Psychological Monographs*, *54*(5), i–34. https://doi.org/10.1037/h0093499

Preuss, U. W., Schaefer, M., Born, C., & Grunze, H. (2021). Bipolar Disorder and Comorbid Use of Illicit Substances. *Medicina (Kaunas, Lithuania)*, *57*(11), 1256. https://doi.org/10.3390/medicina57111256

Puig, M. V., Antzoulatos, E. G., & Miller, E. K. (2014). Prefrontal dopamine in associative learning and memory. *Neuroscience*, *282*, 217–229. https://doi.org/10.1016/j.neuroscience.2014.09.026

Rescorla, R., & Wagner, A. (1972). A theory of Pavlovian conditioning: Variations in the effectiveness of reinforcement and nonreinforcement. In *Classical Conditioning II: Current Research and Theory: Vol. Vol. 2*.

Santana, N., Mengod, G., & Artigas, F. (2009). Quantitative analysis of the expression of dopamine D1 and D2 receptors in pyramidal and GABAergic neurons of the rat prefrontal cortex. *Cerebral Cortex (New York, N.Y.: 1991)*, *19*(4), 849–860. https://doi.org/10.1093/cercor/bhn134

Schultz, W. (2016). Dopamine reward prediction-error signalling: A two-component response. *Nature Reviews. Neuroscience*, *17*(3), 183–195. https://doi.org/10.1038/nrn.2015.26

Smith, J. W., Fetsko, L. A., Xu, R., & Wang, Y. (2002). Dopamine D2L receptor knockout mice display deficits in positive and negative reinforcing properties of morphine and in avoidance learning. *Neuroscience*, *113*(4), 755–765. https://doi.org/10.1016/s0306-4522(02)00257-9

Sylte, O. C., Muysers, H., Chen, H.-L., Bartos, M., & Sauer, J.-F. (2024). Neuronal tuning to threat exposure remains stable in the mouse prefrontal cortex over multiple days. *PLoS Biology*, *22*(1), e3002475. https://doi.org/10.1371/journal.pbio.3002475

Vander Weele, C. M., Siciliano, C. A., Matthews, G. A., Namburi, P., Izadmehr, E. M., Espinel, I. C., Nieh, E. H., Schut, E. H. S., Padilla-Coreano, N., Burgos-Robles, A., Chang, C.-J., Kimchi, E. Y., Beyeler, A., Wichmann, R., Wildes, C. P., & Tye, K. M. (2018). Dopamine enhances signal-to-noise ratio in cortical-brainstem encoding of aversive stimuli. *Nature*, *563*(7731), 397–401. https://doi.org/10.1038/s41586-018-0682-1

Vander Weele, C. M. V., Siciliano, C. A., & Tye, K. M. (2019). Dopamine tunes prefrontal outputs to orchestrate aversive processing. *Brain Research*, *1713*, 16–31. https://doi.org/10.1016/j.brainres.2018.11.044

Wise, R. A. (2004). Dopamine, learning and motivation. *Nature Reviews. Neuroscience*, *5*(6), 483–494. https://doi.org/10.1038/nrn1406

Zelikowsky, M., Hersman, S., Chawla, M. K., Barnes, C. A., & Fanselow, M. S. (2014). Neuronal Ensembles in Amygdala, Hippocampus, and Prefrontal Cortex Track Differential Components of Contextual Fear. *The Journal of Neuroscience*, *34*(25), 8462–8466. https://doi.org/10.1523/JNEUROSCI.3624-13.2014

Zhao, Y.-J., Du, M.-Y., Huang, X.-Q., Lui, S., Chen, Z.-Q., Liu, J., Luo, Y., Wang, X.-L., Kemp, G. J., & Gong, Q.-Y. (2014). Brain grey matter abnormalities in medication-free patients with major depressive disorder: A meta-analysis. *Psychological Medicine*, *44*(14), 2927–2937. https://doi.org/10.1017/S0033291714000518

Zweifel, L. S., Fadok, J. P., Argilli, E., Garelick, M. G., Jones, G. L., Dickerson, T. M. K., Allen, J. M., Mizumori, S. J. Y., Bonci, A., & Palmiter, R. D. (2011). Activation of dopamine neurons is critical for aversive conditioning and prevention of generalized anxiety. *Nature Neuroscience*, *14*(5), 620–626. https://doi.org/10.1038/nn.2808

Chapter 4: Discussion

Integrated summary of the thesis

The ability to study complex behaviors is limited by the tools available to record and analyze the behavior of animals, especially when definitions of behavior go beyond mere motor patterns and intersect with spatiotemporal cues. Automating analysis of animal behaviors from video recordings has greatly enhanced our ability to understand the neural signals that give rise to complex behaviors. But many existing analysis programs specialize in analysis of a single behavior, cannot report where the animal was located during behavior, and fail when used with head-mounted implants that include visible cables.

To study PMA in mPFC, I needed the ability to analyze multiple behaviors with respect to threat-predicting tones and a safe location. Further, I needed to do this analysis in animals that included head-attached cables and implants that partially obstructed the view of a top-down camera. When using DeepLabCut, a deep learning-based approach to track animal position across space and time, I identified a need for a tool that could convert pose tracking into behavioral data. Ideally such a tool could help me analyze behavioral data during PMA while flexibly meeting the needs of other behavioral neuroscientists.

In Chapter 2, I reported a new software program that I created and published for automated analysis of animal behavior. BehaviorDEPOT uses heuristics to convert key point tracking data into discrete behaviors. BehaviorDEPOT is a user-friendly MATLAB app designed for analyzing data in commonly used experimental assays including fear conditioning, open field test, and novel object exploration. It is highly flexible and guides users through the creation of custom analysis pipelines. This tool provides a new way of studying animal behavior that is accessible and easy-to-use for users with limited programming experience. Importantly, BehaviorDEPOT was critical for the analysis of data presented in Chapter 3. By allowing detailed, framewise analysis of mouse behavior during PMA, I was able to easily synchronize

behavioral analysis with miniscope recordings. In doing so, I expanded our knowledge of how aversive learning drives rapid emergence of representations of danger-predicting cues, safe locations, and avoidance actions in mPFC.

BehaviorDEPOT: a pipeline for heuristic-based classification of behavior

The advent of computer vision and machine learning have opened new doors to link neural activity to observed behavior. The growth of computer vision has provided new ways to robustly extract meaningful data from video recordings of behavior. Using tools such as DeepLabCut, experimenters can robustly track keypoints of animals in great detail, reducing the need for human annotation and the variability it can produce. Machine learning has made impossible problems trivial to solve and have enabled deeper exploration of detailed animal poses during behaviors of interest. Supervised algorithms can replace human raters, using samples of annotation to make observations and predictions about complex neural datasets. Unsupervised machine learning can reveal patterns in activity that are difficult for humans to observe and without the need for any human bias.

A major limitation to the rapidly advancing machine learning tools for animal tracking are that they generate estimates of animal position but not descriptions of discrete behaviors. In Chapter 2, I present BehaviorDEPOT – an open source software program I developed to capitalize on the capabilities of deep learning-based keypoint tracking and generating highly detailed reports of animal behaviors that can easily be aligned with streams of neural data.

BehaviorDEPOT is a user-friendly behavioral analysis software package that utilizes keypoint tracking to produce robust readouts of naturalistic behavior, BehaviorDEPOT allows users to analyze specific behaviors with respect to spatiotemporal cues. By providing framewise behavioral readouts, BehaviorDEPOT also facilitates alignment of neural and behavioral data streams.

Established automated methods for quantifying animal behavior rely on techniques that do not track the location of the animal, rely on centroids to approximate position, and fail when animals have obstructive implants and headgear. Using established algorithms to track locations across the animal's body (Mathis et al., 2018; Pereira et al., 2019), BehaviorDEPOT leverages the high fidelity of keypoint tracking to establish a framework for easy quantification of many different behaviors. Users can employ existing classifiers for commonly studied behaviors and spatially-defined tasks (e.g. open field test, elevated plus maze). This pipeline can be customized for the needs of each user and includes support modules that assist with identification, optimization, and validation of new classifiers.

Existing software pipelines for behavior classification are subject to constraints that limit their usefulness in critical situations. An increasingly common feature of behavioral neuroscience experiments is the inclusion of attached headwear and cables used for observing or manipulating neural activity. Some existing software packages can circumvent this issue by cropping out cables; however, these options require side-view cameras, which constrains analysis of movement and spatial features (Anagnostaras et al., 2010; Pennington et al., 2019). BehaviorDEPOT's use of keypoint tracking eliminates this constraint by allowing users to detect animals regardless of experimental condition, even permitting analysis of previously recorded videos. Other software approaches to behavior classification involve use of machine learning. Compared to methods using supervised machine learning (Nilsson et al., 2020; Segalin et al., 2021; Bohnslav et al., 2021), BehaviorDEPOT's heuristics are easier to interpret and can be easily modified for out-of-sample videos. Unsupervised machine learning methods have been successful at unbiased annotation of behavior but are aimed at subtle behaviors that cannot be reliably labeled by humans and may be challenging to use without computational expertise. BehaviorDEPOT is free and open source, focuses on ease-of-use and customization, and is robust in any experimental condition.

Though BehaviorDEPOT represents an improvement on the currently available slate of classification tools for behavioral neuroscience, it has some limitations. Importantly, the accuracy of keypoint tracking is critical for accurate labeling of behavior. Though keypoint tracking software attempts to minimize the need for computational experience, its use, including setting up the software-hardware interface, may still prove challenging for inexperienced users. BehaviorDEPOT attempts to control the impact of human bias on behavior, but it does not eliminate it entirely. Instead, our heuristic classifiers attempt to capture and standardize biased human definitions for behavior across users, using the provided support modules to compare inter-rater agreement levels and reach consensus. Other pipelines are more successful at mitigating bias in behavior through use of machine learning methods, though at a cost to the interpretability and ease-of-use of these methods. Supervised machine learning methods are subject to similar biases in human annotations of behavior but provide an unbiased approach to parameter tuning that could produce more rigorous labeling of behavior. Unsupervised algorithms eliminate the need for human annotations and thus the bias introduced by using them but can require computational experience to use and may result in more granular assessments of behavior than can be reasonably interpreted.

Since its release, BehaviorDEPOT has been used in several research projects within and outside the lab. As of May 2024, BehaviorDEPOT has been cited in 20 publications and has been included in the OpenBehavior Project – a public and widely accessed repository of cutting-edge, open-source tools for advancing behavioral neuroscience research. Since its initial release, BehaviorDEPOT has been iteratively improved based on feedback from the community. Support for additional behaviors such as jumping, rearing, and escape have been added, bringing the total number of ready-to-use classifiers to 12. I also added compatibility for new keypoint tracking algorithms (such as LEAP). In addition to minor improvements in performance and additional customization features, I added support for parallel processing that can double or triple the speed of analysis. After the request of users, I expanded

BehaviorDEPOT to function without any classifiers, simply generating detailed reports of animal position and kinematics that can be used with downstream analyses.

In the future, to help BehaviorDEPOT reach more users and become truly open source, I would recreate the software in Python, an open-source programming language that is universally accessible. Though its classifiers are powerful and easy to understand, BehaviorDEPOT would also benefit from a module that helps users apply machine learning algorithms to new or existing classifiers. BehaviorDEPOT's current heuristic classifiers are only useful for behaviors that humans can reliably view and annotate. Machine learning approaches to behavior classification can find consistent 'micro' behaviors that are not detectable with current classifiers and could potentially be used to enhance the performance of existing classifiers.

Dynamics of mPFC activity during PMA learning

Learning to use predictive cues to avoid danger is critical for survival and has relevance to psychiatric disease states. In Chapter 3, I used miniscope imaging and BehaviorDEPOT to analyze the neural activity and behavior of mice as they learned PMA. I aimed to elucidate how encoding of threatening cues, safe locations, and adaptive actions emerge in mPFC during rapid aversive learning. I focused on the PL subregion of mPFC, a region that is required for active avoidance and encodes threat-predictive cues and avoidance behaviors (Giustino & Maren, 2015; Diehl et al., 2020; Jercog et al., 2021). I discovered changes in individual neuron and population activity patterns that emerged across learning, some of which correlated with estimated learning rates from a behavioral model of PMA. This work demonstrated the existence of distinct population activity patterns that evolve with learning, precede changes in behavior, and are not visible on the single cell level.

Many previous studies of active avoidance used an assay called two-way active avoidance (or shuttle box), that has limited relevance to clinical avoidance. I chose to use PMA

because of 2 major advantages. In versions of the shuttle box assay, the avoidance action terminates the threat-predicting tone, providing unrealistic control of the environment. On the other hand, in PMA the conditioned tone continues to play regardless of whether an animal enters the safety platform. PMA also features a safe location (the platform) that is always accessible, allowing investigation of neural correlates of both danger and safety.

I first investigated single cell responses to behaviorally relevant features as mice rapidly learned PMA. One of the first changes to emerge during learning was a population of PL neurons that increased their activity when animals exited the safety platform. Because this change emerged on the first day of training, it may be necessary to establish a new behavioral strategy required to preemptively avoid foot shocks. On the other hand, the proportion of neurons that encoded the tone did not evolve across learning or differ from non-shocked controls. We did observe a learning-dependent increase in the population neurons that encoded combinations of the tone, the safety platform and freezing behavior. We also discovered that conditioned tones significantly modulate activity associated with platform entries and exits. However, these patterns were only evident on the second day of PMA when mice reliably performed PMA. This suggests that integrated coding of cues and actions is a product of learning that reflects the newly adopted behavioral strategy.

I also revealed dynamic changes in PL population activity that were associated with learning. Decoding the trial outcomes was possible on day 1, before behavioral performance reached its peak, and cells that were significantly modulated by conditioned cues and avoidance actions were more informative for decoding than cells that did not. I used dimensionality reduction to reveal how salient events alter trial-by-trial population dynamics in PL. On the first day of training, highly stable patterns of activity in the epoch immediately preceding the foot shock period emerged in shocked mice but not non-shocked controls. This stabilization may be necessary for learning and may be related to increased representation of impending threat or could reflect increasingly stereotyped behavior during the tone (e.g. waiting on the platform until

the end of the tone). On the first day, the ability of cue-evoked population activity to distinguish between successful vs. shocked trials was correlated with learning rates estimated with the R-W model. On the second day of PMA, population activity during the tone onset epoch dramatically shifted if the animal received a shock. Since animals already exhibited a consistent avoidance strategy at this point, this shift in activity may reflect an update of the predictive relationships between cues, outcomes, and actions.

Together these data reveal how and when changes encoded in individual neurons and in the overall population emerge in PL as animals learn PMA. My findings suggest that during aversive learning, PL first establishes new representations of safe and threatening locations and establishes reliable patterns of activity (e.g. during the pre-shock period) that promote threat avoidance. Establishing a reliable avoidance strategy is associated with the eventual formation of integrated representations of danger-predicting cues, avoidance actions, and locations associated with safety. Though representations of threat are clearly important for aversive learning, representations of safety also impact response to threat. The value of overcoming threat is linked to the perception of safety, and 'safe' behaviors can interfere with treatment of psychiatric disease, especially anxiety disorders (Blakey & Abramowitz, 2016; Goetz et al., 2016). Maladaptive safety seeking could drive disease just as maladaptive perception of threats does.

Limitations and Future Directions

We chose to study PMA because animals learn within just a few trials, as they do in the natural world. However, analyzing neural activity during a low number of trials poses challenges. Many techniques for analyzing neural activity rely on observing activity across hundreds of trials. With sufficient trial averaging, it is possible to discover small but reliable changes in neural activity. In our assay, such changes are harder to observe because we had few trials and behavior changed rapidly throughout the assay. We are partly able to overcome these

limitations by recording from hundreds of neurons at once. In the future, we can lengthen the learning process by adding a competing reward to amplify the approach-avoidance conflict and increase the cost of staying on the platform and encourage additional exploration. This would allow us study how PL activity evolves over more trials.

While neuronal recordings are critical to reveal the specific patterns of neural activity associated with new behavioral strategies, they cannot tell us which aspects of activity are causally related to behavioral changes. In future we can design optogenetic studies in which we test specific predictions informed by our studies presented in Chapter 3. For instance, we can precisely manipulate PL activity during particular epochs of the conditioned tone and at different stages of learning. Silencing PL during the tone onset or pre-shock periods could reveal the importance of population activity identified in my study to learning and allow important comparison to similar experiments done using the shuttle box (Jercog et al., 2021). Manipulation of PL-VTA projections would help us understand how top-down communication with the VTA contributes to aversive learning and could be important for understanding the dynamics of the VTA's role in activating the DA system.

Miniscope imaging allows the simultaneous recording of hundreds of neurons in freely moving animals. However, use of miniscopes requires a lens to be implanted just above the region of interest. In the case of PL, this requires aspiration of some tissue from the adjacent anterior cingulate cortex (ACC), which is also implicated in learning processes of the mPFC (Monosov et al., 2020). In our study, this issue is mitigated by our use of non-shock controls that undergo identical aspirations to the experimental animals. Although unilateral lesions in this region typically do not cause large changes in behavior performance, there is evidence suggesting such lesions could impact decision making (Croxson et al., 2014). It remains possible that aspirating a portion of ACC could alter natural behaviorally-relevant patterns of PL activity.

Another limitation of our imaging approach lies in the temporal resolution of our calcium indicator. Miniscopes rely on the use of calcium indicator proteins as a proxy for observed neural activity. Though frequently used to study the activity of neurons, the dynamics of the fastest calcium indicators are currently orders of magnitude slower than the neural events that underlie their activity. Thus, the reported calcium activity will always be disconnected from the temporal structure of the neural activity it reports. GCaMP proteins have undergone iterative improvement to increase sensitivity and speed, but future studies could compare the Ca^{2+} activity patterns we observed with neuronal spikes measured with extracellular electrodes or genetically encoded voltage sensors.

Though temporal resolution may be limited, miniscopes offer distinct benefits over alternative imaging techniques that can be utilized in future research. One such benefit is the ability to easily record from genetically-, activity- or projection-defined subsets of mPFC cells. We speculated that many of the cells underlying dynamic responses to the tone were projection neurons from PL to the amygdala. Future studies could answer this definitively by using miniscope recordings to compare the neuronal activity patterns among PL-BLA and other anatomically defined populations.

Future studies can address the specific mechanisms that drive plasticity in mPFC activity patterns during learning. Recent research has implicated dopamine as an important substrate of aversive learning in cortical regions, and dopamine in mPFC has been shown to enhance signal-to-noise ratio in neurons encoding aversive stimuli (Vander Weele et al., 2018). The primary source of dopamine for cortical regions is from neurons of the ventral tegmental area (VTA). Recent work from our lab has implicated this region directly in PMA, showing that PL-VTA projection neurons are active when animals enter the safety platform (Gongwer et al., 2023). Unpublished data from our lab has also suggested that PL dopamine release is important for PMA learning, with significant release during shock and, after learning, during the tone period. It is possible that dopamine release during shocks drives the lasting changes in PL

activity that are important for linking predictive cues with avoidance actions. Future studies could record from genetically encoded dopamine sensors in PL or manipulate the activity of DAergic projections from the VTA to assess how DA signaling contributes to the evolution of PL activity during learning.

Previous studies identified sex differences during threat avoidance behaviors. Male rodents acquire active avoidance strategies more rapidly than females (Beck et al., 2011, Yokota et al., 2017). Additionally, when a safety cue is included in the avoidance task, female rodents extinguish learned avoidance faster than males (Beck et al., 2011; Radell et al. 2015). This sex difference has also been observed in humans (Sheynin et al. 2014). Though my study included both male and female animals, it was under powered to rigorously examine sex differences. Future experiments could specifically examine these differences and compare how patterns of mPFC activity differ between sexes who undergo avoidance learning.

Dysfunction within mPFC is closely linked to a variety of psychiatric diseases –including anxiety disorders, depression, phobias, schizophrenia, substance use disorder, and bipolar disorder – that arise with different frequency in males and females (Buxhoeveden et al., 2006; Maner & Schmidt, 2006; Papaleo et al., 2012; Xu et al., 2019; Ironside et al., 2020). In depression and anxiety, excessive avoidance of perceived threats interferes with productive behaviors (Stein & Stein, 2008; DiMartini et al., 2019). Anxiety disorders are the largest category of diagnosed psychiatric disorders and are linked to increased activity in mPFC after presentation of ambiguous stimuli in humans (Nitschke et al., 2009; Mack et al., 2023). Our PL recordings during PMA build a foundation for understanding how disease risk factors like chronic stress may alter mPFC activity and lead to inappropriate levels of threat avoidance. Such research, especially when combined with circuit-specific imaging and manipulations, can ultimately inform better therapeutic interventions.

REFERENCES

Anagnostaras, S. G., Wood, S. C., Shuman, T., Cai, D. J., Leduc, A. D., Zurn, K. R., Zurn, J. B., Sage, J. R., & Herrera, G. M. (2010). Automated assessment of pavlovian conditioned freezing and shock reactivity in mice using the video freeze system. *Frontiers in Behavioral Neuroscience*, *4*, 158. https://doi.org/10.3389/fnbeh.2010.00158

Beck, K. D., Jiao, X., Ricart, T. M., Myers, C. E., Minor, T. R., Pang, K. C. H., & Servatius, R. J. (2011). Vulnerability factors in anxiety: Strain and sex differences in the use of signals associated with non-threat during the acquisition and extinction of active-avoidance behavior. *Progress in Neuro-Psychopharmacology & Biological Psychiatry*, *35*(7), 1659–1670. https://doi.org/10.1016/j.pnpbp.2011.05.002

Blakey, S. M., & Abramowitz, J. S. (2016). The effects of safety behaviors during exposure therapy for anxiety: Critical analysis from an inhibitory learning perspective. *Clinical Psychology Review*, *49*, 1–15. https://doi.org/10.1016/j.cpr.2016.07.002

Bohnslav, J. P., Wimalasena, N. K., Clausing, K. J., Dai, Y. Y., Yarmolinsky, D. A., Cruz, T., Kashlan, A. D., Chiappe, M. E., Orefice, L. L., Woolf, C. J., & Harvey, C. D. (2021). DeepEthogram, a machine learning pipeline for supervised behavior classification from raw pixels. *eLife*, *10*, e63377. https://doi.org/10.7554/eLife.63377

Buxhoeveden, D. P., Semendeferi, K., Buckwalter, J., Schenker, N., Switzer, R., & Courchesne, E. (2006). Reduced minicolumns in the frontal cortex of patients with autism. *Neuropathology and Applied Neurobiology*, *32*(5), 483–491. https://doi.org/10.1111/j.1365-2990.2006.00745.x

Croxson, P. L., Walton, M. E., Boorman, E. D., Rushworth, M. F. S., & Bannerman, D. M. (2014). Unilateral medial frontal cortex lesions cause a cognitive decision-making deficit in rats. *The European Journal of Neuroscience*, *40*(12), 3757–3765. https://doi.org/10.1111/ejn.12751

DeMartini, J., Patel, G., & Fancher, T. L. (2019). Generalized Anxiety Disorder. *Annals of Internal Medicine*, *170*(7), ITC49–ITC64. https://doi.org/10.7326/AITC201904020

Diehl, M. M., Iravedra-Garcia, J. M., Morán-Sierra, J., Rojas-Bowe, G., Gonzalez-Diaz, F. N., Valentín-Valentín, V. P., & Quirk, G. J. (2020). Divergent projections of the prelimbic cortex bidirectionally regulate active avoidance. *eLife*, *9*, e59281. https://doi.org/10.7554/eLife.59281

Giustino, T. F., & Maren, S. (2015). The Role of the Medial Prefrontal Cortex in the Conditioning and Extinction of Fear. *Frontiers in Behavioral Neuroscience*, *9*, 298. https://doi.org/10.3389/fnbeh.2015.00298

Goetz, A. R., Davine, T. P., Siwiec, S. G., & Lee, H.-J. (2016). The functional value of preventive and restorative safety behaviors: A systematic review of the literature. *Clinical Psychology Review*, *44*, 112–124. https://doi.org/10.1016/j.cpr.2015.12.005

Gongwer, M. W., Klune, C. B., Couto, J., Jin, B., Enos, A. S., Chen, R., Friedmann, D., & DeNardo, L. A. (2023). Brain-Wide Projections and Differential Encoding of Prefrontal Neuronal Classes Underlying Learned and Innate Threat Avoidance. *Journal of Neuroscience*, *43*(32), 5810–5830. https://doi.org/10.1523/JNEUROSCI.0697-23.2023

Ironside, M., Amemori, K.-I., McGrath, C. L., Pedersen, M. L., Kang, M. S., Amemori, S., Frank, M. J., Graybiel, A. M., & Pizzagalli, D. A. (2020). Approach-Avoidance Conflict in Major Depressive Disorder: Congruent Neural Findings in Humans and Nonhuman Primates. *Biological Psychiatry*, *87*(5), 399–408. https://doi.org/10.1016/j.biopsych.2019.08.022

Jercog, D., Winke, N., Sung, K., Fernandez, M. M., Francioni, C., Rajot, D., Courtin, J., Chaudun, F., Jercog, P. E., Valerio, S., & Herry, C. (2021). Dynamical prefrontal population coding during defensive behaviours. *Nature*, *595*(7869), 690–694. https://doi.org/10.1038/s41586-021-03726-6

Mack, N. R., Deng, S., Yang, S.-S., Shu, Y., & Gao, W.-J. (2023). Prefrontal Cortical Control of Anxiety: Recent Advances. *The Neuroscientist: A Review Journal Bringing Neurobiology, Neurology and Psychiatry*, *29*(4), 488–505. https://doi.org/10.1177/10738584211069071

Maner, J. K., & Schmidt, N. B. (2006). The role of risk avoidance in anxiety. *Behavior Therapy*, *37*(2), 181–189. https://doi.org/10.1016/j.beth.2005.11.003

Mathis, A., Mamidanna, P., Cury, K. M., Abe, T., Murthy, V. N., Mathis, M. W., & Bethge, M. (2018). DeepLabCut: Markerless pose estimation of user-defined body parts with deep learning. *Nature Neuroscience*, *21*(9), 1281–1289. https://doi.org/10.1038/s41593-018-0209-y

Monosov, I. E., Haber, S. N., Leuthardt, E. C., & Jezzini, A. (2020). Anterior Cingulate Cortex and the Control of Dynamic Behavior in Primates. *Current Biology: CB*, *30*(23), R1442–R1454. https://doi.org/10.1016/j.cub.2020.10.009

Nilsson, S. R., Goodwin, N. L., Choong, J. J., Hwang, S., Wright, H. R., Norville, Z. C., Tong, X., Lin, D., Bentzley, B. S., Eshel, N., McLaughlin, R. J., & Golden, S. A. (2020). *Simple Behavioral Analysis (SimBA) – an open source toolkit for computer classification of complex social behaviors in experimental animals* (p. 2020.04.19.049452). bioRxiv. https://doi.org/10.1101/2020.04.19.049452

Nitschke, J. B., Sarinopoulos, I., Oathes, D. J., Johnstone, T., Whalen, P. J., Davidson, R. J., & Kalin, N. H. (2009). Anticipatory activation in the amygdala and anterior cingulate in generalized anxiety disorder and prediction of treatment response. *The American Journal of Psychiatry*, *166*(3), 302–310. https://doi.org/10.1176/appi.ajp.2008.07101682

Papaleo, F., Yang, F., Garcia, S., Chen, J., Lu, B., Crawley, J., & Weinberger, D. (2012). Dysbindin-1 modulates prefrontal cortical activity and schizophrenia-like behaviors via dopamine/D2 pathways. *Molecular Psychiatry*, *17*(1), 85–98. https://doi.org/10.1038/mp.2010.106

Pennington, Z. T., Dong, Z., Feng, Y., Vetere, L. M., Page-Harley, L., Shuman, T., & Cai, D. J. (2019). ezTrack: An open-source video analysis pipeline for the investigation of animal behavior. *Scientific Reports*, *9*(1), 19979. https://doi.org/10.1038/s41598-019-56408-9

Pereira, T. D., Aldarondo, D. E., Willmore, L., Kislin, M., Wang, S. S.-H., Murthy, M., & Shaevitz, J. W. (2019). Fast animal pose estimation using deep neural networks. *Nature Methods*, *16*(1), 117–125. https://doi.org/10.1038/s41592-018-0234-5

Radell, M. L., Beck, K. D., Pang, K. C. H., & Myers, C. E. (2015). Using signals associated with safety in avoidance learning: Computational model of sex differences. *PeerJ*, *3*, e1081. https://doi.org/10.7717/peerj.1081

Segalin, C., Williams, J., Karigo, T., Hui, M., Zelikowsky, M., Sun, J. J., Perona, P., Anderson, D. J., & Kennedy, A. (2021). The Mouse Action Recognition System (MARS) software pipeline for automated analysis of social behaviors in mice. *eLife*, *10*, e63720. https://doi.org/10.7554/eLife.63720

Sheynin, J., Beck, K. D., Pang, K. C. H., Servatius, R. J., Shikari, S., Ostovich, J., & Myers, C. E. (2014). Behaviourally-inhibited temperament and female sex, two vulnerability factors for anxiety disorders, facilitate conditioned avoidance (also) in humans. *Behavioural Processes*, *103*, 228–235. https://doi.org/10.1016/j.beproc.2014.01.003

Stein, M. B., & Stein, D. J. (2008). Social anxiety disorder. *Lancet (London, England)*, *371*(9618), 1115–1125. https://doi.org/10.1016/S0140-6736(08)60488-2

Vander Weele, C. M., Siciliano, C. A., Matthews, G. A., Namburi, P., Izadmehr, E. M., Espinel, I. C., Nieh, E. H., Schut, E. H. S., Padilla-Coreano, N., Burgos-Robles, A., Chang, C.-J., Kimchi, E. Y., Beyeler, A., Wichmann, R., Wildes, C. P., & Tye, K. M. (2018). Dopamine enhances signal-to-noise ratio in cortical-brainstem encoding of aversive stimuli. *Nature*, *563*(7731), 397–401. https://doi.org/10.1038/s41586-018-0682-1

Xu, P., Chen, A., Li, Y., Xing, X., & Lu, H. (2019). Medial prefrontal cortex in neurological diseases. *Physiological Genomics*, *51*(9), 432–442. https://doi.org/10.1152/physiolgenomics.00006.2019

Yokota, S., Suzuki, Y., Hamami, K., Harada, A., & Komai, S. (2017). Sex differences in avoidance behavior after perceiving potential risk in mice. *Behavioral and Brain Functions: BBF*, *13*(1), 9. https://doi.org/10.1186/s12993-017-0126-3